

https://dspace.org/

Fabrication of a polymeric microneedle array for the decalcification of blood vessels

Moodley, Kimaya

2024

University of the Witwatersrand, Johannesburg

https://hdl.handle.net/10539/46361

Moodley, Kimaya . (2024). Fabrication of a polymeric microneedle array for the decalcification of blood vessels [Master`s dissertation, University of the Witwatersrand, Johannesburg]. WIReDSpace. https://hdl.handle.net/10539/46361

Downloaded from a DSpace repository. https://dspace.org/

Fabrication of a polymeric microneedle array for the decalcification of blood vessels

Kimaya Moodley



A dissertation submitted to the Faculty of Health Sciences, University of the Witwatersrand, in fulfilment of the requirements for the degree of Master of Pharmacy

Supervisor:

Professor Yahya E. Choonara

Wits Advanced Drug Delivery Platform, Department of Pharmacy and Pharmacology, School of Therapeutic Sciences, Faculty of Health Sciences, University of the Witwatersrand, Johannesburg, Gauteng, South Africa

Co-supervisors:

Associate Professor Thashree Marimuthu

Professor Pradeep Kumar

Wits Advanced Drug Delivery Platform, Department of Pharmacy and Pharmacology, School of Therapeutic Sciences, Faculty of Health Sciences, University of the Witwatersrand, Johannesburg, Gauteng, South Africa

Doctor Armorel Van Eyk

Department of Pharmacy and Pharmacology, School of Therapeutic Sciences, Faculty of Health Science, University of the Witwatersrand, Johannesburg, Gauteng, South Africa

Johannesburg, 2024

Declaration

I, Kimaya Moodley, declare that this Dissertation is my own, unaided work. It is being submitted for the Degree of Master of Pharmacy by dissertation at the University of the Witwatersrand, Johannesburg. It has not been submitted before for any degree or examination at any other University.



_____ (Signature of candidate)

_20__day of __July_____ 20_24___

Publications envisaged from this research work

Kimaya Moodley, Yahya E. Choonara, Thashree Marimuthu, Pradeep Kumar and Armorel van Eyk. Comparative Analysis of chitosan and alginate polymer blend microneedle arrays in the delivery of EDTA for calcium chelation in vascular calcification (*to be submitted*).

Kimaya Moodley, Yahya E. Choonara, Thashree Marimuthu, Pradeep Kumar and Armorel van Eyk. Microneedle drug delivery and its potential as a vascular drug delivery system (*to be submitted*).

Presentations

Authors: K. Moodley, T. Marimuthu, P. Kumar, A. Van Eyk, Y.E. Choonara (Appendix 2)

Title: Design and Characterisation of EDTA Loaded Polymer Microneedles: Fabricated from Chitosan and Alginate

Wits School of Therapeutic Sciences Biennial Research Day 2023 Poster Presentation

Acknowledgements

Upon the completion of this dissertation, there are several individuals without whom I would not have been able to complete this research project to whom I would like to offer my sincere appreciation.

To my Mum and Dad, thank you for always supporting my every venture and believing in me when I had my doubts – there were many. Your unwavering support and belief in me has given me the ability to persevere through any obstacle to get me where I am today. Thank you for always having an understanding ear available when the shoulders were too far away and for never getting tired of listening when you couldn't understand.

To my Brother, for being my inspiration always and reminding me that the world is bigger than I think it is. You have made me brave and resilient beyond belief and I am so grateful for that.

To my Grandparents, for the words of inspiration that got me through not only this dissertation, but my previous studies as well. Your encouragement, belief and wisdom will live with me always.

To my cousin Devyansh, my sweet baby boy. Thank you for reminding me of the child-like wonder that made me love science in the first place, for being my reason to carry on in the most difficult of times. You are the light I didn't know I needed.

To my supervisors, Professor Yahya Choonara, Associate Professor Thashree Marimuthu Professor Pradeep Kumar and Doctor Armorel van Eyk. Thank you for providing direction and support when needed. I am immensely grateful for the time you invested in this project and the guidance you have provided to me over the course of this research project.

To my incredible colleagues at WADDP, thank you for your assistance and for allowing me to spring ideas off you. Your support means the world to me.

To the life-long friends I made in the lab, Kruti Naik, Kate Da Silva, Divesha Essa, Variksha Singh, Theresa Varughese and Alexis Schwulst. Thank you for the laughs, ice cream and tea dates and your unwavering support, especially in the difficult stages of this work. Thank you for being my sounding board, voices of reason and for the endless assistance and encouragement.

To the Ladies and management at Old Parks' for giving me a space to keep my sanity throughout my research, it has been indispensable.

To Dr Hillary Mndlovu, Mr Siyabonga Maphumulo, Mr Kleinbooi Mohlabi, Mr Bafana Temba and Ms Tshidi Mosete, thank you for your efforts in ensuring my work always ran smoothly, this research would not have been possible without your invaluable assistance.

Financial support received from the National Research Foundation (NRF) for this project is acknowledged.

Dedication

This dissertation is dedicated to all the young girls who have been made to believe that science isn't made for them.

"Never allow a person to tell you no who doesn't have the power to say yes."
— Eleanor Roosevelt

Abstract

Blood tissue calcification involves the deposition of calcium and phosphate minerals, predominantly within blood vessel walls, impacting cardiovascular health. Blood vessel calcification remains a significant concern in cardiovascular health, contributing to various complications such as medial arterial calcification (MAC) and intimal atherosclerotic calcification. While traditional treatment options have limitations, emerging research suggests that ethylenediaminetetraacetic acid (EDTA) could serve as a promising chelating agent to reverse calcification. When delivered in close proximity to the calcification site, EDTA has shown potential for mitigating calcification progression and restoring vascular function.

This study aimed to develop a dissolvable polymeric microneedle (MN) array to be loaded with EDTA to treat vascular calcification in a site specific manner. Two MN formulations were prepared, the first from a combination of chitosan, polyvinyl alcohol and hydroxypropyl cellulose and the second from a cross-linked sodium alginate solution using a mould-based method. EDTA was successfully loaded into both MN formulations for further evaluation. Chitosan MN arrays were loaded with 340 µg of EDTA while alginate arrays were loaded with 965.8 µg of EDTA. The arrays were analysed by, differential scanning calorimetry (DSC), powder x-ray diffraction (PXRD) spectroscopy and Fourier transform infrared (FTIR) spectroscopy. The morphological features and mechanical strength, were investigated by scanning electron microscopy and texture analysis respectively. The fabricated arrays were of 8 mm x 8mm patch size containing 10 x 10 needles. Each needle has a length of 300 µm, needle base of 100µm and needle pitch of 500µm. It was shown that MN arrays were mechanically sufficiently strong to penetrate the vascular tissue. The typical failure force ranged from 0.338 to 0.345 Newton per needle for chitosan and alginate MN arrays respectively. Chitosan MN arrays achieved a 315 µg release within 24 hours while alginate arrays released 789 µg in the same period. Drug permeation studies were carried out on porcine venous tissue and showed in enhanced permeation ability of the alginate arrays after 6 hours. The MN arrays also both showed good hemocompatibility via hemolysis testing, with no significant increase in hemolysis and calcium chelating ability based on the quantity of EDTA permeating the tissue layer.

Overall, this study resulted in the successful preparation of two dissolvable, EDTA loaded MN arrays from natural polymers using a simple, mould-based method. These MNs were found to penetrate the vascular tissue with minimal application forces and release bioactive over a 24 hour period. These polymeric MNs could prove useful for the delivery of many other drugs to the vascular system which would benefit therapeutic outcomes of patients greatly.

Table of Contents

Declaration ..... **i**

Publications envisaged from this research work ..... **ii**

Presentations ..... **iii**

Acknowledgements ..... **iv**

Dedication ..... **v**

Abstract ..... **vi**

Table of Contents ..... **vii**

List of Abbreviations ..... **xv**

List of Equations ..... **xvii**

List of Figures ..... **xviii**

List of Tables ..... **xx**

CHAPTER 1 INTRODUCTION AND OVERVIEW OF THE STUDY 1
1.1 Background to this study 1
1.2 Rationale and Motivation 3
1.3 Applications 5
1.4 Novelty 5
1.5 Aims and Objectives 5
1.6 Overview of this Dissertation 6

CHAPTER 2 MICRONEEDLE FABRICATION TECHNIQUES AND POTENTIAL USE AS A VASCULAR DRUG DELIVERY SYSTEM 7

2.1 Introduction 7

2.2 Types of microneedles and their applications 9

2.2.1 Hollow MN arrays and recent application in the vascular system 9

2.2.2 Solid MN arrays and recent application in the vascular system 10

2.2.3 Coated MN arrays and recent application in the vascular system 10

2.2.4 Hydrogel forming/Swellable MN arrays and recent application in the vascular system 11

2.2.5 Dissolving MN arrays and recent application in the vascular system 12

2.3 Microneedle fabrication methods and material considerations 13

2.4 Conclusion 21

CHAPTER 3 FORMULATION AND DESIGN OF MICRONEEDLE ARRAYS FOR VASCULAR APPLICATIONS..... 22

3.1 Introduction 22

3.2 Formulation Considerations..... 22

3.3 Materials 24

3.4 Design Concepts and Prototyping 24

3.5 Results and Discussion 25

3.6 Conclusions..... 30

CHAPTER 4 COMPARATIVE ANALYSIS OF EDTA-LOADED CHITOSAN AND ALGINATE MICRONEEDLE ARRAYS FOR CALCIUM CHELATION IN VASCULAR CALCIFICATION 32

4.1 Introduction 32

4.2 Methods and Materials 33

4.2.1 Materials 33

4.2.2 Methods 33

4.2.2.1 Chitosan microneedle fabrication 33

4.2.2.2 Alginate microneedle fabrication 34

4.2.2.3 Characterisation of the Fabricated Microneedle (MN) Array using Fourier-Transform Infrared Spectroscopy (FTIR) 34

4.2.2.4 Evaluation of the surface morphology of the MN array using optical Microscope and Scanning Electron Microscopy (SEM) 35

4.2.2.5 Assessment of the physicomechanical properties of the MN array using Texture Analysis 35

4.2.2.6 X-Ray diffraction analysis to determine crystallinity of the MN Array 35

4.2.2.7 Determination of the thermal behaviour of the MN array using Differential Scanning Calorimetry (DSC) 36

4.2.2.8 Determination of *in vitro* degradation 36

4.2.2.9 Determination of *in vitro* water uptake 36

4.2.2.10 Drug loading and encapsulation via ferric UV-Vis spectrophotometry 37

4.2.2.11 Determination of EDTA release from MN formulations 37

4.2.2.12 Collection and storage of venous porcine tissue 37

4.2.2.13 Determination *ex vivo* tissue permeation of EDTA from MN arrays using flow diffusion cells 38

4.2.2.14 *Determination of in vitro* hemocompatibilty 39

4.2.2.15 Statistical analysis 39

4.3 Results and Discussion 39

4.3.1 Fabrication of microneedles (MN) arrays 39

4.3.2 Polymer characterization by Fourier Transform Infrared Spectroscopy (FTIR) 40

4.3.3 Examination of MN array using Scanning Electron Microscopy (SEM) 44

4.3.4 Texture Analysis evaluation of the MN array 44

4.3.5 Powder X-ray Diffraction analysis of the polymeric blends 48

4.3.6 Differential Scanning Calorimetry (DSC) analysis of the polymeric blends 49
4.3.7 *In vitro* degradation of alginate and chitosan MN arrays 51
4.3.8 Water uptake analysis of the MN array 51
4.3.9 EDTA loading and encapsulation 52
4.3.10 *In vitro* release of EDTA from alginate and chitosan MN arrays 55
4.3.11 *Ex vivo* assessment of EDTA diffusion across excised porcine venous tissue 56
4.3.12 Evaluation of calcium chelating ability of array 58
4.3.13 Evaluation of *In Vitro* Hemocompatibility of the MN arrays 58
4.4 Concluding remarks 59

CHAPTER 5 CONCLUSIONS AND RECOMMENDATIONS 61
5.1 Conclusions 61
5.2 Limitations 62
5.3 Recommendations 62
5.4 Future Outlook 62

References **64**

Appendix 1 - Ethical Certificates **75**

Appendix 2 - Research Presentations **78**

List of Abbreviations

2D – Two Dimensional

3D – Three Dimensional

AR – Aspect Ratio

$Cacl_2$ – Calcium Chloride

CAD – Computer Aided Drawing

CLIP – Continuous Liquid Interface Production

CMC - Carboxymethylcellulose

CVD – Cardiovascular Disease

DLP – Digital Light Photolithography

DNA – Deoxyribonucleic Acid

DSC – Differential Scanning Calorimetry

EDTA – Ethylenediamine Tetraacetic Acid

FDA – Food and Drug Administration

FDM – Fused Deposition Model

FITC – Fluorescein Isothiocyanate

FTIR – Fourier Transform Infrared

GelMA – Gelatin Methacrylate

HA – Hyaluronic Acid

HPMC – Hydroxypropyl Methylcellulose

KOH – Potassium Hydroxide

MN - Microneedle

PBS – Phosphate Buffer Solution

PC - Polycarbonate

PCL - Polycaprolactone

PDMS - Polydimethylsiloxane

PEG – Polyethylene Glycol

PLA – Polylactic Acid

PLGA – Poly (Lactic-Co-Glycolic Acid)

PMMA – Polymethyl Methacrylate

PVA – Polyvinyl Alcohol

PVP - Polyvinylpyrrolidone

PXRD – Powder X-Ray Diffraction

SEM – Scanning Electron Microscopy

SLA - Stereolithography

SLS – Selective Laser Sintering

TBI – Traumatic Brain Injury

UV-Vis – Ultraviolet Visible

WHO – World Health Organisation

List of Equations

$Remaining\ mass\ \% = 100 - (mi - mf/mi \times 100)$ **Equation 4.1** 36

$Water\ Uptake\% = (md - mw/md) \times 100$ **Equation 4.2** 36

$\%EE = (Di - Df/Di) \times 100$ **Equation 4.3** 37

$\%\ release = (DR/DL)\ \times 100$ **Equation 4.4** 37

Qt = $i = 0t$VtCt **Equation 4.5** 38

Qt/A **Equation 4.6** 38

$\%\ Haemolysis =\ (Ra - Sa/Ra)\ \times 100$ **Equation 4.7** 39

List of Figures

Figure 1.1 Schematic diagram of vascular calcification formation within vessel walls created using BioRender.com. 1
Figure 2.1 Schematic diagram of the various non-dermal applications of microneedle arrays to date created using BioRender.com. 7
Figure 2.2 Schematic illustration of the types of microneedle applications used for drug delivery purposes. Reproduced from Rad et al., 2021 under the Creative Commons License. 9
Figure 2.3 Parameters to be considered when designing MN arrays. This image is reproduced from Damiri et al., 2022 under the Creative Commons License. 13
Figure 2.4 Schematic diagram of the three steps of the thermal drawing process. (a-c) contact drawing affecting the aspect ratio of the array, (d-e) body drawing affecting the aspect ratio and needle height and (g-i) tip drawing affecting the sharpness of the apex. This image is reproduced from Lee et al., 2019 under the Creative Commons License. 17
Figure 3.1 *Images of failed alginate polymer MN arrays.* 26
Figure 3.2 *Images of failed chitosan polymer blend MN arrays.* 26
Figure 3.3 Image of selected chitosan (left) and alginate (right) MN array formulations. 26
Figure 4.1 Schematic diagram of the formulation process for the alginate and chitosan microneedle arrays created using BioRender.com. 34
Figure 4.2 *a) SEM image of single needle within the array, and b) fabricated MN array.* ..... **Error! Bookmark not defined.**
Figure 4.3 FTIR spectra of chitosan formulation arrays and pristine polymers. 41
Figure 4.4 FTIR spectra of alginate formulation and pristine powders. 42
Figure 4.5 SEM images of individual alginate needle (A), alginate microneedle array (B), individual chitosan needle (C) and chitosan microneedle array (D). 43
Figure 4.6 *Schematic of the texture analyser setup for measurements of mechanical strength of the MN arrays.* 44
Figure 4.7 Manual penetration test of a) chitosan MN array and b) alginate MN array in agar gel. 45
Figure 4.8 Schematic diagram showing the application of MN arrays to various surfaces mimicking human vessel tissue for penetration ability testing. 45
Figure 4.9 Light microscopy images of penetration testing in Parafilm M layers after a 30 N application force. a) chitosan MN array, all layers, b) chitosan MN array layer 1, c) chitosan MN array layer 2, d) alginate MN array all layers and e) alginate MN array layer. 46
Figure 4.10 SEM images of MN post force application showing needle deformations. 47
Figure 4.11 XRD diffractograms of alginate MN arrays and components (above) and chitosan MN arrays and components (right). 48

Figure 4.12 DSC thermograms of alginate MN formulation and pristine polymers. 49
Figure 4.13 DSC thermograms of chitosan MN formulation and pristine polymers. 50
Figure 4.14 72 hour degradation profile of EDTA loaded alginate and chitosan MN arrays. 51
Figure 4.15 Calibration curve of Fe-EDTA at concentrations 10, 20, 30, 40 and 50 µg/mL. 52
Figure 4.16 schematic diagram providing the process of cross-linking sodium alginate by calcium chloride. 53
Figure 4.17 schematic diagram providing the reversal process of cross-linking sodium alginate by calcium chloride in the presence of EDTA. 54
Figure 4.18 Percentage EDTA released over a 24 hour period in PBS (pH 7.4) at 37 °C. .. 55
Figure 4.19 The diffusion kinetics of EDTA for the alginate and chitosan arrays across excised porcine venous tissue. 56
Figure 4.20 FTIR spectra of tissue samples before and after the permeation study was run. 57
Figure 4.21 Mass of calcium that can be chelated over time based on EDTA release. 58
Figure 4.22 Colour chart used in the detection of heamolysis showing heamolysis as mg/dl. Reused under CC BY-NC-SA 3.0..... 58
Figure 4.23 Centrifuged blood samples showing serum colour for hemolysis assessment a) untreated, b) unloaded alginate array, c) EDTA loaded alginate array, d) pristine EDTA equal to alginate loaded MN array, e) unloaded chitosan array, f) EDTA loaded chitosan array and g) pristine EDTA equal to chitosan loaded MN array. 59

List of Tables

Table 3.1 Results obtained from the preliminary testing of the chitosan formulation 28

Table 3.2 Results of the preliminary alginate formulation testing with a calcium chloride cross-linker 29

Table 3.3 Results of the preliminary alginate formulation testing using a magnesium chloride cross-linker 30

Table 4.1 showing total maximum force as well as force per needle each microneedle array was able to withstand without breakage 45

Table 4.2 *DSC peaks of the pristine powders and their corresponding thermal event* 50

Chapter 1 Introduction and overview of the study

1.1 Background to this study

Blood vessel calcification occurs when calcium and phosphate minerals are deposited within the walls of the vasculature (Schweighofer *et al*., 2016). Whilst previously considered an age-related consequence, it is now understood to be an actively regulated process of a similar nature to bone homeostasis (Wu *et al*., 2013). The three main types of vascular calcification are: calcific aortic valve disease, intimal calcification and medial calcification (Schantl *et al*., 2019). Calcific aortic valve disease involves initial cellular changes of the leaflets to final-stage calcification which results in left ventricular outflow obstruction (Rajamannan *et al*., 2011). Intimal calcification, illustrated in **Figure 1.1**, is the most likely to rupture and is associated with atherosclerosis, leading to obstructed blood flow, acute coronary syndromes and decreased organ perfusion (Schantl *et al*., 2019; Wu *et al*., 2014). Medial calcification occurs within the vascular smooth muscle layer and results in the stiffening of the vessel wall, increasing blood pressure. Increased vessel stiffness is directly linked to a greater likelihood of adverse cardiovascular events and mortality.

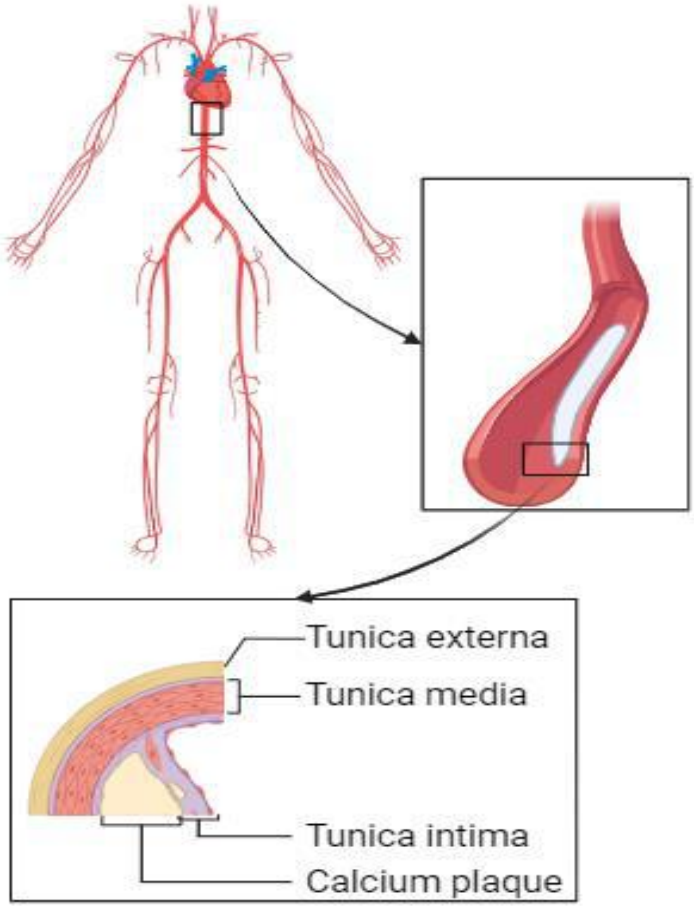


Figure 1.1 *Schematic diagram of vascular calcification formation within vessel walls created using BioRender.com.*

Patients with chronic kidney disease have a greater morbidity of cardiovascular disease compared to individuals with normal renal clearance, and although no single cause has been established, with vascular calcification proposed to have numerous significant contributing factors. (Karamched *et al*., 2019). The presence of medial calcification in particular correlates strongly with the risk of cardiovascular events and amputation in diabetic patients (Lei *et al*., 2013). Vessel calcification may also lead to calcified cerebral embolism, a rare condition that is known to result in more severe cerebral infarctions when compared to other types of embolisms. The cerebrovascular recurrence of such embolism is significant, with 40 % of patients experiencing recurrent stroke (Raghib *et al*., 2018).

Current options to treat calcification mainly include physical mechanisms such as surgical procedures, the most common being rotational atherectomy where a drill-like mechanism is used (Goel *et al*., 2020). Pharmacological interventions such as vitamin K and sodium thiosulfate amongst others are currently under clinical investigation for the treatment of vascular calcification however there is little evidence currently available in literature to support the use of these drugs at this time (Schantl *et al*., 2019). Ethylenediaminetetraacetic acid (EDTA) is a chelating agent with the ability to dissolve and remove the calcium deposits if administered near the site of calcification (Karamched *et al*., 2019). Although Food and Drug Administration (FDA) approval for the use of EDTA to treat vascular calcification has not been granted at this time, an increasing number of cardiovascular disease patients are being treated in this manner (Ibad *et al*., 2016). Typical chelation therapy is administered intravenously and is generally well tolerated however, often leads to a burning sensation at the site of administration (Ibad *et al*., 2016). However, systemic administration of EDTA may lead to adverse effects such as hypocalcaemia, bone resorption, heart failure, hypotension, kidney damage, and bone marrow suppression, limiting its utility (Ibad *et al*., 2016; Karamched *et al*., 2019). These adverse effects represent a significant limitation in the use of EDTA chelation therapy in the treatment of vascular calcification.

Polymeric microneedle arrays have been shown to enhance the efficacy of loaded dosages by increasing tissue permeation as well as allowing for site specific delivery of bioactives (Avcil and Çelik, 2021; Damiri *et al*., 2022). This effect reduces the required effective dose and thus could potentially reduce the possibility of presenting with adverse effects. Polymer based materials have recently been evaluated for MN systems due to them showing improved biocompatibility, biodegradability, minimal toxicity, and cost-effectiveness when compared to previously used materials such as metals and silicon (Damiri *et al*., 2022). MN arrays can be fabricated using a variety of methods including but not limited to 3D printing, etching, laser-mediated and micro-moulding techniques. The selected technique impacts the shape and other physical characteristics of the array and is affected by the type of drug to be incorporated,

required pharmaco- kinetics and dynamics, required dosage and the materials to be used (Damiri *et al.*, 2022).

Recent studies of MN based delivery systems relating to the vascular system are mainly concentrated around the diseases of hypertension, atherosclerosis, and myocardial infarction. These arrays have been used to deliver anti-thrombotic and anti-inflammatory agents as well as therapeutic peptides (R. Zhou *et al*., 2022).

This study proposes to address the need for suitable therapy to treat calcification of vascular tissue by providing a polymeric microneedle array loaded with EDTA for the sustained, local delivery of EDTA for calcium chelation. An EDTA loaded polymeric microneedle array will provide local delivery of EDTA within the affected vessel as well as allow for sustained release. This proposed delivery system allows for diverse application in vessel calcification treatment and will mitigate the risks associated with systemic EDTA use by providing a route whereby EDTA will be delivered to the site of calcification only. Successful treatment of medial calcification could drastically reduce the mortality rate of cardiovascular disease as well as lower the risk of stroke and other neurovascular incidents amongst many population groups but most especially for those with chronic kidney disease and diabetes.

1.2 Rationale and Motivation

Polymeric microneedle arrays allow for the site specific, sustained release of EDTA within calcified vessels in the body while allowing for the usual movement of blood within the affected vessels due to the film like structure of the array, allowing for flexibility to accommodate the curved shape of a blood vessel (Rambhia and Ma, 2015). Polymeric materials have been extensively used as delivery vehicles of a wide-spectrum of drugs (Rafiei and Haddadi, 2019). A few major advantages of these types of materials include longer clearance time, enhanced therapeutic efficacy and reduced toxicity (Sur *et al*., 2019).

Chitosan is a widely available carbohydrate polymer. It has been studied for its properties such as wound healing, hemostasis, biocompatibility, biodegradability, antimicrobial and antifungal activity, as well as many other valuable properties (Badhe *et al*., 2017). Chitosan was utilised in this study due to its biocompatibility, biodegradability and bioadhesivity (Wu *et al*., 2020). Polyvinyl alcohol (PVA) is a commercially significant water soluble plastic and has been frequently utilised in various industries including the food and medical industry. Due to the heightened hydrolysis of the hydroxyl groups within its molecular structure, PVA exhibits qualities of being nontoxic and biodegradable. (Nagarkar and Patel, 2019). Additionally, its hydrophilic nature allows for superior water solubility which proves significant when considering applications in living tissue (Nagarkar and Patel, 2019). Hydroxypropyl

methylcellulose has a great swellability which impacts the drug release profile from a system designed using this polymer creating the ability for controlled release systems (Siepmann and Peppas, 2012). It is hypothesised that by using this combination of polymers will produce a polymeric blend that allows for sufficient mechanical strength of the arrays to penetrate vascular tissue while still being flexible, and allowing for the fabrication of dissolvable needles. The muco-adhesive property of chitosan will aid in ensuring that the MN array remains in place within the vessel.

Alginate is a block copolymer of (1-4)-linked b-D-mannuronic acid with varying proportions and sequential arrangements of its epimer a-L-guluronic acid residues. Sodium alginate is routinely used in the pharmaceutical and biotechnology fields due to its nontoxic, unbranched structure, nonimmunogenic and biodegradable characteristics (Topuz *et al*., 2012). Sodium alginate is frequently crosslinked with divalent calcium ions to form ionic bridges with the guluronic units of alginate to form a network structure with improved mechanical properties (Russo *et al*., 2007). Although polymer based materials generally possess a lower mechanical strength when compared to other materials used for the development of MN arrays, their other advantageous properties make them and enticing prospect for MN development.

When administered near the site of calcification, EDTA has been shown to have the potential to slow down the vascular calcification progress and improve vascular function in calcific disease conditions (Lei *et al*., 2014a). EDTA is a successful chelator of calcium which allows for the breakdown and removal of calcium build ups from the vessel wall and safe transportation out of the body (Lei *et al*., 2014a). EDTA therapy has not been implemented as common treatment for calcification due to the large side effect profile associated with systemic administration. Addressing the unanswered questions of an optimal delivery method, dosing regimen and long term efficacy of EDTA therapy may provide significant insights into developing therapies to combat various calcification-related cardiovascular complications.

The use of a polymeric microneedle array in the delivery of EDTA will minimise the adverse effects of EDTA chelation therapy as the EDTA will be delivered directly to the site of calcification. It has also been shown that EDTA therapy prevents the return of vascular calcification for a time period after the cessation of treatment (Karamched *et al*., 2019). Vessel calcification is of great impact and value particularly in already vulnerable patient groups such as those with chronic kidney disease and diabetes, having a negative effect on patient outcomes. It is therefore of great value to the patient population to find a successful method of treating this calcification before it leads to potential mortality and limb amputations.

1.3 Applications

The polymer blend array will be inserted at site of vascular calcification immediately after surgical intervention at tissue trauma sites for example, neuro trauma (TBI, stroke). The prototype delivery system may also allow for broader application in other sites of vascular calcification treatment to mitigate the risks posed by the use of intravenous (non-targeted) EDTA therapy. Successful treatment of vascular calcification could drastically reduce the mortality rate of CVD as well as lower the risk of stroke and other neurovascular incidents amongst patients afflicted with chronic conditions such as kidney disease and diabetes.

MN arrays have the potential to aid in the delivery and effective dosing of cardiovascular related drugs in a way that provides improved patient outcomes and more rational drug use as they can be dosed site specifically. The MN arrays ability to penetrate membrane barrier allows for enhanced drug permeability to the affected site. Due to the formulations ability to locally deliver drugs the associated side effect profile may be reduced as the drug will avoid systemic interactions.

1.4 Novelty

Formulation of polysaccharide MN arrays: fabrication of a novel polymeric microneedle array for the decalcification of blood vessels using a chitosan polymeric blend and a crosslinked alginate polymeric matrix. The approach presented in this study shows the development of a unique polymeric microneedle array for vascular applications as the materials presented herein have not been applied to vascular MN technology previously.

1.5 Aims and Objectives

This study aims to design and develop polysaccharide formulations for the fabrication of an EDTA loaded dissolvable microneedle patch for the treatment of calcified blood tissue. This was achieved through the following objectives:

1. Formulation of suitable polysaccharides, cross-linkers and/or auxiliary polymers to fabricate an EDTA loaded microneedle array through a mould-based method to obtain two candidate MN patches.
2. Characterisation of the pertinent morphological, physiochemical, mechanical, and penetration properties of the MN patches by SEM, FTIR, Texture Analysis and thermal analysis to ensure design parameters suitability for vascular applications.
3. Evaluation of the *in vitro* drug release and tissue permeation of EDTA loaded MN patches across excised porcine venous tissue using an in-line flow-through

diffusion system to explore the effect of the delivery system on the rate of release as well as the bioactive ability for tissue penetration.

4. Evaluation of the *ex vivo* effectiveness of EDTA via calcium chelation model to verify biological performance.
5. Assessment of the hemocompatibility of the EDTA loaded MNs via hemolysis to ensure biocompatibility.

1.6 Overview of this Dissertation

Chapter 1 of this dissertation presents a background and introduction to the current study by outlining the impact and current treatment failures for vascular calcification. This chapter also focuses on the aim and objectives as well as the potential benefits and rationale of the development of the microneedle arrays presented in this study.

Chapter 2 of this dissertation critically reviews the current available MN formulations that have been designed for vascular and non-dermal drug delivery. This chapter discusses the types of microneedle arrays and the advantages and disadvantages of each type in relation to their desired function. Furthermore, the methods that have been commonly utilised for fabrication of microneedle arrays are outlined herein whilst the materials commonly used are also evaluated.

Chapter 3 of this dissertation outlines the pertinent parameters to be considered during the preliminary phase of the microneedle array fabrication process, particularly for vascular applications. This chapter shows the various methods, polymers, cross-linkers and fabrication methods that were evaluated for the development of the optimised formulation that was tested further.

Chapter 4 of this dissertation explores the fabrication process and assessment of characteristics of the MN arrays. The physiochemical (Differential scanning calorimetry (DSC), X-ray diffraction (PXRD) and Fourier Transform Infrared (FTIR)), morphological (scanning electron microscopy (SEM)) and physicomechanical (water uptake and material strength) properties of the MN array are described. The release and tissue permeability of the bioactive from the two fabricated MN arrays is also evaluated in this chapter and a comparison between the two formulations is presented.

Chapter 5 concludes this thesis, by addressing the limitations and provides recommendations for future use of the MN arrays evaluated in this study.

Chapter 2 Microneedle Fabrication Techniques and Potential Use as a Vascular Drug Delivery System

2.1 Introduction

Microneedles, micron-sized needles with lengths varying from 100 to 1000 μm (Panda *et al*., 2021), were initially developed to effectively deliver drug molecules across tissue barriers such as the skin as a transdermal drug delivery system and have only recently been expanded into drug delivery into other organ systems such as the gastrointestinal tract, the vascular system, and the ocular system as shown in **Figure 2.1** below (Lee *et al*., 2020a, 2014a; Panda *et al*., 2021). Microneedle delivery systems provide a minimally invasive system which possesses the ability to deliver drugs across impermeable membranes (Panda *et al*., 2021). Microneedles can be fabricated using a plethora of materials as well as various methods. Common materials used for microneedle formulation include silicon and other metals, carbohydrate-based materials, and synthetic polymers. Microneedles have been proven to circumvent many known delivery obstacles through the local delivery of the drug, as dosages are reduced and efficacy is maximized (Panda *et al*., 2021).

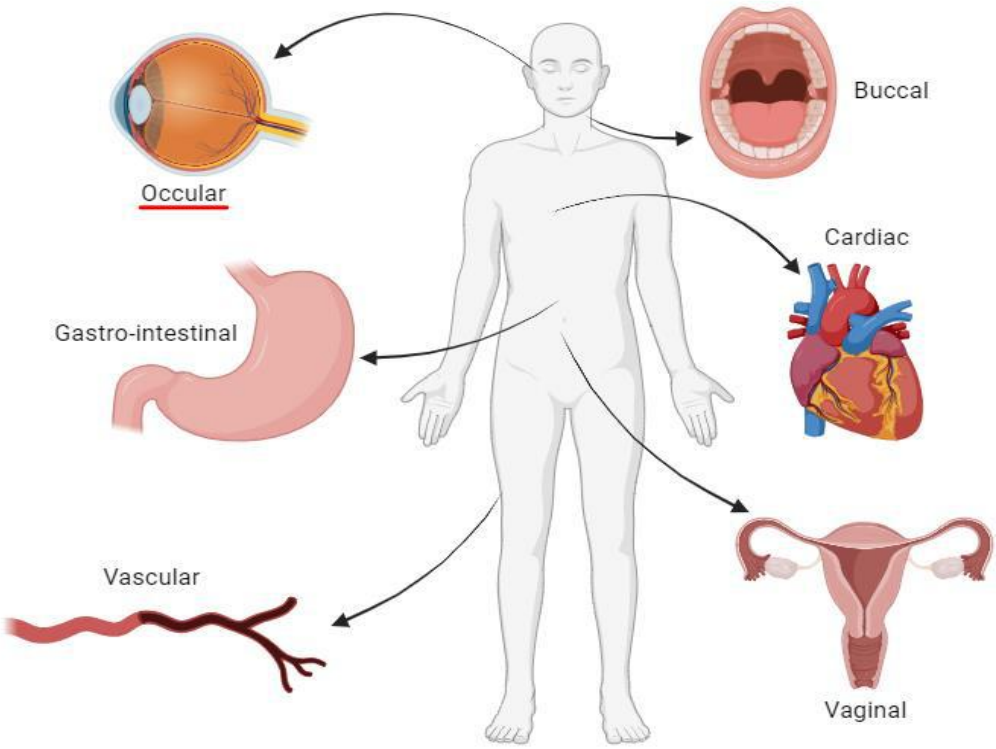


Figure 2.1 *Schematic diagram of the various non-dermal applications of microneedle arrays to date created using BioRender.com.*

2.1.1 Vascular disease and current treatment

Cardiovascular diseases (CVD) are one of the world's leading health threats, causing significant morbidity and mortality (Zhou *et al.*, 2022). Common cardiovascular diseases include; hypertension, dyslipidemia, atherosclerosis, thrombosis and myocardial diseases.

According the World Health Organization (WHO) stroke and ischemic heart disease are the two most prevalent vascular diseases causing the highest global mortality. Alarmingly, in 2012 nearly 17 million people succumbed to a cardiovascular disease related causes (Im *et al*., 2017).

2.1.2 Limitations to vascular treatment

Surgical bypasses using vein or arterial grafting are frequently used for the treatment of coronary and peripheral atherosclerosis, however, this treatment often requires secondary surgery in a large portion of the population due to the likelihood of patients developing restenosis or occlusion at the site of surgery (Choi *et al*., 2012). Many drugs have been investigated to reduce the likelihood of patients developing restenosis or occlusion post-surgery but are limited in their efficacy due to an inability to reach the sight of smooth muscle cell proliferation (Choi *et al*., 2012). Local drug delivery systems for vascular tissue have included the usage of drug eluting stents and cuff like devices that deliver drug to the external wall of the vessel. Drug eluting stents often cause damage to the endothelium post insertion which could lead to the development of restenosis and occlusion whereas cuff like devices mitigate this risk but pose their own difficulties including unpredictable drug distribution (Choi *et al*., 2012). Many side effects of vascular drug delivery are as a result of poorly compatible materials that cause the adhering of platelets and also allows vascular smooth muscle cells to proliferate easily causing restenosis (Jang *et al*., 2019).

2.1.3 Microneedles as vascular delivery system

Endothelial cells have become an interesting potential therapeutic target for molecular interventions. Endothelial cells represent diverse subpopulations and therefore offer characteristics that can be used for targeted drug delivery (Ding *et al*., 2006). Recent advances in microneedle technology has expanded this delivery system away from primarily transdermal delivery systems to a complex system that can be applied in various organ systems including the vascular system (Zhou *et al*., 2022). MN have been investigated for various vascular applications due their wide array of suitable materials and custom designs of physical properties (Lee *et al*., 2020a). MN arrays also allow for targeted delivery of drugs, avoiding first pass metabolism and thus allowing for a reduced dosage which could potentially mitigate many associated side effects of cardiovascular drugs (Panda *et al*., 2021).

This concise review will focus on the various types of microneedles and how these may be used to improve drug delivery to the vascular system as well as what materials would be most suitable to this function. This review aims to evaluate current trends in the field and identify the suitability of microneedle arrays as a delivery system for the vascular system.

2.2 Types of microneedles and their applications

The types of microneedle arrays that can be designed, as shown below in **Figure 2.2**, are; hollow, solid, dissolving, coated and hydrogel-forming needles. Each of these microneedle types has specific methods of formulation, most suitable materials, unique methods of drug delivery and various advantages and disadvantages (Waghule *et al*., 2019).

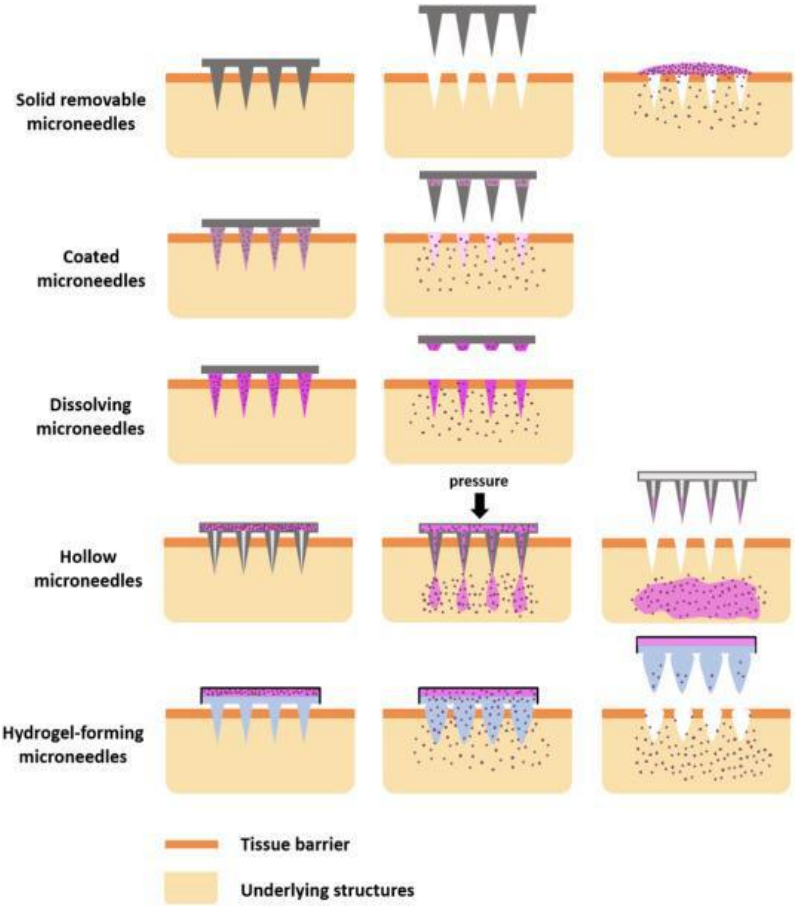


Figure 2.2 *Schematic illustration of the types of microneedle applications used for drug delivery purposes. Reproduced from Rad et al., 2021 under the Creative Commons License.*

2.2.1 Hollow MN arrays and recent application in the vascular system

Hollow microneedles are designed to consist of a cavity of a certain length, usually filled with drug solution, with an oblique angled opening at the tip of the needle (Waghule *et al*., 2019). Hollow microneedles are mainly used for drug delivery and for extraction of interstitial fluid for analysis (Wu *et al*., 2022). Common materials used for the development of these needles include glass, metal, silicon and ceramic. Of these materials silicon offers the most ideal physical properties however, considerable disadvantages are involved including the high

material cost as well as complex fabrication processes (Wu *et al*., 2022). Hollow microneedles are one of the highest costing microneedle type and production requires the use of a pump (Avcil and Çelik, 2021). Hollow microneedles are mainly utilized in protein and other high molecular weight drug molecules delivery and are therefore useful in the administration of vaccines (Waghule *et al*., 2019). This type of microneedle allows for the adjustment of the flow rate of administered drug as well as high dose volumes (Waghule *et al*., 2019). An increased bore size increases the flow rate but could result in a needle array with substantially lower mechanical strength (Waghule *et al*., 2019). Stoeber *et al*. 2000 assessed the injection of fluid through hollow microneedles fabricated via etching and showed that needles 200 µm in height were able to successfully delivery drug 100 µm under the surface of the skin using a chicken thigh model (Stoeber and Liepmann, 2000). Pérennès *et al*. presented a cheaper and more easily accessible method for the fabrication of sharp beveled tip hollow microneedles using X-ray lithography (Pérennès *et al*., 2006). This study eliminated some of the limitations of hollow microneedle synthesis however in terms of vascular applications, there are limited uses for hollow microneedles as a breach in vascular membranes may cause more harm than it does good.

2.2.2 Solid MN arrays and recent application in the vascular system

Solid microneedles are mainly used as a pre-treatment, creating channels in the membrane layer to create improved permeation across the barrier through the passive diffusion mechanism (Damiri *et al*., 2022; Waghule *et al*., 2019). Solid microneedle drug delivery is effected by various considerations including the force of insertion, needle density and needle tip sharpness (Damiri *et al*., 2022). A major disadvantage of solid microneedles involves the sharp waste that they create (Avcil and Çelik, 2021). Li *et al*. used solid microneedles for transdermal delivery and proved that these needles may be inserted multiple times (Li *et al*., 2017). This however is limited to transdermal applications and a single patient as cross-contamination would be detrimental. Another example of solid microneedles would be the work of Narayanan and Raghavan of solid silicon microneedles also utilised in transdermal delivery (Pradeep Narayanan and Raghavan, 2017, 2019). Kundu *et al*. designed stainless steel solid microneedles for delivery of chemicals into plant vascular tissue (Kundu *et al*., 2019). Although this proves useful in plant tissue, it is not feasible in human models as solid microneedles will need to be removed and this would require multiple invasive surgeries.

2.2.3 Coated MN arrays and recent application in the vascular system

Coated microneedles are charcaterised by the presence of a layer of drug solution around the needle structure. The drug system being on the surface of the needles allows for rapid dissolution of drug, however, the amount of loaded drug is dependent on the thickness of the coating and the needle surface available and is usually a minimal amount (Damiri *et al.*, 2022;

Waghule *et al*., 2019). Coated microneedles have been reported for the successful delivery of DNA, peptides and proteins (Damiri *et al*., 2022). The homogenous coating of the surface of the microneedles is an important parameter that needs to be considered during the fabrication process (Damiri *et al*., 2022). The viscosity, surface tension and capillary action of the drug loading solution influences the quality of the microneedle coating, while a more viscous solution with a decreased surface tension may be beneficial these alterations may result in a needle coating only at the tip due to the resultant decrease in capillary action and may negatively affect the penetrating ability of the array due to a decrease in needle sharpness (Baek *et al*., 2017; Chen *et al*., 2017). This tip only coating may be useful when the drug loss from the array substrate is considered. Coated microneedles involve sophisticated layering procedures to prevent loss of integral needle sharpness (Avcil and Çelik, 2021). Several methods have been utilised in the coating of these microneedles including dip coating and spray coating. Li *et al*. showed the possibility for microneedles to be individually coated allowing for co-delivery of multiple drugs within a single array (Li *et al*., 2018). This practice would however be limited by the volume of drug able to be loaded onto the surface of each needle to achieve a therapeutic dose. Tang et al. designed a microneedle patch for the treatment of myocardial infarction whereby the array was then basally coated with hydrogel containing cardiac stem cells for delivery into the damaged cardiac tissue to aid in tissue regeneration, reducing scar formation (Tang *et al*., 2018). Lee *et al*. developed a UV curable microneedle drug eluting balloon for vascular delivery to prevent in stent restenosis. The microneedle array was fabricated, pipette coated with drug (Paclitaxel) and attached to the balloon prior to insertion (Lee *et al*., 2020c). The insertion test performed showed that not only did the array remain attached to the balloon but also that the needles were able to penetrate both the healthy and unhealthy simulated tissue with a deeper insertion depth into the calcified simulated tissue (102 ± 11 μm) than the normal tissue (72 ± 6 μm). Both insertions depth were able to penetrate the endothelium at 10 μm without compromising the integrity of the medial layer at 500 μm (Lee *et al.*, 2020c).

2.2.4 Hydrogel forming/Swellable MN arrays and recent application in the vascular system

Hydrogel forming microneedle arrays are the most recently developed microneedle type. These needles are formulated from highly swellable polymer materials which possess a hydrophilic structure allowing them to uptake a large volume of water into their polymeric network. These needles are used to disrupt the barrier membrane by forming channels between capillary circulation and the drug patch. The needles swell on insertion due to the absorption of interstitial fluid and once swollen they act as a rate controlling membrane (Waghule *et al.*, 2019). Hydrogel-based microneedles are versatile devices which allow for

personalized treatment options owing to their ability to incorporate drugs with different therapeutic windows (Damiri *et al*., 2022). Zhou et al. describes a swelling microneedle array fabricated from crosslinked alginate for transdermal drug delivery (Zhou *et al*., 2022). This study aimed to expand the suitable materials for swellable microneedles. Results showed that optimal array fabrication was dependent on the concentration of cross-linker used as with great crosslinking concentrations, as the needles swell, the excess cross-linker dissolves leaving cavities which cause structural instability to the needle. These arrays were inserted to a depth of 155.33 ± 9.44 µm in porcine skin although florescence imaging using a model drug (FITC) showed drug penetration up to 900 µm into the skin. Lui *et al*. performed a study utilizing GelMA as the material for microneedle synthesis of a biodegradable and swellable microneedle array. This study concurred that crosslinking produced notable effects on the arrays swelling behavior, although a photo-cross linker was used as opposed to the chemical cross linker previously discussed. The swelling ratio of the array was found to be inversely proportional to the crosslinking time with a shorter time corresponding to the highest swelling ratio (Liu *et al*., 2021).

2.2.5 Dissolving MN arrays and recent application in the vascular system

Dissolving microneedles are fabricated using biodegradable polymers with drug encapsulated into the polymer solutions (Waghule *et al*., 2019). It has been shown that dissolvable microneedles are able to successfully deliver both small and large molecules (Demir *et al*., 2013a). Dissolving microneedles involve a once off application only as it is not necessary to remove the needles after insertion, this is an attractive property for vascular drug delivery as it eliminates the need for further invasive surgeries. This type of microneedle allows for controlled release of drug as the polymer encapsulation acts as a regulator of the release rate (Waghule *et al*., 2019). One of the biggest problems faced when developing this type of needle is the adequate distribution of drug within the needles and thus effective drug polymer mixing is a vital step in formulation (Waghule *et al*., 2019). Dissolving microneedles also possess low mechanical strength and therefore have minimal penetration ability as well as only being able to deliver small doses of drug (Avcil and Çelik, 2021). Due to the attractive property of this type of microneedle it is the most common type studied for vascular and other non-dermal applications. Due to the polymeric nature of these dissolvable arrays they allow for alteration to the shape of the traditional array with many studies involving a curved or cuff like device for vascular delivery as this has been shown to reduce the negative impact these devices have on the vasculature (Choi *et al*., 2012; Kim *et al*., 2017; Lee *et al*., 2017, 2014b). Most commonly these vascular delivery systems have been designed for the delivery of anti-proliferation drugs such as sirolimus, paclitaxel and sunitinib to prevent the formation of intimal hyperplasia at sites of tissue injury (Kim *et al.*, 2017; Lee *et al*., 2017, 2014b). The dissolution

time of these dissolvable microneedles can be altered based on the type of polymer used as the polymer hydrophilicity is a rate determining factor in array dissolution (Coyne *et al*., 2017)

Combining types of microneedles could result in more optimal properties being created by utilizing the advantageous properties of one type to enhance the properties of another for example Lee *et al*. performed a study in which drug loading was carried out via a dip coating method but the initial microneedle array was fabricated to be a dissolving needle. Seeing as dissolving needles have a low drug loading ability, dip coated the fabricated array could allow for more drug to be loaded into each array resulting in a higher dosing ability of a dissolvable array (Lee *et al*., 2017, 2014b). Dissolvable microneedles have been shown to have poorer insertion capabilities than solid microneedles and thus Zhu *et al*. fabricated a separating array with both solid and dissolving microneedles to improve tissue insertion (Zhu *et al*., 2016).

2.3 Microneedle fabrication methods and material considerations

Various fabrication methods for microneedle synthesis have been developed and are outlined below. The selection of fabrication technique is based on the required properties of the microneedle system as outlined below in **Figure 2.3** (Damiri *et al*., 2022; Waghule *et al*., 2019). Desired properties to be considered include the drug type for incorporation, the dose required, the necessary needle geometry and materials, pharmacokinetic and pharmacodynamics requirements as well as the target and materials (Damiri *et al*., 2022; Waghule *et al*., 2019).

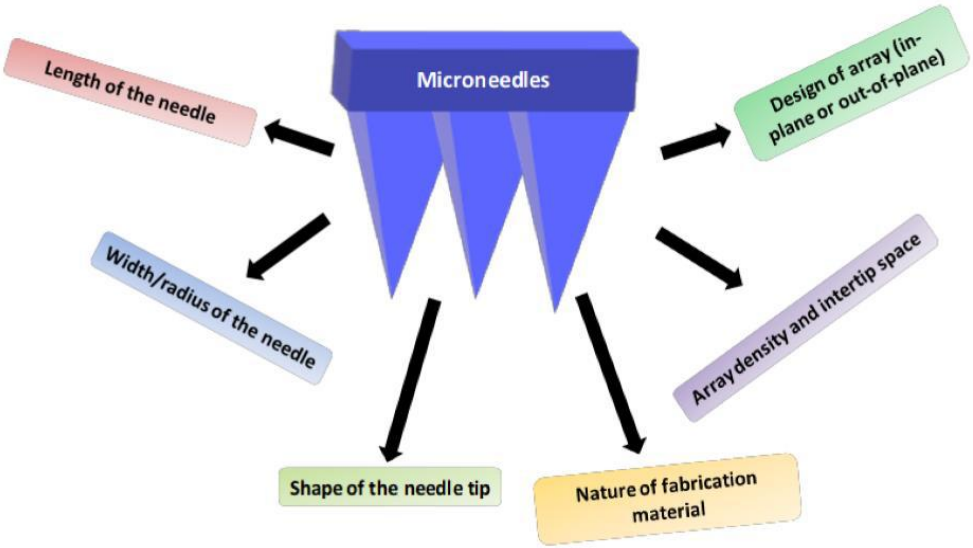


Figure 2.3 *Parameters to be considered when designing MN arrays. This image is reproduced from Damiri et al., 2022 under the Creative Commons License.*

Fabrication techniques can broadly be divided into two main categories, namely, printing based methods and micro-molding based methods.

For vascular drug delivery in particular, the type of material used is of vital importance as blood is a particularly complex body fluid consisting of various proteins and peptides as well as a variety of cells. These various components are integral in several biological pathways such as the inflammatory response and the clotting cascade (Hedayati *et al*., 2019). Many blood contacting medical interventions are administered worldwide, these interventions include stents, heart valves and life support systems (Hedayati *et al*., 2019). Poorly compatible materials result in an inflammatory response within the vessels. This reaction includes the adhering of platelets and the proliferation of vascular smooth muscle cells. This leads to further vessel obstruction and injury. When the risk-benefit ratio deems the use of such materials appropriate, it is necessary to administer pharmaceutics, such as anticoagulants, to manage the risks associated with these materials (Hedayati *et al*., 2019). These therapies involve their own risks and side effects as well as requiring patient compliance and are not 100 % effective (Hedayati *et al*., 2019). It is thus of vital importance to the treatment of vascular diseases to investigate and identify the most compatible materials.

2.3.1 Printing based MN array fabrication techniques

Three of the common printer types utilized in the printing of plastic based materials are selective laser sintering (SLS), fused deposition modeling (FDM), and stereolithography (SLA) (Luzuriaga *et al*., 2018). Each has their own benefits and limitations as discussed below.

2.3.1.1 3D printing techniques

Fused deposition modeling

FDM is a cost effective and flexible method of printing and is suitable to print biocompatible and biodegradable materials such as polyvinyl alcohol and polyacetic acid (Luzuriaga *et al*., 2018). FDM, however possesses a very low resolution in comparison to other printing methods and is therefore not usually capable of printing fine details such as microneedles. Studies have concluded that the main features responsible for the reduction of inflicted pain was the size and amount of needles present in the array with needles of maximum length of 1450 µm, thickness of 100 µm, width of 465 µm, and a tip diameter <75 µm (Kaushik *et al*., 2001). Luzuriaga *et al*. however designed a method using FDM printing combined with a post fabrication etching process that was able to yield successful needles within the above mentioned size range. These needles not only possess the ability to penetrate the skin but also have been designed with a break-away system allowing for the needles to remain embedded in the skin for longer periods of time. PLA was used to synthesize these needles allowing for later degradation via hydrolysis in the skin. This combination method shows great potential for its ability to allow alterations in the parameters of the microneedles when compared to previous methods (Luzuriaga *et al*., 2018). These needles however, showed a

limitation in regards to the length with a minimum needle length of 600 µm. Although this would be acceptable for dermal applications, given the thickness of vascular tissue to optimum penetration depth is approximately 300 µm and as such the limitation of this method would prevent its use in vascular applications.

Stereolithography (SLA) and selective laser sintering (SLS)

SLA and SLS printers are more suitable to the printing of details smaller than 100 µm but are more costly and most of the suitable materials are not biocompatible and thus cannot be used in designing microneedle delivery systems (Luzuriaga *et al.*, 2018). Although SLA is unsuitable for direct applications as a drug delivery system, it has been used to print MN templates which are further designed into master molds for MN fabrication. Krieger *et al*. was able to produce favourable resolution printed needles using this method and a clear resin. This study found that decreasing the layer height parameter when printing improved the surface finish of the fabricated needles (Krieger *et al*., 2019). This method does however show a discrepancy in the input print height and the acquired height of needles which may pose a problem when designing arrays for vascular implementation.

Digital light processing (DLP)

Digital light processing is based on stereolithography and involves the utilization of a projector to develop a cross-sectional image signal of an object into a digital signal which is then introduced into a photosensitive resin for the photo-curing synthesis (Yang *et al*., 2021). Unlike other printing techniques DLP is well suited to creating high resolution, smooth surfaced transdermal microneedles (Yang *et al*., 2021). Yao *et al*. used this technique to fabricate hydrogel based microneedles manufactured from polyethylene glycol diacrylate using a blue light curing step. The fabricated needles possessed a balance between stiffness and precision and it was found that the exposure time to the curing agent was directly linked to the stiffness of the needles with 300 ms being regarded as the optimal curing time for dermal applications (Yao *et al*., 2020).

Continuous liquid interface production (CLIP)

Continuous liquid interface production is a faster and more advanced method of 3D printing process based on the DLP technique (Yang *et al*., 2021). This fabrication method avoids the use of support during the printing process, without which it is possible to reduce and/or eliminate the stair stepping effect without impacting the mechanical properties and fabrication time. This results in an improved surface quality (Yang *et al*., 2021). Johnson *et al*. used this specific type of SLA printing to design square pyramidal microneedles of various heights (1000, 700 and 400 µm) (Johnson *et al*., 2016). This method of fabrication allows for

customizable design of microneedle properties and is fast to print once the CAD design is complete, however, this method like others mentioned requires a UV reactive substance to be used which is often not biocompatible. Johnson *et al*. did demonstrate the printing ability of photopolymerisable derivatives of PEG using this CLIP method as well as PCL, polyacrylic acid and acrylic acid, all of which are FDA approved for medical devices (Johnson *et al*., 2016). It was further shown that these arrays were able to penetrate the skin as well as release drug into the skin however using CLIP as a direct fabrication method for vascular applications may prove more difficult as these polymers are known to have large toxicity profiles and the degradation profiles of these altered derivatives is not well established (Johnson *et al*., 2016). This method may however prove useful in designing PDMS molds for further fabrication as it is highly customizable and faster than many other printing techniques.

2.3.1.2 Lithography based printing

Photolithography

Photolithography is a technique used largely in creating hollow or solid microneedles. Needles are fabricated using an inverse mold method (Damiri *et al*., 2022). Photolithographic techniques are frequently combined with etching techniques (Li *et al*., 2018; Narayanan and Raghavan, 2017, 2019).

Thermal lithography

Drawing lithography, involves the shaping of a viscoelastic polymer into the desired microstructure shape by controlled polymer heating (Lee *et al*., 2010). Thermal drawing processes by nature expose MN materials to high temperatures and therefore it is necessary to monitor any changes in properties due to this thermal exposure, particularly when polymer components are involved (Choi *et al*., 2013).

A common drawing method for needle fabrication which involves heating a polymer above its glass transition temperature, drawing it to the desired height before allowing it to cool and fracturing it at its neck, often results in enlarged two-step tips rather than sharp tips as required for MNs (Choi *et al*., 2012). To avoid this problem a spatially discrete thermal drawing system has been designed, allowing for the controlled heating of the top and bottom sides of the microneedles individually to adequately control needle tip dimensions by drawing to the desired height before cooling. This process has been shown to produce needles of varying heights (200 and 500 µm) (Choi *et al*., 2012) as well as being able to control the shape of the needle tip by controlling the drawing temperature, distance and speed (Choi *et al*., 2013).

Kim *et al*. fabricated a cuff shaped MN array using a thermal drawing method of fabrication and a PLGA polymer base. This method required drug loading via a separate process

(dipping) as the heat needed for the needle formation may interfere with drug properties. Needle shape was controlled by altering the drawing speeds and temperature (Kim *et al*., 2017).

The spatially discrete thermal drawing method as shown below in **Figure 2.4** has been used to produce mainly PLGA needles (Choi et al., 2013, 2012; Kim et al., 2017; Lee et al., 2019, 2014b) and although the method used by Choi et al. was shown to have minimal effect on the polymer crystallinity, this is still a major limitation of this method as alterations to the crystallinity may result in inadequate mechanical properties (Choi *et al*., 2013). PLGA needles

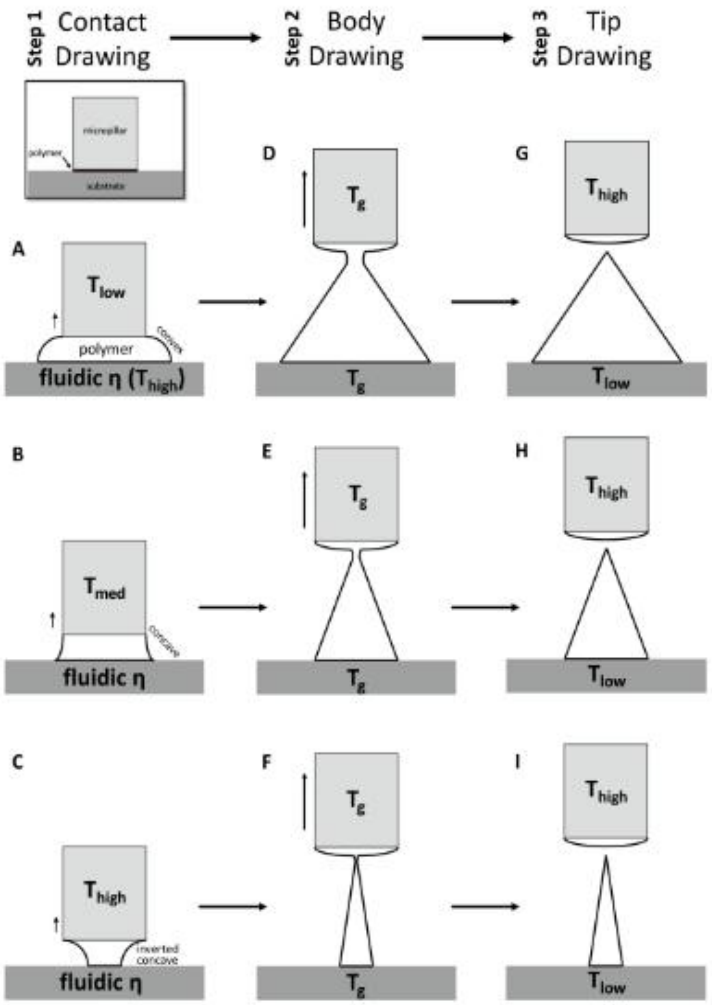


Figure 2.4 *Schematic diagram of the three steps of the thermal drawing process. (a-c) contact drawing affecting the aspect ratio of the array, (d-e) body drawing affecting the aspect ratio and needle height and (g-i) tip drawing affecting the sharpness of the apex. This image is reproduced from Lee et al., 2019 under the Creative Commons License.*

have a limitation in regards to mechanical strength (Lee *et al*., 2014b). The main influence on whether a needle (Rad *et al*., 2021) array could suitably penetrate the vascular tissue is the aspect ratio of the needles. Lee *et al.* performed a study based on the method previously discussed (Choi *et al*., 2013) to test the optimal aspect ratio of needles. Needles with aspect

ratios (AR) of 1.5, 3.5 and 7.0 were tested via an insertion test and the results showed that lower AR needles although able to penetrate the tissue, resulted in large tissue damage not suitable to vascular delivery while higher AR arrays were unable to adequately penetrate the tissue. It was found that arrays with an AR of 3.5 was suitable for penetration while minimizing the tissue damage making this most suitable for vascular delivery (Lee *et al*., 2014b).

2.3.1.3 Etching based printing

Etching is a process whereby material is removed from an already existing scaffold or wafer to create a controlled and specific geometry. Stoeber and Liepmann used a combination method of fabrication using photolithography and two types of etching. This method was able to produce sharp tipped hollow needles with a height of 200 µm and a lumen diameter of 40 µm (Stoeber and Liepmann, 2000). Yang and Zahn used a reactive ion etching system to design silicon microneedles which were then used to assess the effect of vibrational force on needle insertion properties (Yang and Zahn, 2004). This system of etching uses a chemically reactive plasma to remove specific material from the surface of an existing wafer until the desired shape is created. Another variety of etching processes is the wet etching process. This process involves the use of KOH as the etching material (Wilke *et al*., 2005). Shakya *et al.* fabricated stainless steel microneedles using a wet etch process, these microneedles were fabricated to be 700 µm in height and each array contained 57 individual needles (Shakya *et al*., 2019).

2.3.1.4 Laser mediated printing

The laser cutting method is mainly utilized in fabricating polymer based or metal microneedles. A computer aided design system is utilized in designing the correct orientation and dimensions of the microneedles. The needles are cut by the laser in a 2 dimensional (2D) form onto a metal sheet and then bent at 90º to create a 3 dimensional (3D) structure (Damiri *et al*., 2022). Banks *et al*. used a laser cutting technique to fabricate stainless steel microneedles for transdermal applications using an infrared laser. The fabricated needles were 750 µm in length, had a base width of 180 µm and a less than 1 µm tip diameter (Banks *et al*., 2010). Martanto *et al*. used a similar method and produced arrays of 105 needles with a base dimension of 50 by 200 µm, and a height of 1000 µm (Martanto *et al*., 2004). Due to these needles being synthesized from stainless steel they would not be an ideal candidate for vascular drug delivery as they may cause vascular irritation and will also require surgery for implantation as well as removal. Laser ablation is a similar laser technique utilized frequently in the fabrication of polymer or metal based microneedles. This technique, unlike laser cutting, engraves the plate into 3 dimensional microneedle plates (Damiri *et al*., 2022). Nejad *et al*. used a CO_2 laser ablation technique to fabricate microneedle molds. This study used a specific 2D geometric pattern of lines traced by the laser, these lines overlapped at certain points and

due to this the laser passed over these points more frequently resulting in a greater depth of ablation. These overlapped areas are what created the needle geometry in the mold (Nejad *et al*., 2018).

2.3.2 Micro-molding based method of MN array fabrication

Micro-molding techniques are far more common in the microneedle field as they are less costly, reproducible and simpler to fabricate than printed needles (Lee *et al.*, 2020a). Molding techniques do however have the disadvantage of being difficult to customize MN properties and alter needle parameters. Many mold based methods incorporate some form of printing in the development of the master mold but this process is a once off rather than a continuous method of production.

2.3.2.1 Solvent casting

The process of solvent casting involves dissolving of the required medium into solution which is filled into the mold then allowing the solvent to evaporate leaving behind a film like solid. This method is popular with many polymeric scaffolds and has also been frequently used to fabricate biocompatible microneedle arrays. Solvent casting is most frequently utilized when fabricating with polymer materials such as alginate (Bonfante *et al*., 2020; Guimarães *et al*., 2022; Zhang *et al*., 2018a), PVP (Su *et al*., 2023), hyaluronic acid, cellulose derivatives (Bonfante *et al*., 2020), PVA and PLGA (Arsalan Abu-Much *et al*., 2022).

Amongst the research reviewed for this paper it was shown that alginate is frequently used for solvent casting methods, however pure alginate lacks the mechanical strength required for needle penetration into the skin and therefore various measures have been taken to circumvent this shortcoming such as crosslinking (Zhang *et al*., 2018b; Zhou *et al*., 2022) or combination polymer solutions (Guimarães *et al*., 2022).

Zhang *et al*. was able to successfully fabricated MN made of alginate however stable needles possessing adequate strength was only possible when crosslinking was combined with the addition of another polymer with crosslink only arrays showing significant shrinkage in comparison to the mold as well as not possessing the mechanical strength to penetrate the skin (Zhang *et al*., 2018b). Zhou *et al.* looked at the different gelling methods for alginate based formulations and resulted in a similar conclusion, alginate crosslinked with Ca^{2+} showed irregular formation but when combined with another gelling agent, in this case D-(+)-glucono-1,5-lactone, the arrays were uniformly structured with little crinkling and shrinkage (Zhou *et al., 2022)*.

Bonfante *et al.* demonstrated the comparison between various polymers and concentrations using a PDMS mold technique. Polymers evaluated in this comparison were alginate,

hyaluronic acid and carboxymethyl cellulose. MN arrays were evaluated based on physical structure, in particular the tip sharpness, and piercing ability. This study showed promising results for HA and CMC however the alginate arrays were found to be brittle and had a poor needle structure (Bonfante *et al*., 2020).

These studies all show signs of alginate being a poor candidate for MN synthesis without alteration, however alginate is frequently used for vascular drug delivery due to its compatibility and ability to contain and deliver sensitive molecules like proteins (Gu *et al*., 2004) Although alginate MN have not been very successful in the past this polymer is of interest for vascular drug delivery as it possesses the ability to encapsulate and deliver proteins and other sensitive molecules (Gu *et al*., 2004).

Arsalan *et al*. and Lee *et al*. both used PLGA but of varying ratios (80:20 and 50:50). Arsalan *et al*. used a straightforward casting-mold technique by casting a PLGA solution onto a PDMS mold and kept overnight, this method produced quadrangular pyramid needle tips with a flexible back due to the addition of glycerol as a plasticizer (Arsalan Abu-Much *et al*., 2022). These arrays were able to withstand a force of 20 N applied by patients required for dermal insertion. *Lee et al*. used a silicon mold but a more complex fabrication method using multiple steps including etching, deposition and lithography. Arrays produced had variable heights 480, 640 and 780 µm (Lee *et al*., 2017).

PVP and PVA are also frequently used in mold based microneedle synthesis (Coyne *et al*., 2017; Su *et al.*, 2023; Tang *et al*., 2018). Su *et al*. used PDMS molds and a PVP solution and then loaded with a drug. Coyne *et al*. used a combination of PVP and PVA and a PDMS mold for the fabrication of microneedles. Tang *et al.* used PVA alone to produce polymer based needles. PVP has been approved and used as a plasma volume enhancer for trauma victims and PVA is frequently used for scaffolds and grafts due to its biocompatibility (Coyne *et al.*, 2017). PVA and PVP combination needles produced needles with a height of 600 µm, a base width of 200 µm and a tip diameter of 10 µm, these measurements were used as they have showed a low aspect ratio that has been proven to improve mechanical strength. The needles were able to withstand a compressive force of approximately 5.6 N (Coyne *et al*., 2017). PVA only needles had a mechanical strength of 2 N per needle in the array and dimensions of 600 µm (height), 300 µm (base width) and 5 µm (tip diameter). PVP alone needles, were not evaluated for mechanical strength or formulated dimensions but the mold used had a needle height of 300 µm and a base width of 300 µm (Coyne *et al*., 2017).

Mold based fabrication methods have a wider variety of suitable materials which is of great significance when looking at vascular applications of microneedle arrays as the vascular

system is highly sensitive and requires special precaution to be taken when introducing foreign bodies.

2.4 Conclusion

Although many types of microneedles have been created for different dermal applications, not all of these are suitable for vascular applications as the vascular system is an internal body system without easy access. This nature of vascular tissue largely rules out the usage of solid and hollow microneedles. It is evident from current trends in literature that although printing methods provide a new avenue of microneedle fabrication which could allow easier alterations to a design, the precision offered and materials suitable for such are often not suitable to vascular delivery. Mold based microneedle fabrication techniques are far more adaptable in terms of the materials that can be used and are therefore more likely to be able to be used to fabricate microneedles for vascular applications.

Overall, microneedles provide an interesting newly developing field to be explored for the progression and advancement of the treatment of vascular diseases with the potential to enhance patient outcomes and reduce the immense disease burden cardiovascular diseases currently possess.

Chapter 3 Formulation and design of microneedle arrays for vascular applications

3.1 Introduction

Microneedles can be easily and vastly modified via the use of different materials and fabrication methods to acquire detailed and specific needle structures to suit their wide variety of applications. Features such as needle height and diameter, array size, needle pitch and needle aspect ratio can all be altered to ensure optimal needle structure for drug delivery (Lee *et al*., 2019).

Various MN technologies have been proposed for the adequate delivery of therapeutic agents in the vascular system. Many of these are to address intimal hyperplasia or for the more precise delivery of current therapeutics such as beta blockers (Zhou *et al*., 2021). It has been found that a greater degree of flexibility is required for vascular delivery than is for dermal delivery due to the curved nature of the blood vessels and tissue structures (Lee *et al.*, 2017). Vascular MN delivery also has a more limited material base, as it is unlikely that non-degradable substances be placed into the vasculature as they would require additional invasive surgery to be removed. The vascular system is also particularly sensitive to foreign material due to the white blood cells causing immune response and therefore the materials used for these MN arrays have to be very carefully selected.

3.2 Formulation Considerations

When fabricating an implantable microneedle array, material considerations are of vital importance as the materials utilised need to be of sufficient mechanical strength to form microneedles as well as be safe for use in tissue without significant negative biologic response such as inflammation or apoptosis. The type of microneedle to be developed also has a significant impact on material selection as each type of needle has specific requirements and fabrication techniques that cannot be met by all materials, for example materials that are thermo-sensitive cannot be utilised in many printing techniques as the exposure to heat required by the method would potentially alter the chemical properties and material strength of the selected polymer (Choi *et al*., 2012; Lee *et al*., 2019).

Most frequently the microneedles used for implantation devices are polymers due to the need for these devices to dissolve and not need to be removed or to create medical sharp waste (Indermun *et al*., 2014). These polymers are either natural or synthetic with natural polymers being used more frequently. Commonly used natural polymers include carbohydrate based polymers such as well as derivatives of cellulose including carboxmethylcellulose (CMC) which have been utilised in the fabrication of degradable or coated MNs (Cholkar *et al*., 2017).

Other common polymers used for MN fabrication include chitosan, hyaluronic acid (HA), alginate, silicon, polyvinyl alcohol (PVA), polyvinylpyrrolidone (PVP). A polymers biocompatibility is evaluated based on its ability to mitigate the body's immune response to a foreign body presence. Due to the nature of the array sought to be designed in this study (vascular) the material consideration is of great significance as the blood carries immunoresponsive materials and would therefore be quick to react to foreign bodies. Polymethyl methacrylate (PMMA) and polycarbonate (PC) have been shown to restrict the foreign body response and therefore have been utilised in many medical disciplines despite their synthetic nature (Cholkar *et al*., 2017).

Drug loading of microneedles can be done via various mechanisms. One common method is the incorporation of drug molecules directly into the microneedle material matrix (Huang *et al.*, 2022). The method of drug incorporation chosen is influenced by the type of materials to be used in the fabrication process, the type of drug to be loaded, type of release profile required and the fabrication method.

Although individual polymers may not always provide the exact physical properties needed for MN fabrication, often a combination of polymers and other additives may be used to enhance the physical properties of the resultant polymer blend (Calori *et al.*, 2020; Cholkar *et al*., 2017). Auxiliary polymers may be added for numerous functionality reasons such as plasticizing agents, viscosity enhancers or additional compressive and tensile strength (Calori *et al*., 2020; Cholkar *et al*., 2017). Microneedles particularly for vascular drug delivery are required to be flexible as they need to be able to be fitted to the cylindrical shape of the vessel wall whether applied perivascularly or intravascularly.

In light of these considerations, the polymers selected for further testing were, sodium alginate, low molecular weight chitosan, polyvinyl alcohol and hydroxypropyl methylcellulose. Sodium alginate has been frequently used for biomedical applications due to its, non-toxic, biocompatible, non-immunogenic, and antimicrobial properties. Chitosan is the most abundant natural occurring polymer possessing, biocompatible, biodegradable and nontoxic characteristics. Although chitosan is sensitive to water its pKa of 6.5 makes it practically insoluble at body pH allowing for a controlled release system to be designed. The biggest disadvantage of using natural polymers to design scaffold-like structures such as microneedles is the lack of mechanical properties that these materials possess. It is for this reason that additional polymers and cross-linkers were evaluated. PVA and was chosen to enhance the mechanical properties of chitosan as it exhibits good mechanical strength and biocompatibility. Both PVA and HPMC are hydrophilic polymers which was hypothesised to

increase the solubility of the chitosan scaffold within body tissue to allow for degradation to occur (Calori *et al*., 2020).

3.3 Materials

Biopolymers and pharmaceutical materials comprising of sodium alginate, polyvinyl alcohol (PVA) (MW=89,000-98,000 g/mol), chitosan (low molecular weight, 30 cp, 1 wt. % in 1 % acetic acid (25 °C, spindle LV1 Brookfield)(lit.) and hydroxypropyl methylcellulose (HPMC) (Mw=806.937 g/mol), were procured from Sigma-Aldrich (Missouri, USA). Ferric chloride dehydrate, ethylenediaminetetraacetic acid (EDTA) disodium and calcium chloride hexahydrate was procured from LabChem (Founder's hill, Johannesburg, SA). Microneedle (MN) moulds (patch size 8x8 mm, array 10x10, needle pitch 500 µm, height 300 µm, base 100 µm) were purchased from DLD Scientific (Durban, South Africa), manufactured by MicroPoint Technologies (Singapore).

3.4 Design Concepts and Prototyping

As discussed in the previous chapter, microneedles can be fabricated using a variety of methods that each possess their own advantages and disadvantages. For this study it was determined that the most suitable method for fabrication on a small scale for prototyping would be a micro-moulding approach as this is a simple method with pre-developed moulds of varying specifications that allow for use of a variety of polymer bases without requiring significant method redevelopment. With the micro-moulding fabrication technique, the selected mould is largely responsible for the geometry of the resultant microneedle arrays and thus it is of vital importance to select a suitable mould size and shape.

Parameters that need to be considered when designing a microneedle array include specification of the needle geometry which includes the needle height and aspect ratio as well as the needle pitch and shape (Johnson *et al.*, 2016). These geometries are determined by the mould dimensions and therefore needed to be considered before selecting the most appropriate mould for this study. The needle height along with the strength of the material determines the penetration depth of the microneedle array. With regards to dermal insertion the needle height influences the pain inflicted with needle heights <1000 µm demonstrating painless insertion (Demir *et al.*, 2013a). This, however, is not as influential of a factor for vascular delivery with more emphasis being placed on the needle size that minimizes the tissue damage as well as the specific layer of vascular tissue to be targeted.

Vascular tissue ranges in thickness from 1500 to 40 µm depending on the type and location of the vessel (Camasão and Mantovani, 2021). In order to minimize tissue damage it would

be best for microneedles to not penetrate entire vessel structures as this could cause micro-bleeds as well as a loss of vessel integrity (Lee *et al*., 2021, 2017). For this reason, the needle height needs to be carefully selected based on the chosen vessel for application. As bioactive molecules could diffuse through tissue layers the ideal height for microneedles for drug delivery into the medial layer of vascular tissue may not necessarily have to penetrate the medial tissue layer. It was thus decided that a microneedle of height 300 µm was a suitable size mould to utilize for the prototyping undertaken in this study.

In order to find the most suitable formulation and method of fabrication various polymer blends and concentrations were tested as outlined in the tables below. The sodium alginate and chitosan MN array formulations were optimised separately.

The chitosan formulation was altered in the concentrations of the various solutions as well as whether dissolution should take place individually, prior to combination or if polymer powders should be mixed before dissolution.

Different cross-linkers were evaluated for the cross-linking of sodium alginate at varying concentrations to establish the most appropriate cross-linking system, as described in the table below. The cross-linkers tested were calcium and magnesium, both divalent ions.

3.5 Results and Discussion

From the preliminary study conducted it was evident that a HPMC concentration of 3.75 %, although soluble, was too viscous to be homogeneously combined with other polymers whereas the 7.5 % HPMC was not fully solubilised. The 6 % chitosan solution was difficult to solubilise and created a resultant polymer solution too viscous to be filled into the silicon mould effectively which caused malformed microneedle arrays with barely any tip formed. Intermediate concentrations of chitosan also showed poorly formed arrays with many samples tearing or having holes when removed from the mould as seen in **Figure 3.1**and

Figure *3.2*. The higher concentrations of PVA caused an increase in rigidity of the resultant microneedle array, and although this may have been reduced when introduced into a biologic simulated environment and water uptake took place, these arrays were deemed unsuitable due to a lack of initial flexibility when removing the array from the mould as well as when evaluated via a mechanical forceps bending test. Findings from this initial study are summarised in **Table 3.1** below.

These results led to the lowest concentrations for each polymer being chosen for further studies.

The MN array produced from only sodium alginate was poorly formed with shrinkage occurring in the mould and needle tips that were bent or non-existent. This led to the consideration of potential cross-linkers to enhance the physical properties of the sodium alginate. The cross-linkers chosen for investigation were both divalent ions, calcium and magnesium chloride shown in **Table 3.2** and **3.3**.



Figure 3.1 *Images of failed alginate polymer MN arrays.*



Figure 3.2 *Images of failed chitosan polymer blend MN arrays.*



Figure 3.3 *Image of selected chitosan (left) and alginate (right) MN array formulations.*

The biggest challenges faced in the design of these microneedle arrays in this study was the development of a polymer solution that was able to produce MN arrays with significant strength and flexibility while maintaining a low enough viscosity that allowed for successful filling of the entire microneedle mould. Another challenge encountered was the selection of the

microneedle size as this determines the aspect ratio of the array. The penetrating ability of the resultant array is highly dependent on the aspect ratio as a very high aspect ratio has been shown to cause needle bending or buckling whereas a low aspect ratio prevents insertion into tissue as the needles are not long enough to reach the desired tissue depth. In further stages of the development process, it was necessary to ensure that the microneedle arrays produced are of a suitable strength for tissue insertion.

Table 3.1 Results obtained from the preliminary testing of the chitosan formulation

Chitosan concentration %(w/v)	**PVA concentration %(w/v)**	**HPMC concentration %(w/v)**	**Results**
1.5	0.75	1.88	Well-formed and flexible MN array
		3.75	HPMC not well incorporated
		7.5	HPMC concentration too high for solubility
	1.5	1,88	Slightly stiff
		3.75	Slightly stiff and HPMC not fully incorporated
		7.5	HPMC concentration too high for solubility
	3	1.88	Slightly stiff array
		3.75	Slightly stiff array with HPMC not fully incorporated
		7.5	HPMC concentration too high for solubility
3	0.75	1.88	Flexible but not well defined needles
		3.75	HPMC not well incorporated
		7.5	HPMC concentration too high for solubility
	1.5	1,88	Needles not well defined
		3.75	HPMC not well incorporated
		7.5	HPMC concentration too high for solubility
	3	1.88	Needles not well defined and array slightly stiff
		3.75	HPMC not well incorporated
		7.5	HPMC concentration too high for solubility
6	0.75	1.88	Chitosan too concentrated for needle formation
		3.75	Chitosan too concentrated for needle formation
		7.5	Chitosan too concentrated for needle formation
	1.5	1,88	Chitosan too concentrated for needle formation
		3.75	Chitosan too concentrated for needle formation
		7.5	Chitosan too concentrated for needle formation
	3	1.88	Chitosan too concentrated for needle formation
		3.75	Chitosan too concentrated for needle formation
		7.5	Chitosan too concentrated for needle formation

Table 3.2 Results of the preliminary alginate formulation testing with a calcium chloride cross-linker

Cross-linker concentration (% w/v)	Alginate concentration (% w/v)	Observations
0.5	1	Cross-linking too weak; array shrunk upon drying
	2	Cross-linked but still low viscosity for mould filling
	4	Uneven cross-linking; solid parts and non-cross-linked sections
	6	Solid hydrogel too stiff for MN casting
1	1	Slightly uneven crosslinking but solution too thick for pouring in mould
	2	Uneven cross-linking; solid parts and non-cross-linked sections
	4	Uneven cross-linking; solid parts and non-cross-linked sections
	6	Solid hydrogel too stiff for MN casting
2	1	Uneven cross-linking; solid parts and non-cross-linked sections
	2	Uneven cross-linking; solid parts and non-cross-linked sections
	4	Uneven cross-linking; solid parts and non-cross-linked sections
	6	Solid hydrogel too stiff for MN casting
4	1	Uneven cross-linking; solid parts and non-cross-linked sections
	2	Solid hydrogel too stiff for MN casting
	4	Solid hydrogel too stiff for MN casting
	6	Solid hydrogel too stiff for MN casting
6	1	Solid hydrogel too stiff for MN casting
	2	Solid hydrogel too stiff for MN casting
	4	Solid hydrogel too stiff for MN casting
	6	Solid hydrogel too stiff for MN casting

Table 3.3 *Results of the preliminary alginate formulation testing using a magnesium chloride cross-linker*

Cross-linker Concentration (% w/v)	**Alginate concentration (% w/v)**	**Observations**
0.5	1	Cross-linking too weak; array shrunk upon drying
	2	Cross-linking too weak; array shrunk upon drying
	4	Cross-linking too weak; array shrunk upon drying
	6	Cross-linking too weak; array shrunk upon drying
1	1	Cross-linking too weak; array shrunk upon drying
	2	Cross-linking too weak; array shrunk upon drying
	4	Cross-linking too weak; array shrunk upon drying
	6	Cross-linking too weak; array shrunk upon drying
2	1	Shrinkage
	2	Uneven crosslinking; shrinkage
	4	Solidified but parts still not crosslinked
	6	Solidified but parts still not crosslinked
4	1	Solidified but parts still not crosslinked
	2	Solidified but parts still not crosslinked
	4	Solidified but parts still not crosslinked
	6	Solidified but parts still not crosslinked
6	1	Solidified but parts still not crosslinked
	2	Solidified but parts still not crosslinked
	4	Solidified but parts still not crosslinked
	6	Solidified but parts still not crosslinked

3.6 Conclusions

In conclusion, through various pre-formulation tests and evaluations, the two most promising polymer blend formulations were identified for further exploration and characterisation based on the MN arrays ability to be fabricated, removed from the mould as a completed array as well as enduring a forceps bending test without breakage. These formulations consisted of a) chitosan, HPMC and PVA blend with respective polymer concentrations of 1.5 % w/v, 1.875

% w/v and 0.75 % w/v and b) 2% w/v sodium alginate based solution cross-linked with a 0.5 % w/v calcium chloride solution. These selected formulations displayed good flexibility as well as well-formed and sharp needle tips. Additionally, this stage of development allowed for the determination of a specific size of MN array which was suitable to the vascular system, ensuring uniformity of design in subsequent stages.

Chapter 4 Comparative Analysis of EDTA-Loaded chitosan and alginate microneedle arrays for calcium chelation in vascular calcification

4.1 Introduction

Blood tissue calcification involves the deposition of calcium and phosphate minerals, predominantly within blood vessel walls, impacting cardiovascular health (Schweighofer *et al.*, 2016). Formerly viewed as an aging-related process, it is now recognized as actively regulated, akin to bone homeostasis (Wu *et al*., 2014). Vascular calcification manifests in three forms: intimal, medial, and aortic valve calcification (Schantl *et al*., 2019). Intimal calcification, associated with atherosclerosis, poses a risk of vessel rupture, leading to acute coronary syndrome and reduced organ perfusion (Schantl *et al.*, 2019; Wu *et al*., 2014). Medial calcification stiffens vessel walls, raising blood pressure and heightening the risk of adverse cardiovascular events and mortality (Lei *et al*., 2013; Shioi *et al*., 2020). Aortic valve calcification, ranging from sclerosis to stenosis, represents a progressive disorder (Freeman and Otto, 2005).

Notably, chronic kidney disease patients are particularly vulnerable to cardiovascular morbidity due to vascular calcification (Karamched *et al*., 2019). Additionally, vascular calcification may lead to calcified cerebral embolism, with a significant recurrence rate of recurrent strokes (Raghib *et al*., 2018). Current treatment options, including surgical interventions and pharmacological agents like vitamin K and EDTA, aim to address vascular calcification (Goel *et al*., 2020; Schantl *et al*., 2019). However, EDTA chelation therapy, while showing promise, presents significant side effects when administered systemically (Ibad *et al*., 2016). Targeted drug delivery approaches offer a potential solution to mitigate these adverse effects, providing hope for improved treatment outcomes in vascular calcification management (Lei *et al*., 2014b).

Microneedle arrays have been shown to be a local delivery system which enhances drug permeability in a minimally invasive manner (Lee *et al*., 2019). As explored in Chapter 2 of this dissertation, recent advances in the field have expanded the technology to be utilised in various tissues and for many disease states (Lee and Prausnitz, 2018; Lee *et al*., 2019). These recent advances have included the development of MN arrays specifically for vascular drug delivery applications, focused mainly on intimal hyperplasia reduction however, the benefits of MN technology expands beyond this and could offer and interesting potential for targeted drug delivery to sites that are considered difficult to reach (Choi *et* al., 2013, 2012; Lee *et al*., 2019).

In this study, two natural biodegradable polymer based MN arrays loaded with EDTA as a model bioactive, supported by previous literature in the field (Lei *et al*., 2014b; Najjar *et al*., 2004) were fabricated, for the potential to treat vascular calcification. In the study it has been shown that these polymers are capable of forming well defined MNs with suitable mechanical properties for vascular drug delivery. It was also shown that these arrays were not harmful to the blood system and did not cause excessive apoptosis of red blood cells and in fact appeared to reduce the hemotoxicity of EDTA. The loaded bioactive was shown to be released from both arrays and permeated porcine venous tissue adequately.

4.2 Methods and Materials

4.2.1 Materials

Biopolymers and pharmaceutical materials comprising of sodium alginate, polyvinyl alcohol (PVA) (MW=89,000-98,000 g/mol), chitosan (low molecular weight, 30 cp, 1 wt. % in 1 % acetic acid (25 °C, spindle LV1 Brookfield)(lit.) and hydroxypropyl methylcellulose (HPMC) (Mw=806.937 g/mol), were procured from Sigma-Aldrich (Missouri, USA). Ferric chloride dehydrate, ethylenediaminetetraacetic acid (EDTA) disodium and calcium chloride hexahydrate was procured from LabChem (Founder's hill, Johannesburg, SA). Phosphate buffered saline (PBS) tablets were procured from Rochelle Chemicals (Electron, Johannesburg, SA). Human whole blood was collected into heparin anticoagulation tubes, from healthy volunteers (ethical clearance number: M180978). Microneedle (MN) moulds (patch size 8x8 mm, array 10x10, needle pitch 500 µm, height 300 µm, base 100 µm) were purchased from DLD Scientific (Durban, South Africa), manufactured by MicroPoint Technologies (Singapore).

4.2.2 Methods

4.2.2.1 Chitosan microneedle fabrication

A chitosan (1.5 % w/v in acetic acid 1 % w/v), HPMC (1.825 % w/v in deionized water), PVA (0.75 % w/v in deionized water) blend was prepared in a 1:1:1 ratio. Each polymer was dissolved separately and then combined to ensure homogeneity. Microneedle arrays were synthesized using a mold based technique whereby 200 µl of the polymer solution blend was cast into a predesigned silicon mold (patch size 8x8 mm, array 10x10, needle pitch 500 µm, height 300 µm, base 100 µm) and left to dry for 48 hours at 25 °C.

4.2.2.2 Alginate microneedle fabrication

A calcium chloride (0.5 %w/v in deionized water) cross-linked alginate solution (2 % in deionized water), prepared in a 1:2 ratio. The mixture was vortexed to ensure homogeneity and complete crosslinking. Microneedle arrays were synthesized using a mold based technique whereby polymer solution blends were cast into a predesigned silicon mold (patch

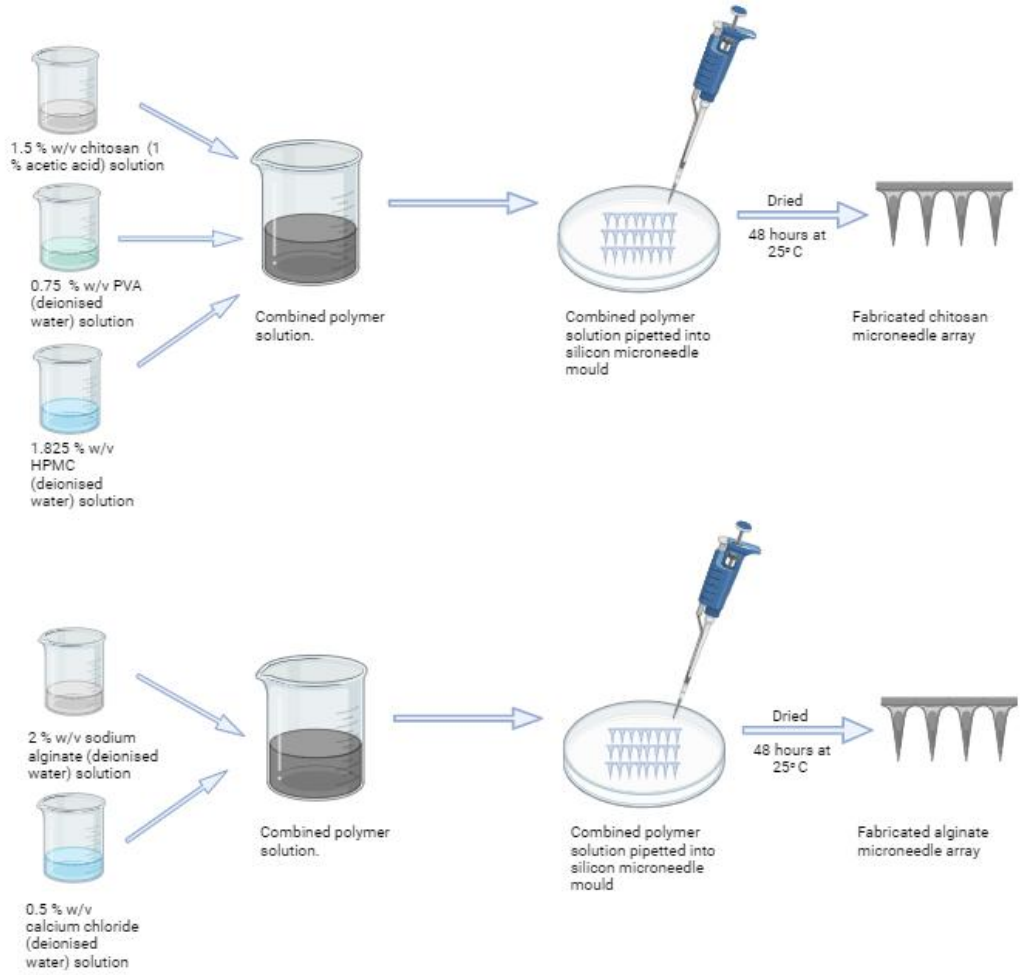


Figure 4.1*Schematic diagram of the formulation process for the alginate and chitosan microneedle arrays created using BioRender.com.*

size 8x8 mm, array 10x10, needle pitch 500 µm, height 300 µm, base 100 µm) and left to dry for 48 hours at 25 °C. The concentration and volume of calcium was optimized to produce a crosslinked polymer of appropriate viscosity for both mechanical strength and mold filling.

4.2.2.3 Characterisation of the Fabricated Microneedle (MN) Array using Fourier-Transform Infrared Spectroscopy (FTIR)

FTIR analysis was conducted using a Spectrum 100 FTIR Spectrometer (Perkin-Elmer, Beaconsfield, BUCKS, UK) to confirm the synthesis of the MNs. Determination of functional groups present in the resultant formulation provides an insight into the potential properties

possessed by the MN array. FTIR was performed on the pure polymers as well as the MN formulations to establish its chemical functional groups. Samples were processed at a resolution of 4 cm^{-1} and were analysed at wave numbers ranging from 650-4000 cm^{-1}.

4.2.2.4 Evaluation of the surface morphology of the MN array using optical Microscope and Scanning Electron Microscopy (SEM)

The surface morphology and characteristics were evaluated using Scanning Electron Microscopy (SEM) (FEI Quanta 400F (Hillsboro, OR, USA)). Morphological analysis allows for an evaluation of the detailed needle structure which impacts the penetrating ability of the arrays. Samples were gold/palladium-coated for 30 s with an SPI-Module Sputter Coater (SPI Supplies, Division of Structure Probe Inc., West Chester, PA, USA) while being mounted on the aluminium stub, prior to analysis.

4.2.2.5 Assessment of the physicomechanical properties of the MN array using Texture Analysis

Mechanical strength of the MNs was determined using a Texture Analyser (TA.XT.*plus Texture Analyser*, Stable Microsystems®, Surrey, UK). An arrays mechanical strength determines the force which can be applied to its surface before bending/breaking occurs. This force needs to be greater than the required application force in order for successful application to occur. A microneedle array was placed on the flat rigid surface of a stainless-steel base plate. An axial force was applied using a cylindrical probe 2 cm in diameter, perpendicular to the axis of the microneedle. The force was measured when the moving sensor touched the uppermost point of the microneedle array. The force-distance graph obtained from evaluations yielded the maximum force required for deformation of the MN. A pre-test speed and post-test speed of 0.5 mm/s was employed. A trigger force of 0.049 N with a load cell weight of 5 kg was used for all tests. A target mode of 10 % strain was used. These test parameters emulate the application force to be applied during surgery.

4.2.2.6 X-Ray diffraction analysis to determine crystallinity of the MN Array

Powder X-Ray diffraction (PXRD) was employed to detect any changes in crystallinity on a X-Ray Diffractometer (Rigaku Miniflex 600, Rigaku Corporation, Matsubara-cho, Akishima-shi, Tokyo, Japan). The dry samples were analysed under a continuous scan mode at 15 °/minute (Wang, 1994; Guirguis *et al.,* 2012) over the diffraction angle range 5–90 ° (2Ɵ).

4.2.2.7 Determination of the thermal behaviour of the MN array using Differential Scanning Calorimetry (DSC)

Thermal analysis of the MN was undertaken employing a Temperature Modulated or Advanced DSC (TMDSC/ ADSC) (Mettler Toledo DSC-1 STARe System, Schwerzenback, ZH, Switzerland) to assess the thermal behaviour of the formulation. The thermal transitions of pure EDTA, chitosan, HPMC and PVA were compared. Samples (2-12 mg) were accurately weighed into standard 40 µL aluminium open pans, hermetically closed and pierced. Samples were then heated from 0-300 °C. The pans were ramped at 10 °C/min between a temperature gradient of 0-300 °C under a constant purge of an inert N_2 atmosphere (100 mL/min). Using differential scanning calorimetry (DSC) system, the glass to rubber transition of MN base materials, delta Cp and melting peak, were investigated. These properties affect the structural integrity of the array and are therefore essential to consider in the fabrication process.

4.2.2.8 Determination of *in vitro* degradation

Microneedle samples were prepared as per the fabrication method in 4.2.2.1 and 4.2.2.2 and weighed prior to being incubated in a shaker bath in phosphate buffer solution (pH 7.4) for various intervals (72, 48, 24, 16, 8 and 1 hours) at 37 °C. The samples were removed at the required time point and centrifuged at 15000 rpm for 5 minutes. The supernatant was then removed and remaining sample was left to dry for 48 hours before being weighed. The percentage degradation was calculated by $Remaining\ mass\ \% = 100 - (\frac{m_i - m_f}{m_i} \times 100$**)** **Equation 4.1** below:

$$Remaining\ mass\ \% = 100 - (\frac{m_i - m_f}{m_i} \times 100) \quad \textbf{\textit{Equation 4.1}}$$

Where m_i is the initial dry mass of the sample in milligrams and m_f is the final dry mass of the sample in milligrams.

4.2.2.9 Determination of *in vitro* water uptake

Microneedle arrays were individually weighed before being placed into 10 ml of PBS (pH 7.4) for various intervals after which the samples were removed, blotted dry on filter paper and reweighed. The change in weight was used to determine the percentage water uptake by the array as calculated by $Water\ Uptake\% = \frac{m_d - m_w}{m_d} \times 100$ **Equation 4.2** below:

$$Water\ Uptake\% = \frac{m_d - m_w}{m_d} \times 100 \quad \textbf{\textit{Equation 4.2}}$$

Where m_d is the dry mass of the sample in milligrams and m_w is the mass of the sample at maximum water uptake state in milligrams.

4.2.2.10 Drug loading and encapsulation via ferric UV-Vis spectrophotometry

To calculate the amount of EDTA in the formulation, an Ultraviolet Visible (UV-Vis) spectrophotometric analysis was conducted.

A MN sample was weighed and then dissolved in 5 mL of a 0.1 M HCl. Concentration of EDTA was assessed using UV-Vis spectroscopy (UV-Visible Spectrophotometer, Varian GmbH, Austria) at wavelength λ=272 nm and compared to a calibration curve. Entrapment efficiency was calculated using $\%EE = Di - DfDi$**×100 Equation 4.3** below,

$$\%EE = \frac{Di - Df}{Di} \times 100 \quad \textbf{\textit{Equation 4.3}}$$

Where Di is the theoretical drug loaded (micrograms) and Df is the entrapped drug evaluated from the calibration curve (micrograms). A calibration curve was established by dissolving a range of known quantities of EDTA (10 – 50 µg/ml), complexation with a 0.5 mg/ml $FeCl_3$solution (0.1 M HCl) and analysing the results on UV-vis (λ=272 nm).

4.2.2.11 Determination of EDTA release from MN formulations

The drug release percentage of the EDTA bioactive was evaluated using a flow cell diffusion apparatus (PermeGear 7-in-line flow-through diffusion system, PermeGear, Hellertown, USA) with a flow rate of 1.5 ml/hour to mimic the effect of *in vitro* blood flow. MN arrays were placed within the cell and the donor compartment was filled with PBS (pH 7.4) to prevent sample drying. The apparatus was run over a 24 hour period at 37 °C, with samples of 3 ml (volume) being collected for evaluation at 2 hourly intervals. Samples were then quantified by utilizing UV-Vis spectrophotometry.

Percentage release was calculated via $\% release = \frac{D_R}{D_L} \times 100$ **Equation 4.4** below:

$$\% release = \frac{D_R}{D_L} \times 100 \quad \textbf{\textit{Equation 4.4}}$$

Where D_R is the quantity of EDTA released and D_L is the quantity of EDTA encapsulated in the formulation.

4.2.2.12 Collection and storage of venous porcine tissue

An ethics waiver for the approved use of porcine skin was obtained from the University of the Witwatersrand School of animal, plant and environmental sciences (19-05-2022-O*) (Appendix*

1). The porcine venous samples were harvested from animals euthanized for other purposes at the central animal unit at the University of the Witwatersrand Medical School. Porcine tissue was selected as the porcine model is the most frequently used model for *in vitro* permeation studies due to is anatomical similarity to human tissue (Albl et al., 2016).

After collection, porcine tissue was immediately placed in phosphate-buffered saline (PBS) (pH 7.4) solution and transported to the laboratory within an hour. Excess fat and connective tissue were removed, and the specimen were cut into strips. The prepared tissue strips were then placed into cryovials, snap frozen in liquid nitrogen (-195 °C) and stored at -70 °C. Any samples showing signs of any disease or damage that may influence results was removed from the study. The process of cryopreservation is a process in which organelles, cells and tissues are preserved by cooling to extremely low temperatures (Jaiswal and Vagga, 2022). This process is widely used for the permeability analysis. Studies have shown that the process of cryopreservation increases the flux of the preserved tissue and therefore has been a method to preserve tissues for permeability analysis (Jaiswal and Vagga, 2022; Keane et al., 2015).

4.2.2.13 Determination *ex vivo* tissue permeation of EDTA from MN arrays using flow diffusion cells

The tissue permeation of the EDTA bioactive was evaluated using a flow cell diffusion apparatus (PermeGear 7-in-line flow-through diffusion system (exposed area 0.039 cm^2, PermeGear, Hellertown, USA) with a flow rate of 1.5 ml/hour. MN arrays were placed onto the porcine venous tissue sample (1 cm^2) within the cell and then the donor compartment was filled with PBS (pH 7.4) to prevent sample drying. The apparatus was run over a 24 hour period at 37 °C, with samples of 3 ml (volume) being collected for evaluation at 2 hourly intervals. Samples were then quantified by utilizing UV-Vis spectrophotometry.

The cumulative amounts of EDTA that diffused across the tissue were calculated by using $Qt = \sum_{i=0}^{t} VtCt$ ***Equation 4.5*** below:

$$Qt = \sum_{i=0}^{t} VtCt \quad \textbf{Equation 4.5}$$

Where Qt is the cumulative quantities (ng), t (min) is the time period, Vt is the volume (ml) of the sample at t and Ct is the concentration of the sample (ng/mL) at t.

Cumulative curves were constructed using the cumulative quantities at each time point per unit of skin surface area exposed (0.0397 cm^2), ***Qt/A Equation* 4.6** below.

$$Qt/A \quad \textbf{Equation 4.6}$$

The linear portion of the cumulative graphs were then analysed further to determine the Steady state fluxes ($Flux_{ss}$) via linear regression and the lag time to reach steady state (x-intercept) values.

To ensure tissue integrity was maintained throughout the experiment run, FTIR was run, as described in section 4.2.2.3, on the freshly thawed tissue sample as well as the tissue sample immediately post experiment. The various bands of the pre and post test runs were compared to evaluate the effect that the test process had on the tissue samples.

4.2.2.14 *Determination of in vitro* hemocompatibilty

Samples were placed in 1 ml of fresh human whole blood and incubated for one hour before blood was centrifuged at 15000 rpm for 15 minutes to prepare serum samples. Serum samples were analysed via UV-vis for the absorbance of hemoglobin (wavelength λ=570 nm). The change in absorbance values were recorded and compared with control to determine the percentage increase in hemolysis using $\% \, Hemolysis = \frac{R_a - S_a}{R_a} \times 100$ **Equation 4.7** below:

$$\% \, Hemolysis = \frac{R_a - S_a}{R_a} \times 100 \quad \textbf{\textit{Equation 4.7}}$$

Where R_a is the absorbance value of the control (untreated blood sample) and S_a is the absorbance value of the sample.

4.2.2.15 Statistical analysis

The experimental data was analysed by one-way analysis of variance (ANOVA) and two-way ANOVA and post hoc tests, or with Student's t-test for a direct comparison of two groups. All tests were run in triplicate. Statistical tests were done using GraphPad Prism 10 software.

4.3 Results and Discussion

4.3.1 Fabrication of microneedles (MN) arrays

Chitosan and alginate were selected as the main polymer components in the formulation of these MN arrays due to their biocompatible and biodegradable properties. Both these polymers are naturally found polymers and are therefore more suitable for biologic applications. These polymers, however, were found to have a lack of mechanical strength which prevented needles from being formed and removed without damage from the silicon mold. In this light, HPMC and PVA were added to the chitosan formulation for their advantageous properties as described in the previous chapter and a calcium chloride cross-linker was added to the alginate formulation to create stronger polymer blends for improved

needle formation seen in **Figure 4.2**. As shown in **Figure 4.1**, individual polymers were dissolved in their respective solvents before being combined. It was then that EDTA was added, and the final solutions cast into the silicon molds. These polymer blends were created in larger volumes than were required for individual arrays as only 200 µl was required per mold.

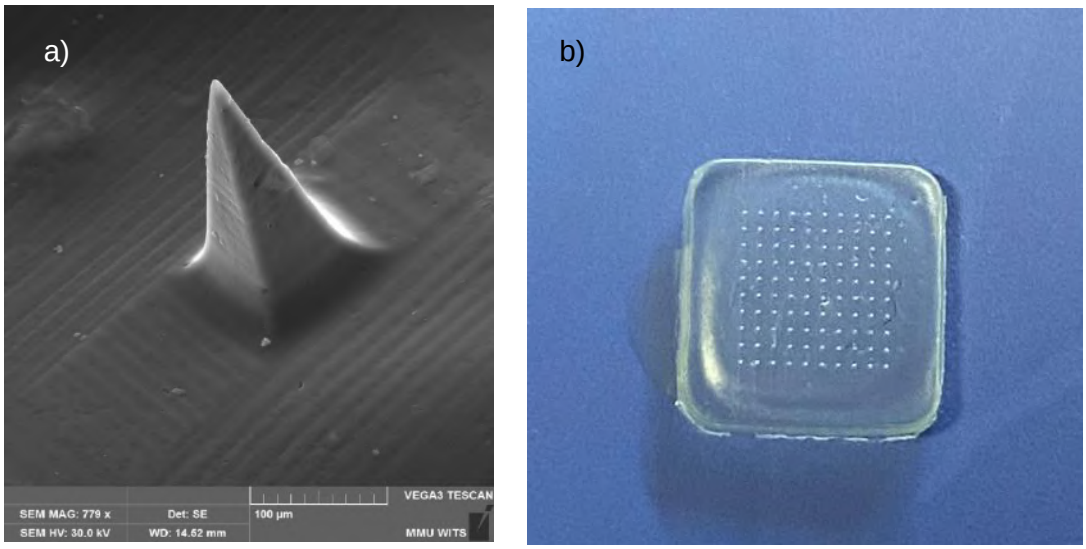


Figure 4.2 a) SEM image of single needle within the array, and b) fabricated MN array.

4.3.2 Polymer characterization by Fourier Transform Infrared Spectroscopy (FTIR)

In **Figure 4.3**, the FTIR spectra for chitosan showed characteristic bands at wavelengths 3285 cm^{-1} (N─H stretching), 2870 cm^{-1} (C─H stretching), residual N-acetyl groups were confirmed by bands at 1649 cm^{-1} (C═O stretching of amide I), 1313 cm^{-1} (C─N stretching of amide III) and 1560 cm^{-1} (N─H bending of amide II) 1374 cm^{-1} (C─H deformations), 1150 cm^{-1} (asymmetric stretching of the C─O─C bridge) and 1023 cm^{-1} (C─O stretching) as previously reported by literature (Queiroz *et al*., 2015).

The spectrum for HPMC in **Figure 4.3** revealed bands at 3425, 1372, 2895 and 1051 cm^{-1} which corresponded to O─H stretching, O─H bending, C─H stretching and C─O stretching, respectively.

PVA spectrum seen in corresponded with findings from (Mansur *et al*., 2008) with peaks being observed at 2907 cm^{-1} (alkyl C─H stretching), 3281 cm^{-1} (O─H stretching), 1714 cm^{-1} (C═O stretching of the acetate group) and 1087 cm^{-1}.

EDTA disodium characteristic peaks as reported by (Baykal and Toprak, 2007 and Lanigan and Pidsosny, 2007) at 3519 cm^{-1} and 3379 cm^{-1} corresponding to O─H and N─H stretching, respectively and peaks at 1671 and 1610 cm^{-1} showing the free carboxylic acid groups.

Sodium alginate FTIR spectrum revealed bands at 3240 cm^{-1} (O─H stretching), 1594 and 1406 cm^{-1} (symmetrical and asymmetrical carboxylic salt stretching, respectively) and 1050 cm^{-1} (C─O stretching).

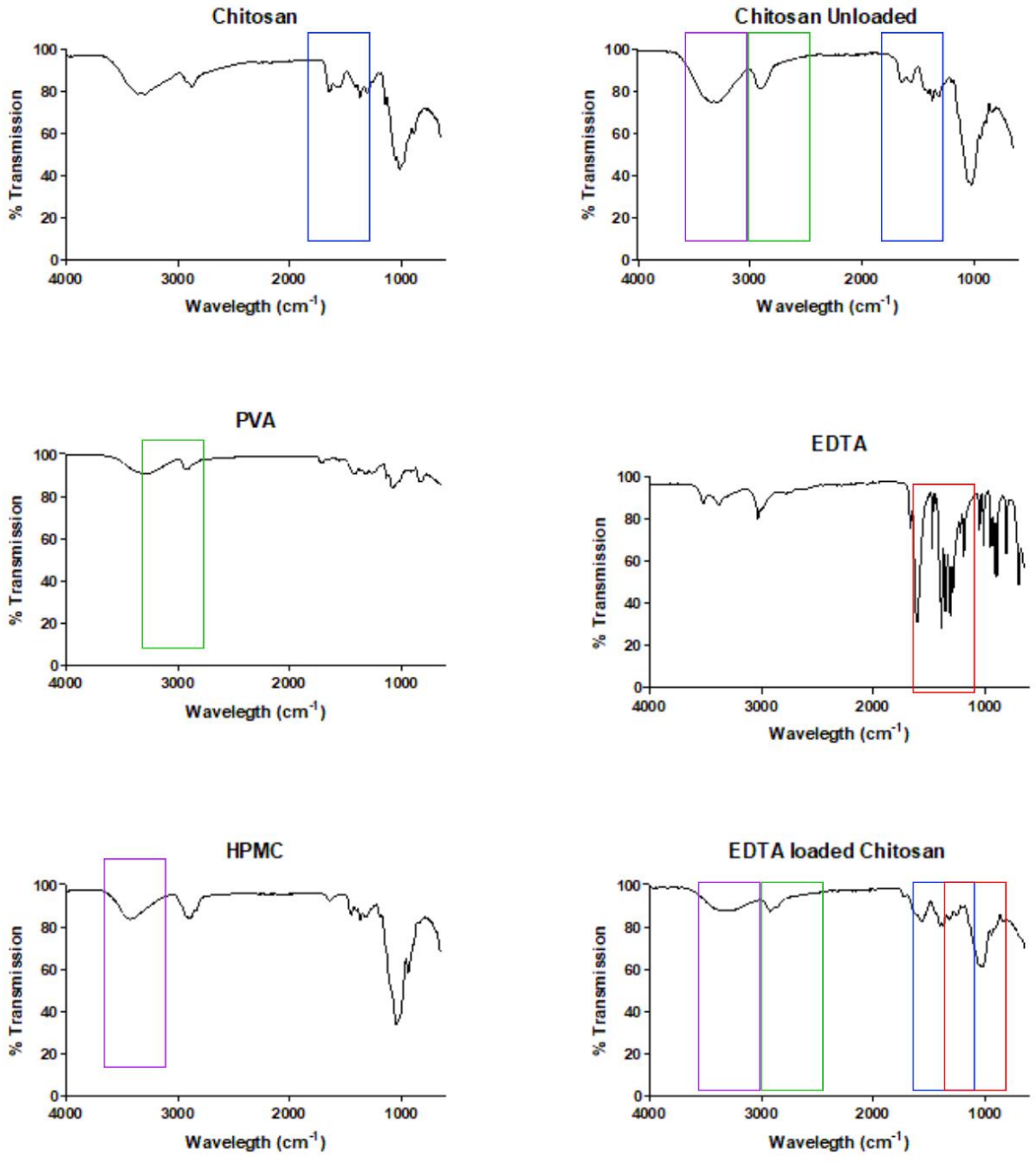


Figure 4.3 *FTIR spectra of chitosan formulation arrays and pristine polymers.*

Upon investigation of the FTIR spectra as shown in **Figure 4.3** for the chitosan MN array formulations and its components before and after combination and the addition of EDTA it was shown that whilst resembling the spectrum for the main parent polymer (chitosan) molecular changes did occur that can be contributed to the addition of the other polymers. Unloaded chitosan blend arrays display a broad peak at 3344 cm^{-1} owing to the O─H stretching of the HPMC moiety, 2915 cm^{-1} as a result of the C─H stretching of the PVA moiety and a peak at 1651 cm^{-1} indicating residual N-acetyl groups from the chitosan moiety. Additionally, EDTA loaded chitosan arrays display an increased intensity of peak 1578 cm^{-1} due to the EDTA interaction (COO^-) (1400 cm^{-1}) at the NH_3+ site (1600 cm^{-1}) of the chitosan moiety (Singh *et al.*, 2012).

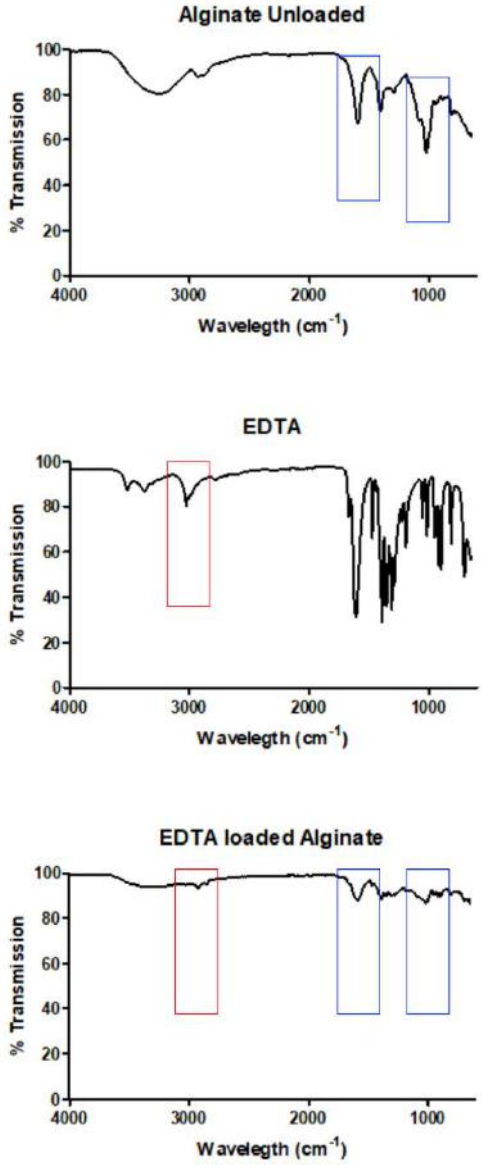


Figure 4.4 *FTIR spectra of alginate formulation and pristine powders.*

Upon examination of the FTIR spectrum for the alginate MN formulation before and after crosslinking shown in **Figure 4.4** it is evident that a change at the molecular-level occurred in response to the crosslinking process. From the two spectra, the most notable distinction observed is an intense absorption band shift of the -COO- groups, which have shifted from 1594 cm^{-1} to 1610 cm^{-1} and from 1406 cm^{-1} to 1407 cm^{-1}. Additionally, there is a broadening and reduction in intensity, as depicted in **Figure 4.4**. This implies a robust interaction between Ca^{2+} and the carbonyl bond (C=O) in the carboxyl functional groups of alginate, confirming the successful crosslinking. A notable similarity was reported by (Li *et al.*, 2016) wherein a crosslinked alginate network was produced by an interaction Ca^{2+} to evaluate the effects of

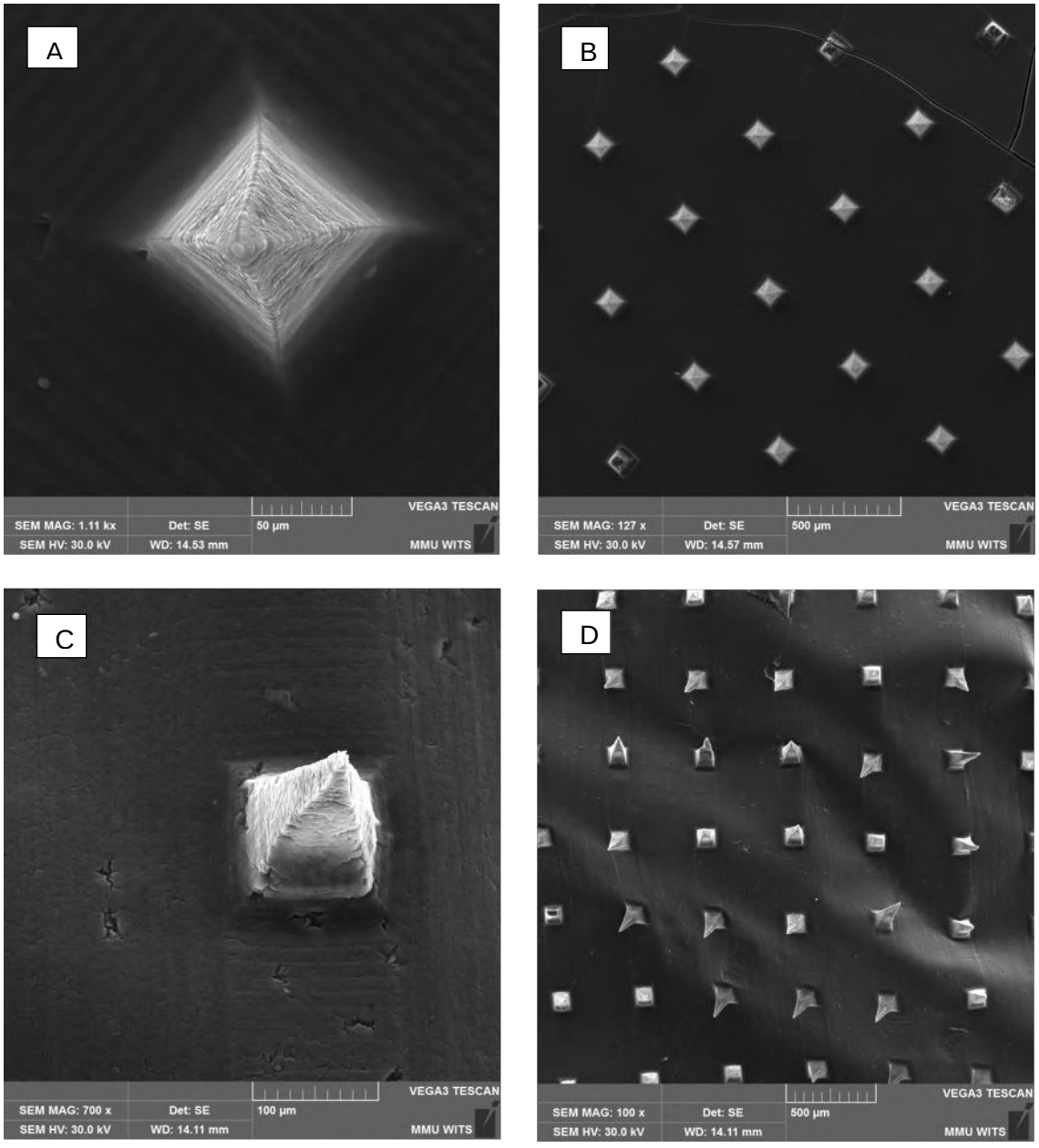


Figure 4.5 SEM images of individual alginate needle (A), alginate microneedle array (B), individual chitosan needle (C) and chitosan microneedle array (D).

calcium concentrations on the gelation process of alginate films. EDTA loaded sodium alginate arrays display a new peak at 3028 cm^{-1} as a contribution from the EDTA moiety. These features are indicative of successful incorporation of EDTA.

4.3.3 Examination of MN array using Scanning Electron Microscopy (SEM)

SEM images revealed well defined and formed square-based pyramidal needles with sharp tips to allow for easier penetration into vessel layers without causing significant tissue trauma and injury (Lee *et al*., 2020a). The uniform structure of both the alginate (**Figure 4.5** B) and the chitosan (**Figure 4.5** D) arrays demonstrates optimal mold formulation. The uniformity of materials within each individual needle as pictured in **Figure 4.5** A and C, demonstrates successful blending and drug incorporation within the formulation process. Furthermore, the SEM images verified the presence of sharper tips and a smoother surface for the alginate arrays.

4.3.4 Texture Analysis evaluation of the MN array

The penetrating ability of microneedle arrays is of paramount importance when designing a drug delivery system of this nature (Demir et al., 2013b). In order for successful penetration of dermal tissue to take place microneedle arrays are required to possess a strength equivalent to between 0.08 and 3.04 N per needle (Lee *et al.*, 2020d; Zhu *et al*., 2016). Texture analyser data for all synthesized arrays showed in **Table 4.1** above, that all needle arrays were able to withstand sufficient force per needle without any breakages being observed upon scanning electron and light microscopy. This demonstrates that all arrays possess a mechanical strength required for insertion into the blood vessel wall.

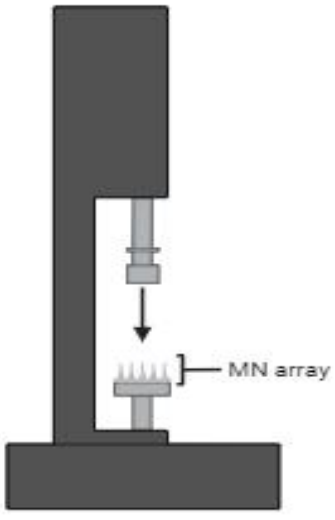


Figure 4.6 *Schematic of the texture analyser setup for measurements of mechanical strength of the MN arrays*.

Table 4.1 *showing total maximum force as well as force per needle each microneedle array was able to withstand without breakage*

	Total max force (N)	Force per needle (N)
Chitosan MN with EDTA	33.847	0.338
Chitosan MN with no EDTA	33.694	0.337
Alginate MN with EDTA	34.492	0.345
Alginate MN with no EDTA	34.516	0.345

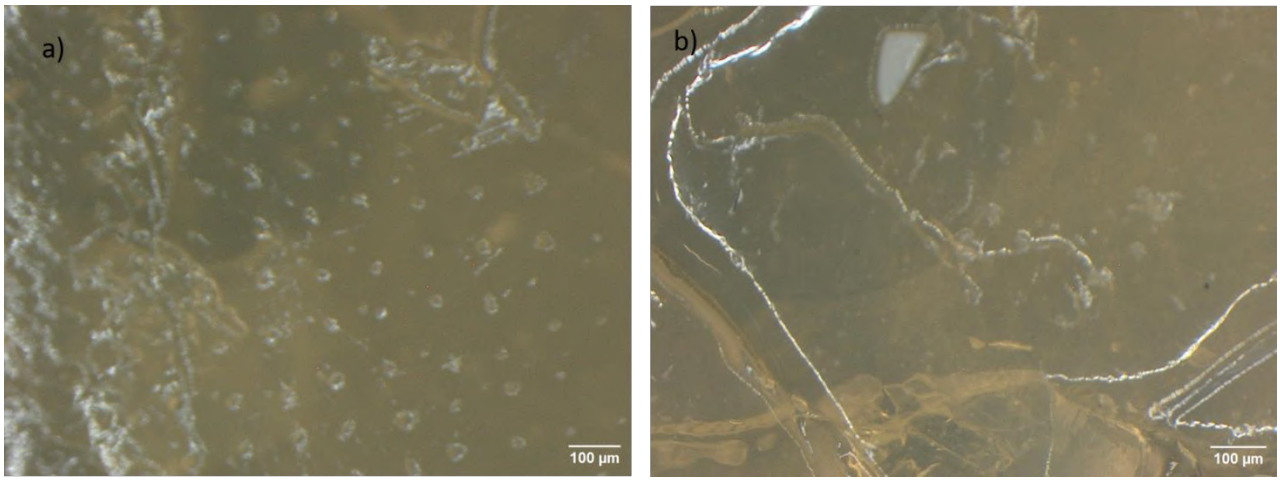


Figure 4.7 Manual penetration test of a) chitosan MN array and b) alginate MN array in agar gel.

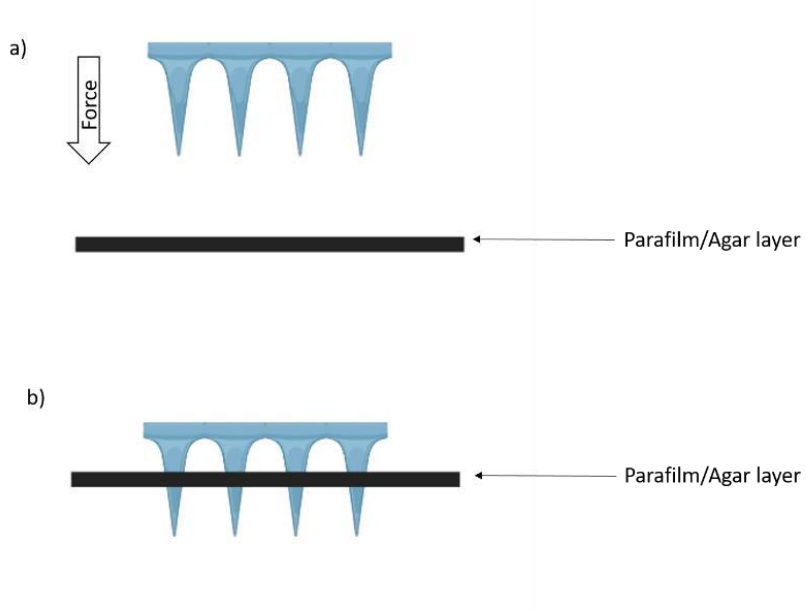


Figure 4.8 *Schematic diagram showing the application of MN arrays to various surfaces mimicking human vessel tissue for penetration ability testing.*

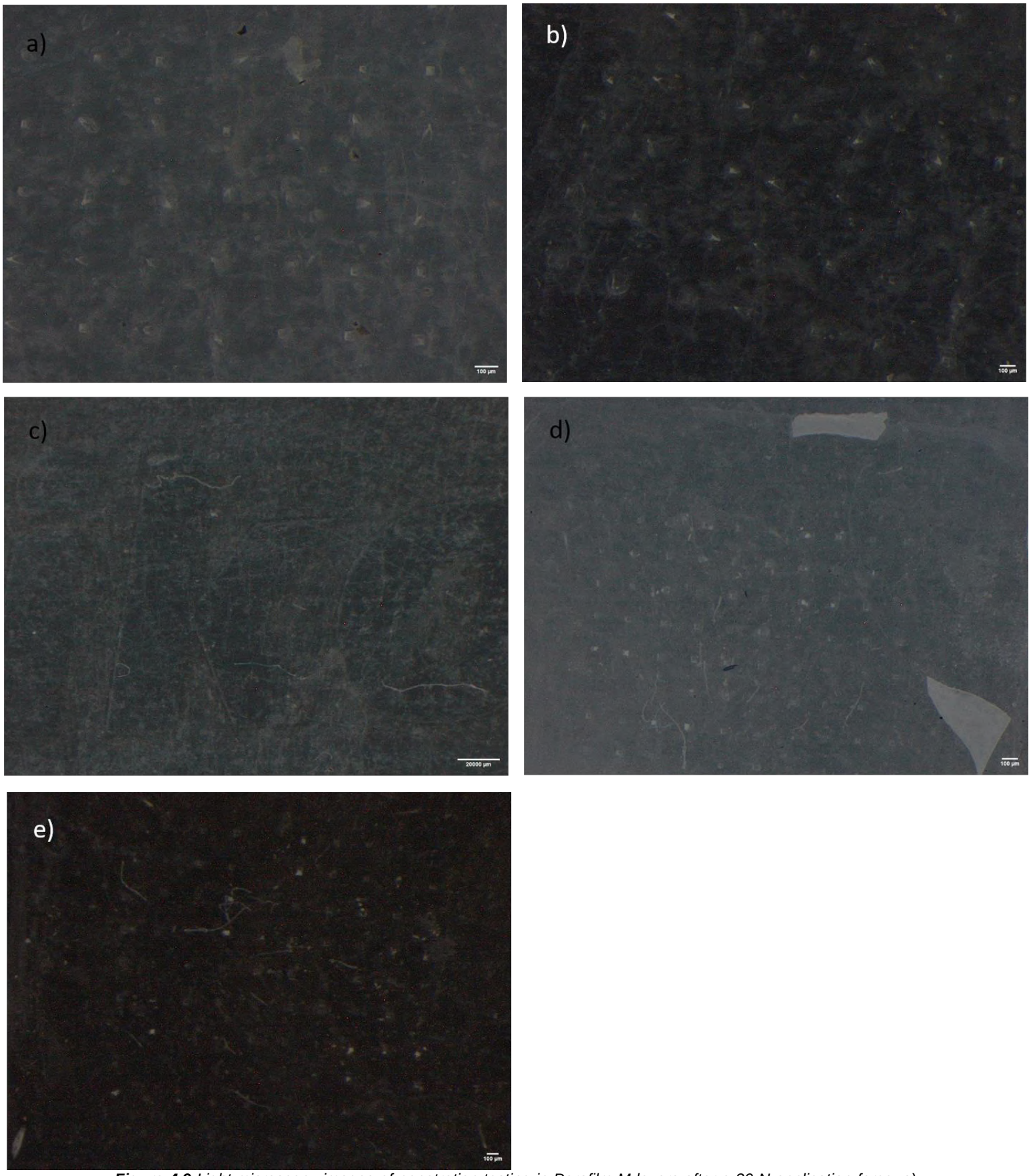


Figure 4.9 *Light microscopy images of penetration testing in Parafilm M layers after a 30 N application force. a) chitosan MN array, all layers, b) chitosan MN array layer 1, c) chitosan MN array layer 2, d) alginate MN array all layers and e) alginate MN array layer.*

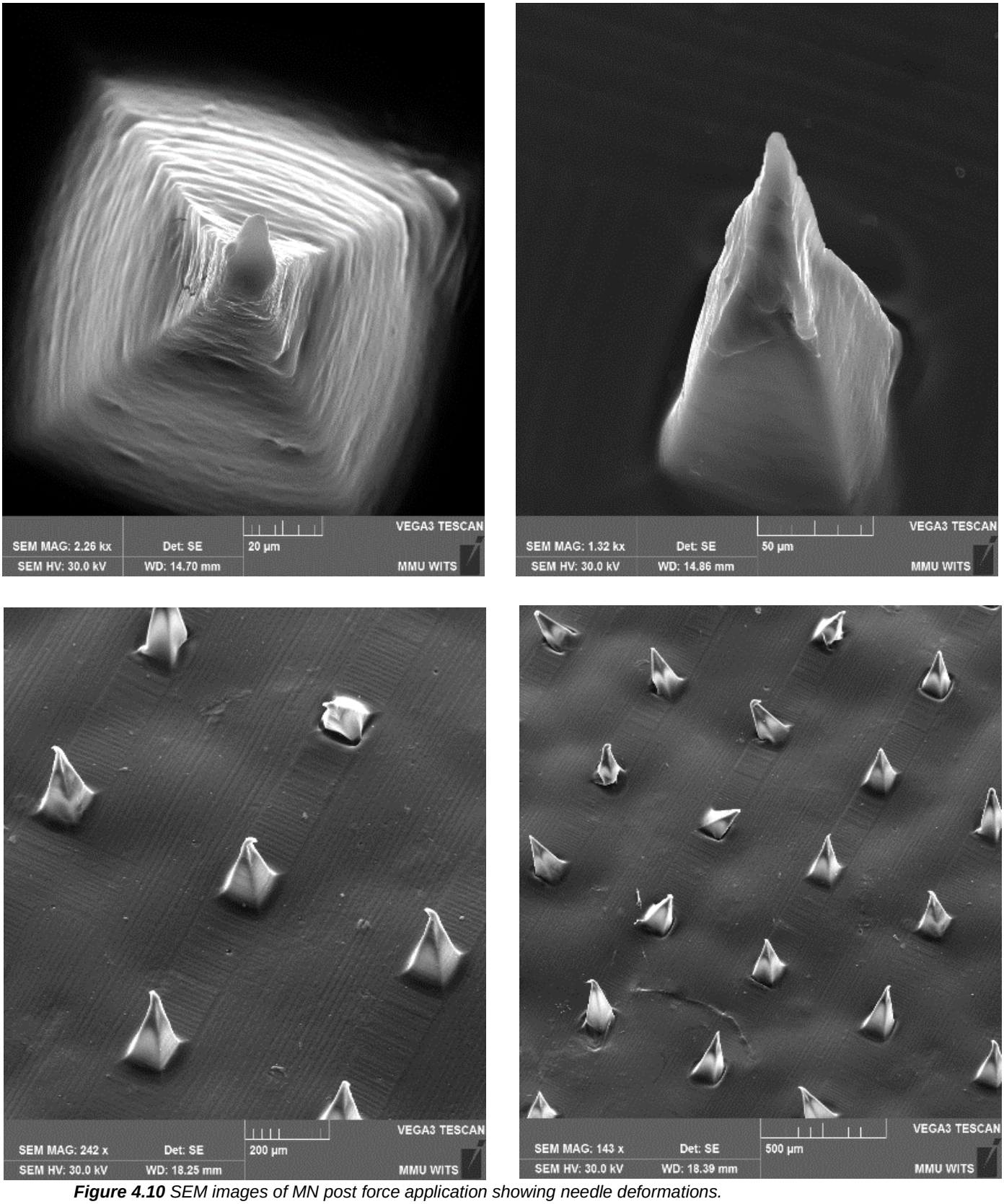


Figure 4.10 *SEM images of MN post force application showing needle deformations.*

4.3.5 Powder X-ray Diffraction analysis of the polymeric blends

The PXRD diffractogram of the pristine compounds were first analysed and then compared to that of the alginate and chitosan loaded arrays as shown in **Figure 4.11** below. The diffraction pattern of sodium alginate showed a semi-crystalline structure with two peaks at 2θ equals to 22.1 °C and 38.4 °C. The diffraction pattern of EDTA disodium, however, contained sharp narrow peaks, pointing to their crystalline structure.

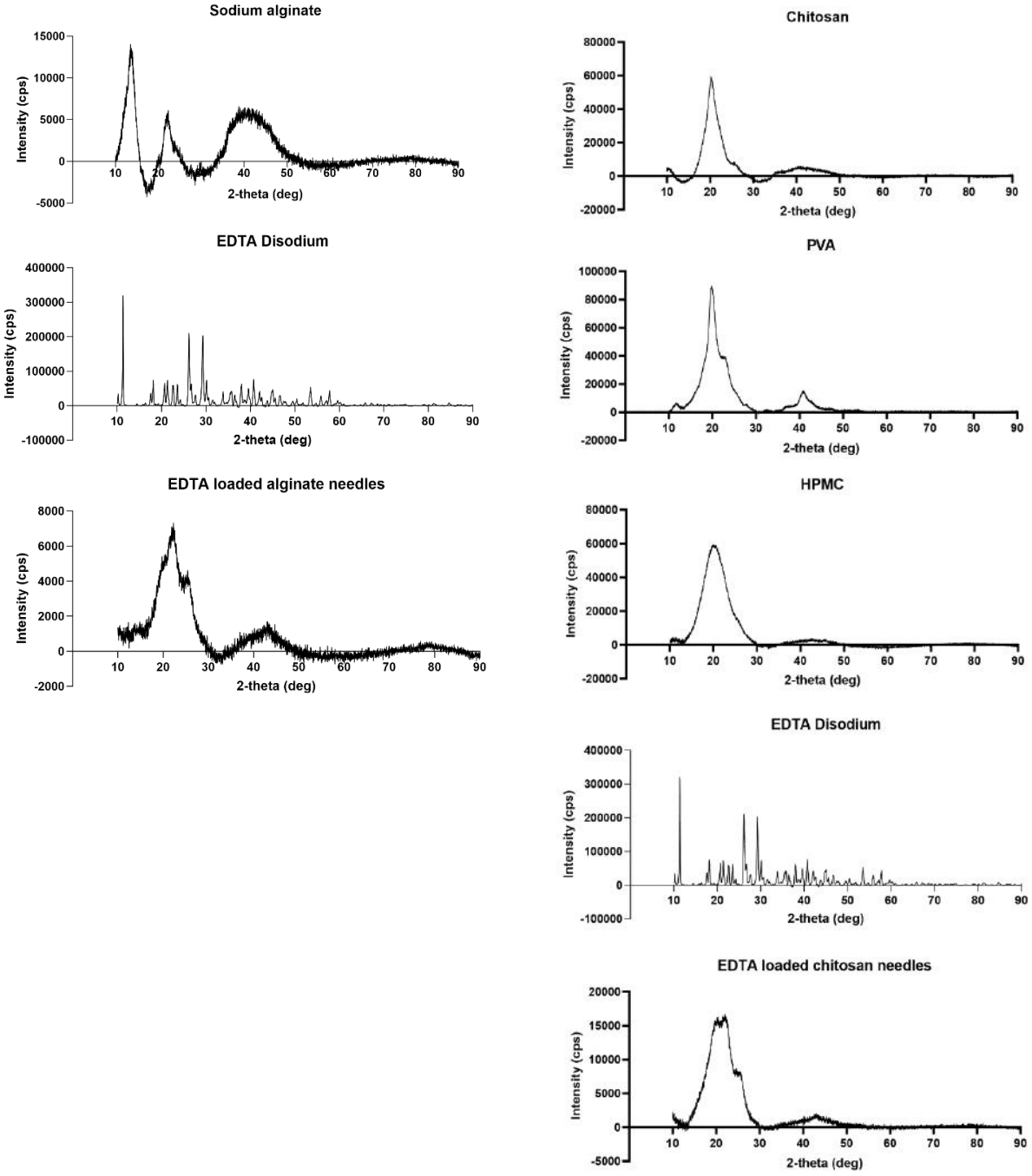


Figure 4.11 *XRD diffractograms of alginate MN arrays and components (above) and chitosan MN arrays and components (right).*

After combining these, the produced EDTA loaded alginate array displayed an amorphous diffraction pattern. The diffraction pattern corresponded to sodium alginate and displayed two peaks at 2θ equals to 21.4 °C and 45.1 °C as well as an amalgamation of overlapping peaks between 20 – 30 °C which could be attributed to the addition of the more crystalline EDTA disodium. The XRD spectra of pristine compounds used in the chitosan formulation revealed a semi-crystalline structure for both chitosan and PVA but a more amorphous structure of HPMC. The combination array produced peaks similar to that of the main component, namely chitosan, but showed a broader peak at approximately 20 °C due to the interactions of both the other polymer components (HPMC and PVA) as well as the addition of EDTA disodium. Due to the more amorphous nature of the sodium alginate in comparison to the chitosan, the alginate arrays show a more amorphous diffraction pattern and this could correlate to the alginate arrays quicker degradation rate (Hideno, 2016).

4.3.6 Differential Scanning Calorimetry (DSC) analysis of the polymeric blends

The DSC findings regarding the chitosan array loaded with disodium EDTA (**Figure 4.13**) showed 3 thermodynamic events all of which were endothermic events. The first of these occurred at 97.33 °C is assigned to the loss of molecular water, the second at 189.54 °C is as a result of melting of the PVA component within the system and the third, occurring at 243.72

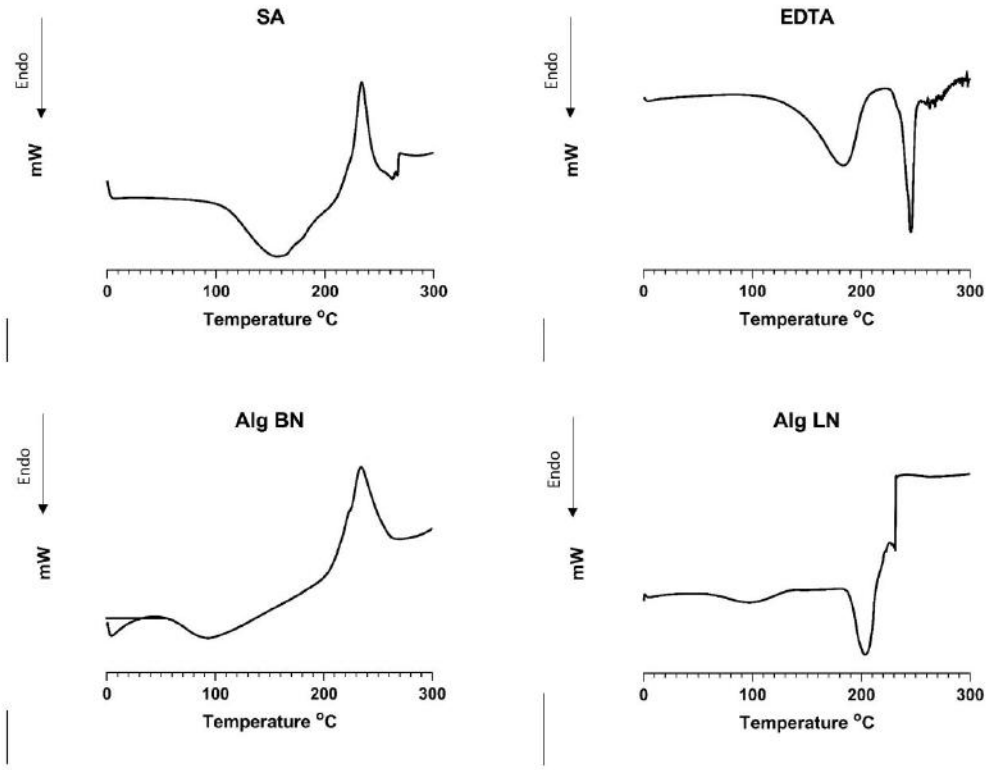


Figure 4.12 *DSC thermograms of alginate MN formulation and pristine polymers.*

°C represents the decomposition of the EDTA within the system. Peaks were observed at similar temperatures as event one and two for the unloaded chitosan arrays.

Table 4.2 *DSC peaks of the pristine powders and their corresponding thermal event*

Sample	Peak Temp (°C)	Corresponding thermodynamic event
Sodium alginate	156	Dehydration
	234	Decomposition
EDTA disodium	183	Dehydration
	244	Decomposition
Chitosan	101	Dehydration
HPMC	85	Melting
PVA	42	Glass transition
	190	Melting

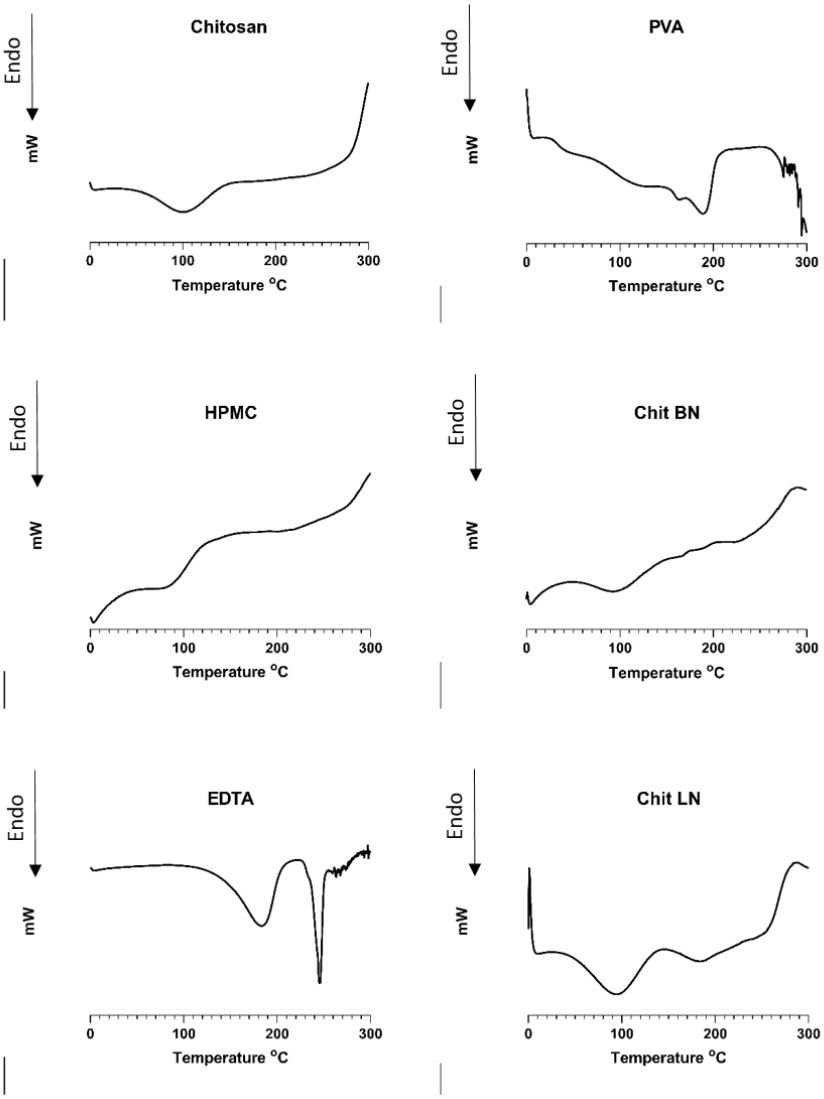


Figure 4.13 *DSC thermograms of chitosan MN formulation and pristine polymers.*

4.3.7 *In vitro* degradation of alginate and chitosan MN arrays

As shown in **Figure 4.14**, after 72 hours, the chitosan arrays were 95.92 % degraded whereas the alginate arrays had completely degraded by this time. Alginate based arrays degrade at a quicker rate than chitosan arrays and therefore make them better suited for dissolvable MN formulations whereas chitosan arrays may be beneficial for longer release formulations with the incorporation of auxiliary polymers as the arrays maintained their structure beyond the 72 hour testing period. Although alginate arrays are not completely degraded prior to the 72 hour time point, they do not maintain an intact array structure for more than a few minutes and are fully dissolved at the one hour time point and can only be separated from solution using centrifugation.

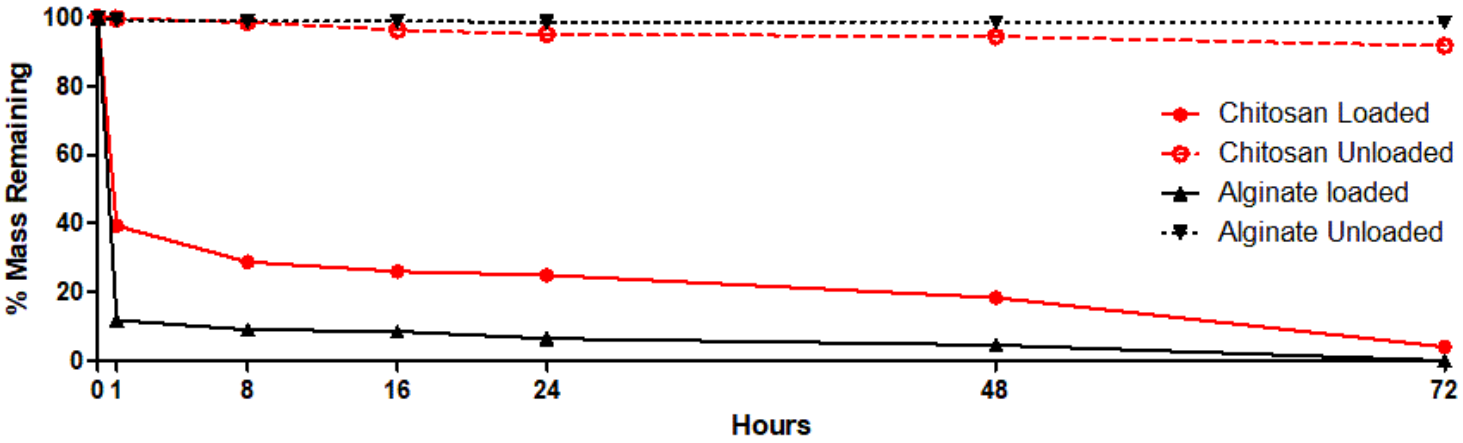


Figure 4.14 *72 hour degradation profile of EDTA loaded alginate and chitosan MN arrays.*

4.3.8 Water uptake analysis of the MN array

Water uptake is an essential part of this system as the array would need to take in water in order for EDTA to be released to permeate the tissue. Water uptake also contributes to the degradation of the arrays. Chitosan-EDTA MN arrays have a maximum water uptake at 10 minutes with an uptake ratio of 3071.62 % when compared to the initial dry mass of the sample. The blank chitosan samples reached maximum water uptake in half the time and possessed a water uptake ratio of 4064.56 %. This shows that by the addition of EDTA disodium into the formulation, the water uptake ability of the polymer base is reduced. This decrease in the water uptake percentage could be attributed to the strong interaction between the $-NH_3$ groups of the chitosan and the -OH and -COOH groups of the EDTA molecule. This strong interaction results in a more densely linked complex with a decreased void space. It is this void space that is occupied with water during water uptake and with less void space, less water is able to be taken into the polymer matrix (Singh *et al.*, 2012). Similar outcomes were observed with the alginate based arrays. EDTA loaded arrays reached peak water uptake of

362.53 % of original mass within one minute, whereas unloaded arrays took longer to reach peak water uptake (two minutes) but had a max water uptake ratio of 2515.10 %.

Seeing as these included polymers and co-polymers possessing the ability for such great water uptake (Siepmann and Peppas, 2012) it is possible that the mechanical strength of the MN array will be reduced, however with the presence of EDTA being a minimizing factor in terms of water uptake, it may lead to only a plasticizing effect being had on the arrays, making them more flexible and conforming to vascular tissue structure. This conformation would aid in vascular delivery as stiff materials have been shown to increase the likelihood of intimal hyperplasia development (Kim *et al.*, 2017).

4.3.9 EDTA loading and encapsulation

During initial fabrication stages, various w/v concentrations of EDTA were evaluated for both polymer arrays. Concentrations evaluated ranged from 1 mg/ml to 30 mg/ml. It was found that higher concentrations of EDTA in the chitosan array produced brittle MNs which were unusable whereas with the alginate array an increase in EDTA created a more pliable and usable MN array.

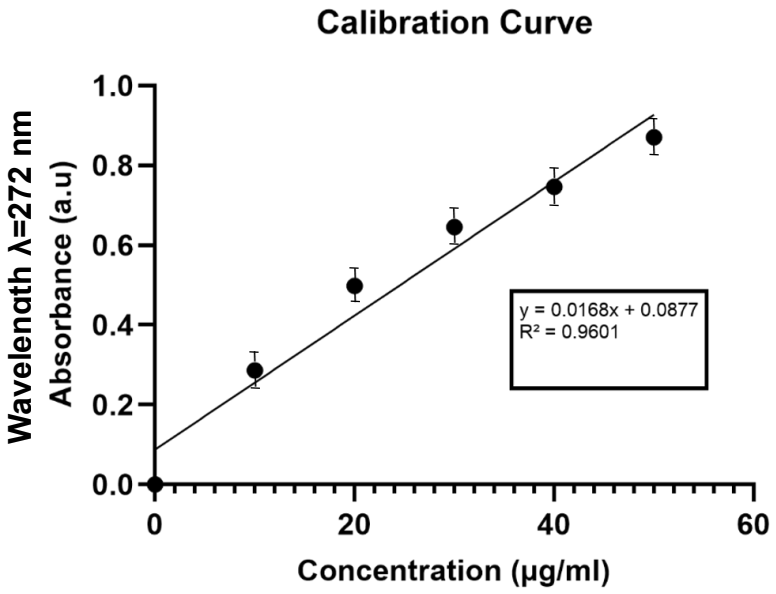


Figure 4.15 *Calibration curve of Fe-EDTA at concentrations 10, 20, 30, 40 and 50 µg/mL.*

It was found that chitosan microneedle arrays possessed a maximum loading capacity of 400 µg of EDTA, as higher EDTA concentrations resulted in mechanical failure of the array due to the brittleness of the formulation.

A loading efficiency of 85.12% (±1.1) was recorded for the chitosan array, translating into a loaded drug weight of 340 µg per array. In comparison, due to the nature of the crosslinking of the alginate formulation, the alginate array possessed a larger loading ability of EDTA. Each alginate array was able to be loaded with 2000 µg of EDTA, however loading efficiency showed a very low percentage of 48.29% (±2.4) equating to 965.8 µg of EDTA. This is potentially due to EDTA's ability to erode the calcium crosslinks formed, as seen in **Figure 4.17**, within the alginate structure resulting in free calcium being chelated by the EDTA prior to complete release as described in **Figure 4.16** and **Figure 4.17** below (Delaney *et al.*, 2010). Although EDTA forms a more stable complex with Fe^{3+} than Ca^{2+} (Corsello *et al*., 2009), its bound state prior to the addition of ferric chloride prevents favourable bonding and therefore EDTA was unquantifiable by previously discussed ferric chloride quantification method utilised in this work.

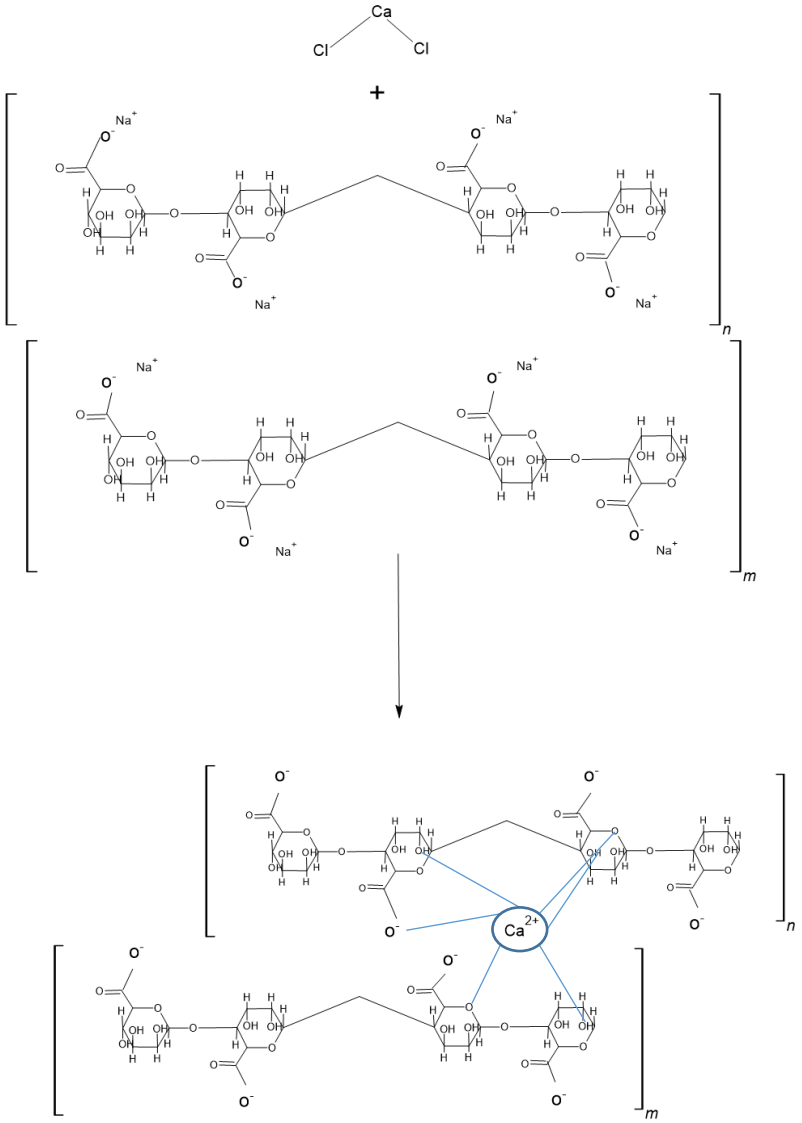


Figure 4.16 *schematic diagram providing the process of cross-linking sodium alginate by calcium chloride.*

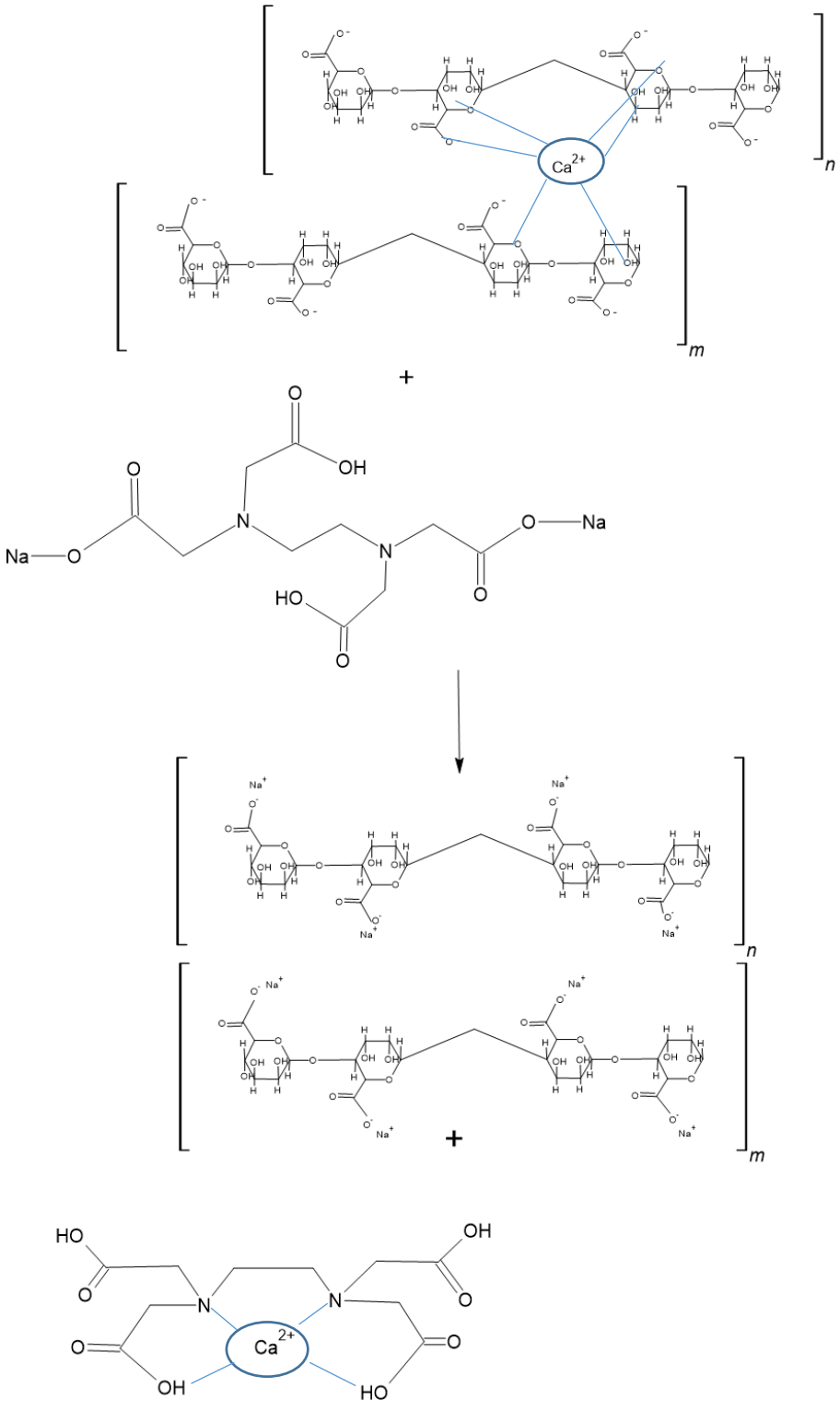


Figure 4.17 *schematic diagram providing the reversal process of cross-linking sodium alginate by calcium chloride in the presence of EDTA.*

4.3.10 *In vitro* release of EDTA from alginate and chitosan MN arrays

Both the chitosan and alginate arrays exhibit similar release profiles for the initial 6 hours (as shown in **Figure 4.18** consistent with findings reported in previous studies of alginate MN arrays (Tiraton *et al.*, 2022; Yu *et al.*, 2017). Subsequently, the release profile of the alginate MN array accelerates, reaching steady-state flux with continuous release up to 24 hours.The release rate of EDTA from the chitosan MN array however decreased after 6 hours with a much lower cumulative release amount compared to the alginate array in line with observations made by other researchers (Wei *et al*., 2022).

This can be attributed to how the arrays breakdown over time due to the reversal of calcium crosslinking upon the addition of EDTA, as the alginate array is dissolved almost immediately resulting in a quick release of EDTA which then steadily permeates through the tissue sample (Tiraton *et al*., 2022).

Conversely, the chitosan array degrades slower and therefore EDTA is released from the array at a more gradual rate and then permeates through the tissue (Wei *et al*., 2022). These findings align with the observed differences in release profiles between the two arrays in our study.

The alginate MN array shows greater cumulative release amount for EDTA due to its higher loading capabilities as mentioned above, however, when compared to initial loading of the array, chitosan arrays display a 92.57 % (±10.15) cumulative release efficacy at 24 hours with the alginate array displaying a lower cumulative release efficacy, the released drug amount in relation to the loaded drug amount percentage of 81.71 % (±8.66).

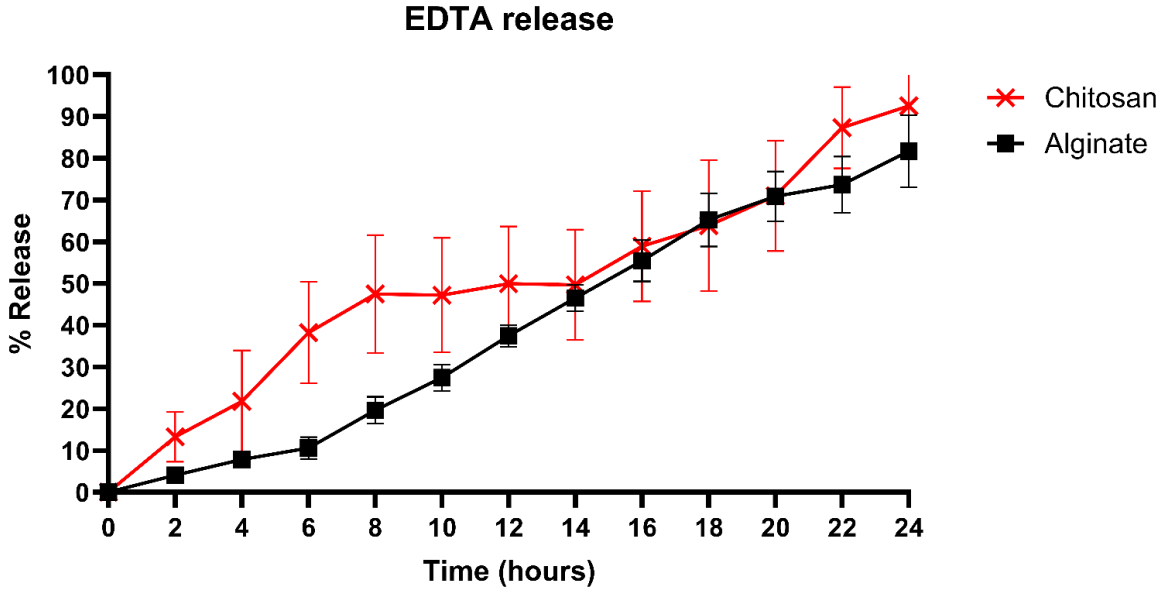


Figure 4.18 *Percentage EDTA released over a 24 hour period in PBS (pH 7.4) at 37 °C.*

4.3.11 *Ex vivo* assessment of EDTA diffusion across excised porcine venous tissue

Up until time point 480 minutes, both arrays display similar permeation values, as illustrated in **Figure 4.19** below. After this point, the permeation of the alginate arrays increases rapidly, while the permeation of the chitosan array remains constant.

There are numerous factors which impact the permeability of a drug molecule including the molecule size, shape, lipophilicity and the pH of the test system. Additional interactions between the tissue membrane and elements of the formulation could also impact the permeability. EDTA at a pH of 7.4 has a molecular charge of negative 3 although when considering the addition of calcium ions in the alginate formulation which would bind to the free EDTA, the charge will change to a more neutral compound which will enhance the cell permeability due to the negative charge within the cell.

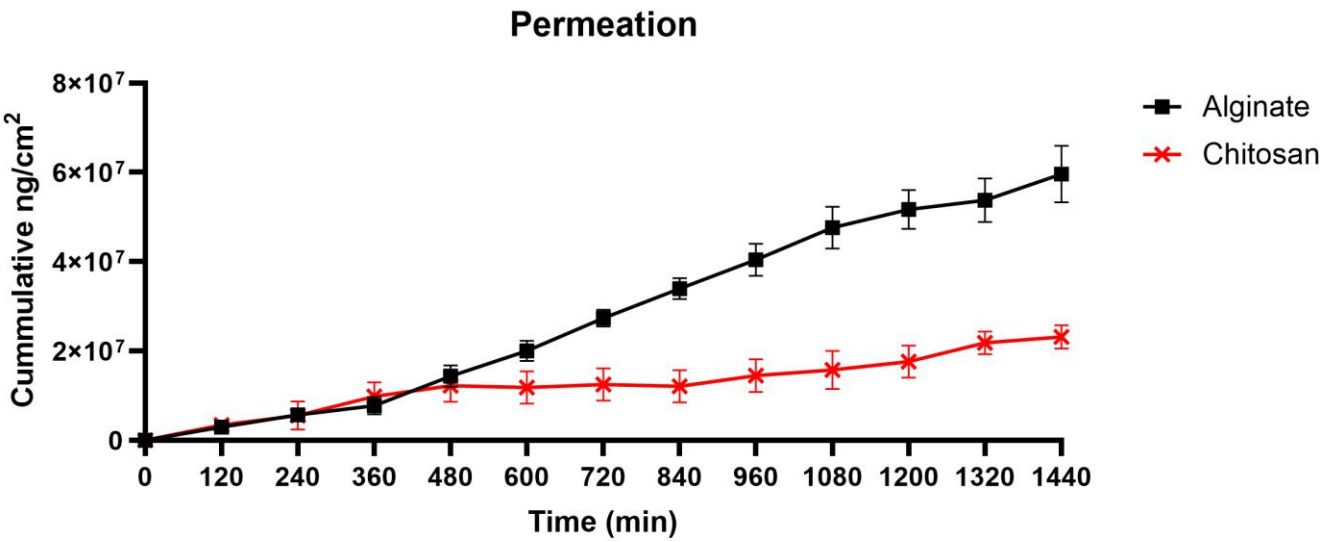


Figure 4.19 *The diffusion kinetics of EDTA for the alginate and chitosan arrays across excised porcine venous tissue.*

The difference in permeability in this study may be contributed to the rapid dissolution time of the alginate array in comparison to the chitosan array. The almost complete degradation of the structure of the alginate array within the first few hours as seen in the degradation study results in the EDTA molecules being more readily available to permeate the membrane whereas the incomplete dissolution of the slower release chitosan array would prevent all the loaded EDTA from permeating the membrane. Although chitosan is a permeation enhancer and one would expect to find it having a higher permeation than the alginate arrays, the incomplete dissolution of the formulation would hinder the polymers ability to influence the membrane (Sadeghi *et al.*, 2008). EDTA itself is a known membrane destabilizer and may aid

in its own transport across the membrane due to the increase in paracellular permeability (Dahlgren *et al*., 2021).

The flux and lag phase of the graphs were calculated via linear regression of the linear portion of the graphs (360 – 1080 minutes for the alginate array and 960 – 1200 minutes for the chitosan array) to be 55299 ng/cm^2/minute and 180 minutes respectively for the alginate arrays and 18713 ng/cm^2/minute and 215 minutes respectively for the chitosan arrays. Flux is described as the amount of bioactive passing through the membrane per unit area into the receptor chamber per unit time, expressed in units of mass/area/time. The calculated flux values indicate that the alginate array had a much higher permeability in comparison to the chitosan array. The lag time represents the delay from onset of permeation to the time at which steady state is reached. Both formulations have similar lag times indicating that they reach steady state between 3-3.5 hours.

The pre and post-test FTIR evaluation as shown in **Figure 4.20** below, indicate no significant changes in the absorption bands between the two FTIR spectra showing that the interaction of the formulations did not alter the makeup of the tissue and tissue integrity was maintained.

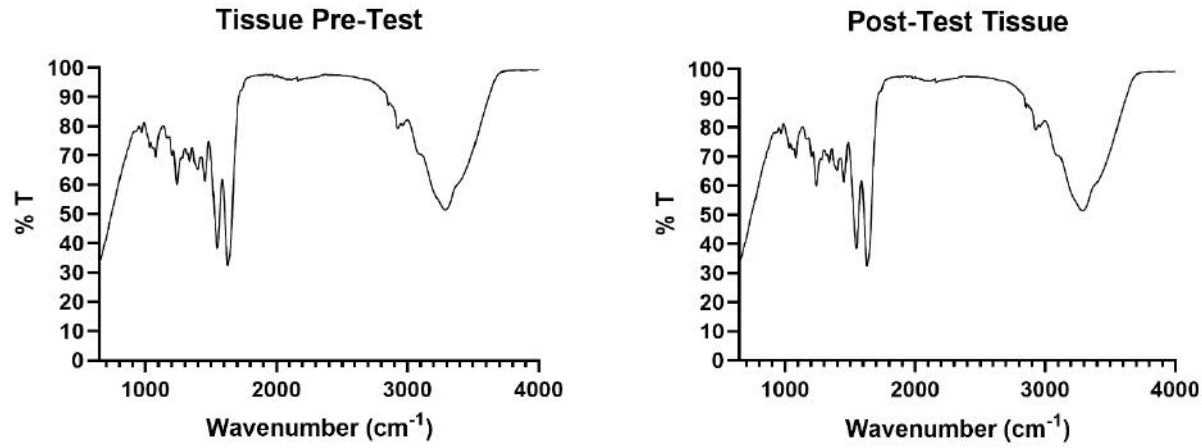


Figure 4.20 *FTIR spectra of tissue samples before and after the permeation study was run.*

4.3.12 Evaluation of calcium chelating ability of array

Although maximum calcium chelating ability based on drug loading for the chitosan and alginate arrays are 112.2 µg and 318.8 µg respectively, actual calcium chelating ability of both alginate and chitosan arrays, shown in **Figure 4.21** Mass of calcium that can be chelated over time based on EDTA release. **Figure 4.21** was determined based on drug release data and a molar ratio of 1:1 (EDTA:$CaCl_2$) (Nkuna *et al*., 2022).

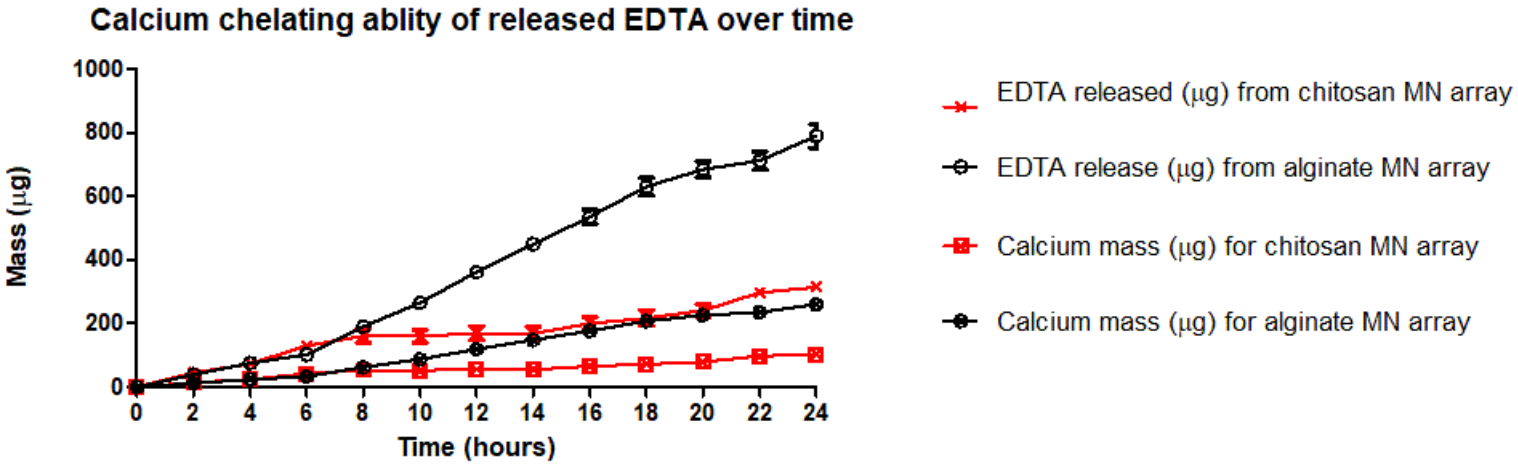


Figure 4.21 *Mass of calcium that can be chelated over time based on EDTA release.*

4.3.13 Evaluation of *In Vitro* Hemocompatibility of the MN arrays

EDTA has been shown to cause an increase in hemolysis by between 45.7(±33.4) and 55.4(±34.7) percent and this creates a challenge when using EDTA as a bioactive (Witeska and Wargocka, 2011). However, results shown in **Figure 4.23** when compared to **Figure 4.22** showed minimal hemolysis. Further UV-vis analysis of the results of the hemocompatibility study performed show that both formulations of EDTA loaded MN arrays showed a decrease in hemolysis in comparison to respective doses of unloaded EDTA disodium MN arrays, with the alginate needles showing a 115.07% decrease in hemolysis and the chitosan a 36.46 % decrease. This proves that the MN array dosage form has the potential

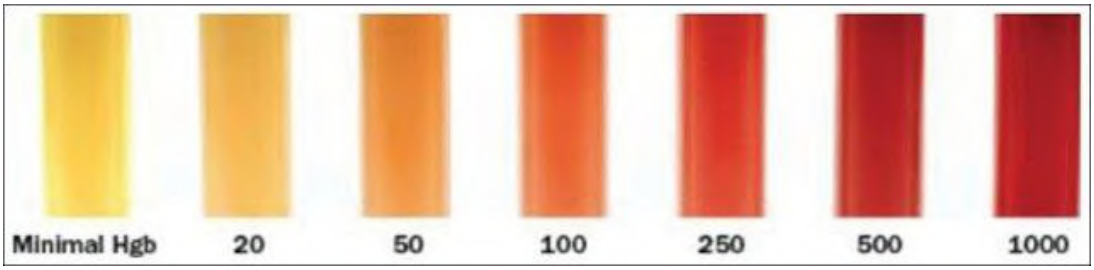


Figure 4.22 *Colour chart used in the detection of heamolysis showing heamolysis as mg/dl. Reused under CC BY-NC-SA 3.0.*

to reduce the toxicity effects of the loaded bioactives, this may be due to the delay in release from the array allowing for smaller amounts of EDTA to interact with the blood cells.

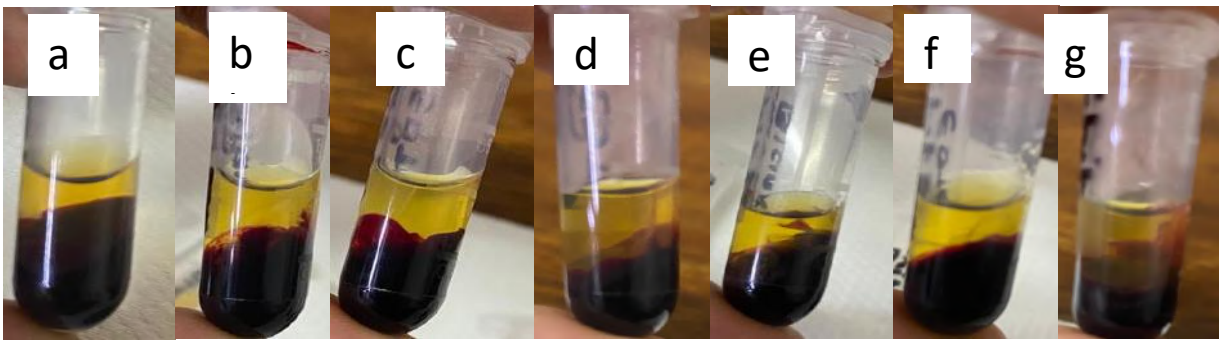


Figure 4.23 *Centrifuged blood samples showing serum colour for hemolysis assessment a) untreated, b) unloaded alginate array, c) EDTA loaded alginate array, d) pristine EDTA equal to alginate loaded MN array, e) unloaded chitosan array, f) EDTA loaded chitosan array and g) pristine EDTA equal to chitosan loaded MN array.*

4.4 Concluding remarks

In this study 10 x 10 (8 mm x 8 mm) MN arrays with a needle height of 300 µm, a needle pitch of 500 and an aspect ratio of 3 were fabricated using two natural polymers and loaded with EDTA disodium as a bioactive for potential use in the decalcification of blood vessels. The fabricated MN's were of pyramidal shape as seen in the SEM images.

The amount of bioactive incorporated and released from the two microneedle formulations was evaluated using UV-Vis spectrophotometry and it was found that the alginate formulation had a loading capacity of 965.8 µg of EDTA and a cumulative release of 789 µg (±83.63) after a 24 hour period whereas the chitosan formulation had a loading capacity of 340 µg with 315 µg (±33.43) being released after the same 24 hour period.

Through the characterisations performed for this study it has been shown that both these natural polymer arrays assist in reducing EDTA hemotoxicity due to their site specific action and slower release profiles, allowing for greater potential for the development of EDTA and other therapies in vascular drug delivery. The alginate array has a faster degradation rate in comparison to the chitosan array showing complete degradation within 72 hours and complete dissolution in PBS in one hour, which would make it a potential candidate for quick release dissolving MN formulations which may prove useful for acute cases of vascular calcification whereas it may be beneficial to look at other polymer blends for more chronic cases.

In this study it was found that both formulations were able to release the EDTA bioactive effectively and permeate the vessel tissue demonstrating the success of the formulation despite substantial bioactive loss in the alginate formulation.

These microneedle arrays also have potential uses in the delivery of other small and large molecule cardiovascular drugs and bioactives due to the simple drug loading and fabrication process used herein with further studies required to evaluate the release efficiency.

Chapter 5 Conclusions and recommendations

5.1 Conclusions

Vascular and blood tissue calcification involves the deposition of calcium and phosphate minerals, predominantly within blood vessel walls, impacting cardiovascular health (Schweighofer *et al.*, 2016). The current treatment of vascular calcification most commonly centres on physical means of removal of the calcium plaque, with reoccurrence being a common feature for patients (Schantl *et al*., 2019). Recently, EDTA has been investigated as a vascular therapeutic and although it is shown to be effective, it is also associated with many harmful and potentially lethal side effects. These concerns are presently restricting the use of this potentially successful bioactive. It has been shown that local targeted delivery of EDTA reduces the side effect profile. Therefore, there is a significant need for novel treatment options.

This study proposed to fabricate a dissolvable MN with key features of vascular compatibility and local drug delivery to mitigate the harmful effects of EDTA chelation therapy. Two polymer blends were created that showed good mechanical strength and drug-release capability; however, drug-loading capacity remains a challenge. Since most drugs cannot be formed into a mechanically strong enough needle that is able to penetrate tissue, a high amount of drug loading is not possible as the majority of the needle must consist of polymer matrix. As microneedles are very small, the maximum total dose that can be loaded into a dissolving polymer MN can be a challenge, however applying multiple MNs to the area may help to achieve the required dosage.

Results showed successfully designed EDTA loaded chitosan blend and alginate cross-linked MN arrays with mechanical strengths suitable for drug delivery to soft tissues such as the vascular system. Chitosan MN arrays possessed a mechanical strength of 0.338 N per needle and the Alginate arrays possessing a slightly lower mechanical strength of 0.345 N per needle.

In conclusion, this study addresses some of the limitations of current vascular delivery systems by fabrication of a dissolving MN intended for single use in vascular tissue. MNs containing EDTA as model bioactive were shown to be able to be formed using a simple mould-casting method. These MNs were found to have a piercing depth of 130 – 260 µm which is suitable for vascular tissue as vessel wall thicknesses range from 1500 – 40 µm. Dissolving chitosan and alginate MNs fabricated in this study were able to deliver 92.57 % (±10.15) and 81.71 % (±8.66), respectively of the loaded bioactive amount. These MN arrays also showed good hemocompatibility and even reduced the natural hemolytic effect of EDTA.

5.2 Limitations

A key limitation of this study is the inherent nature of dissolvable MNs to have a very low drug loading capacity. This could also be overcome by the application of multiple or larger patches of MNs but is limited by the vascular surface area available at the site of calcification This study was also limited by the degradation rate of the selected polymer blends as once the needle structure was dissolved the free bioactive molecules would migrate away from the site of action.

5.3 Recommendations

The present dissertation describes the successful fabrication and implementation of the EDTA-containing MN arrays fabricated from alginate and chitosan upon *in vitro* and *ex vivo* analysis. Characterisation of the MN provided data regarding the chemical stability, reactivity, morphology and degradation of the polymer. One of the key goals of this research was to design a drug delivery system that was safe and suitable for use in the vascular system. To further improve on this, polymers with longer erosion times could be investigated in the future as prolonged release would be of great benefit to vascular applications due to the inherent inaccessibility of the tissue. Redesign of needle geometry could increase the maximum drug loading capacity whilst retaining needle strength. Investigations by Martanto and colleagues suggest that MN density is essential for preventing tissue damage during delivery (Martanto *et al.*, 2004). An inverse relationship exists between the density of a microneedle array and its penetrating ability. This relationship along with findings of ideal vascular delivery needle size is worthy of further investigation to determine the resultant effect on penetration and vascular drug delivery. To adapt the controlled drug release further, different ratios of polymer can be used in order to release drug slower while maintaining the MN array structure.

5.4 Future Outlook

A dissolving polymer MN containing EDTA as a model bioactive has been designed and fabricated in this study. *In vitro* and *ex vivo* results are encouraging and demonstrate good biocompatibility, therefore the next step is to conduct *in vivo* studies to investigate the effect of the MNs in a living organism.

EDTA was used as model bioactive for this study. Other vascular targeted drugs should be investigated in the future for a wider range of therapeutic effects. The use of these polymer MNs may be further extended to other soft tissue sites in the future. These microneedle arrays also have potential uses in the delivery of other small and large molecule cardiovascular drugs

and bioactives due to the simple drug loading and fabrication process used herein with further studies required to evaluate the release efficiency.

References

Albl, B., Haesner, S., Braun-Reichhart, C., Streckel, E., Renner, S., Seeliger, F., Wolf, E., Wanke, R., Blutke, A., 2016. Tissue sampling guides for porcine biomedical models. Toxicol. Pathol. 44, 414–420. https://doi.org/10.1177/0192623316631023

Arsalan Abu-Much, Raya Darawshi, Hala Dawud, Haytam Kasem, Ammar, A.A., 2022. Preparation and characterization of flexible furosemide-loaded biodegradable microneedles for intradermal drug delivery. Biomater. Sci. https://doi.org/10.1039/D2BM01143C

Avcil, M., Çelik, A., 2021. Microneedles in drug delivery: Progress and challenges. Micromachines 12, 1–15. https://doi.org/10.3390/mi12111321

Badhe, R. V., Bijukumar, D., Chejara, D.R., Mabrouk, M., Choonara, Y.E., Kumar, P., du Toit, L.C., Kondiah, P.P.D., Pillay, V., 2017. A composite chitosan-gelatin bi-layered, biomimetic macroporous scaffold for blood vessel tissue engineering. Carbohydr. Polym. 157, 1215–1225. https://doi.org/10.1016/j.carbpol.2016.09.095

Baek, S.H., Shin, J.H., Kim, Y.C., 2017. Drug-coated microneedles for rapid and painless local anesthesia. Biomed. Microdevices 19. https://doi.org/10.1007/s10544-016-0144-1

Banks, S., Pinnintia, R.R., Gill, H.S., Paudel, K.S., Crooks, P.A., Brogden, N.K., Prausnitz, M.R., Stinchcomb, A.L., 2010. Transdermal delivery of naltrexol and skin permeability lifetime after microneedle treatment in hairless guinea pigs. J Pharm Sci 23, 1–7. https://doi.org/10.1002/jps.22083.Transdermal

Baykal, A., Toprak, M.S., 2007. Synthesis and characterization of NiFe 2 O 4 nano-octahedrons by EDTA-assisted hydrothermal method. Turkish J. Chem. 31, 659–666.

Bonfante, G., Lee, H., Bao, L., Park, J., Takama, N., Kim, B., 2020. Comparison of polymers to enhance mechanical properties of microneedles for bio-medical applications. Micro Nano Syst. Lett. 8, 1–13. https://doi.org/10.1186/S40486-020-00113-0/FIGURES/12

Calori, I.R., Braga, G., de Jesus, P. da C.C., Bi, H., Tedesco, A.C., 2020. Polymer scaffolds as drug delivery systems. Eur. Polym. J. 129, 109621. https://doi.org/10.1016/j.eurpolymj.2020.109621

Camasão, D.B., Mantovani, D., 2021. The mechanical characterization of blood vessels and their substitutes in the continuous quest for physiological-relevant performances. A critical review. Mater. Today Bio 10. https://doi.org/10.1016/j.mtbio.2021.100106

Chen, Y., Chen, B.Z., Wang, Q.L., Jin, X., Guo, X.D., 2017. Fabrication of coated polymer

microneedles for transdermal drug delivery. J. Control. Release 265, 14–21. https://doi.org/10.1016/j.jconrel.2017.03.383

Choi, C.K., Kim, J.B., Jang, E.H., Youn, Y.N., Ryu, W.H., 2012. Curved biodegradable microneedles for vascular drug delivery. Small 8, 2483–2488. https://doi.org/10.1002/SMLL.201200441

Choi, C.K., Lee, K.J., Youn, Y.N., Jang, E.H., Kim, W., Min, B.K., Ryu, W., 2013. Spatially discrete thermal drawing of biodegradable microneedles for vascular drug delivery. Eur. J. Pharm. Biopharm. 83, 224–233. https://doi.org/10.1016/J.EJPB.2012.10.020

Cholkar, K., Acharya, G., Trinh, H.M., Singh, G., 2017. Therapeutic applications of polymeric materials, Emerging Nanotechnologies for Diagnostics, Drug Delivery and Medical Devices. Elsevier. https://doi.org/10.1016/B978-0-323-42978-8.00001-2

Corsello, S., Fulgenzi, A., Vietti, D., Ferrero, M.E., 2009. The usefulness of chelation therapy for the remission of symptoms caused by previous treatment with mercury-containing pharmaceuticals: A case report. Cases J. 2. https://doi.org/10.1186/1757-1626-2-199

Coyne, J., Davis, B., Kauffman, D., Zhao, N., Wang, Y., 2017. Polymer microneedle mediated local aptamer delivery for blocking the function of vascular endothelial growth factor. ACS Biomater. https://doi.org/10.1021/acsbiomaterials.7b00718

Dahlgren, D., Olander, T., Sjöblom, M., Hedeland, M., Lennernäs, H., 2021. Effect of paracellular permeation enhancers on intestinal permeability of two peptide drugs, enalaprilat and hexarelin, in rats. Acta Pharm. Sin. B 11, 1667–1675. https://doi.org/10.1016/j.apsb.2020.12.019

Damiri, F., Kommineni, N., Ebhodaghe, S.O., Bulusu, R., Jyothi, V.G.S.S., Sayed, A.A., Awaji, A.A., Germoush, M.O., Al-Malky, H.S., Nasrullah, M.Z., Rahman, M.H., Abdel-Daim, M.M., Berrada, M., 2022. Microneedle-based natural polysaccharide for drug delivery systems (DDS): progress and challenges. Pharmaceuticals 15, 1–26. https://doi.org/10.3390/ph15020190

Delaney, J.T., Liberski, A.R., Perelaer, J., Schubert, U.S., 2010. Reactive inkjet printing of calcium alginate hydrogel porogens - A new strategy to open-pore structured matrices with controlled geometry. Soft Matter 6, 866–869. https://doi.org/10.1039/b922888h

Demir, Y.K., Akan, Z., Kerimoglu, O., 2013a. Sodium alginate microneedle arrays mediate the transdermal delivery of bovine serum albumin. PLoS One 8. https://doi.org/10.1371/JOURNAL.PONE.0063819

Demir, Y.K., Akan, Z., Kerimoglu, O., 2013b. Sodium Alginate Microneedle Arrays Mediate the Transdermal Delivery of Bovine Serum Albumin. PLoS One 8. https://doi.org/10.1371/JOURNAL.PONE.0063819

Ding, B. Sen, Dziubla, T., Shuvaev, V. V., Muro, S., Muzykantov, V.R., 2006. Advanced drug delivery systems that target the vascular endothelium. Mol. Interv. 6, 98–112. https://doi.org/10.1124/mi.6.2.7

Freeman, R. V., Otto, C.M., 2005. Spectrum of calcific aortic valve disease: Pathogenesis, disease progression, and treatment strategies. Circulation 111, 3316–3326. https://doi.org/10.1161/CIRCULATIONAHA.104.486738

Goel, S., Pasam, R.T., Chava, S., Gotesman, J., Sharma, A., Malik, B.A., Frankel, R., Shani, J., Gidwani, U., Latib, A., 2020. Orbital atherectomy versus rotational atherectomy: A systematic review and meta-analysis. Int. J. Cardiol. 303, 16–21. https://doi.org/10.1016/j.ijcard.2019.12.037

Gu, F., Amsden, B., Neufeld, R., 2004. Sustained delivery of vascular endothelial growth factor with alginate beads 96, 463–472. https://doi.org/10.1016/j.jconrel.2004.02.021

Guimarães, T.M.T., Moniz, T., Nunes, C., Zaharieva, M.M., Kaleva, M., Yoncheva, K., Najdenski, H., Costa Lima, S.A., Reis, S., 2022. Polymeric microneedles for transdermal delivery of rivastigmine: design and application in skin mimetic model. Pharmaceutics 14. https://doi.org/10.3390/pharmaceutics14040752

Hedayati, M., Neufeld, M.J., Reynolds, M.M., Kipper, M.J., 2019. The quest for blood-compatible materials: Recent advances and future technologies. Mater. Sci. Eng. R Reports 138, 118–152. https://doi.org/10.1016/j.mser.2019.06.002

Hideno, A., 2016. Comparison of the thermal degradation properties of crystalline and amorphous cellulose, as well as treated lignocellulosic biomass. BioResources 11, 6309–6319. https://doi.org/10.15376/biores.11.3.6309-6319

Huang, Y., Yu, H., Wang, L., Shen, D., Ni, Z., Ren, S., Lu, Y., Chen, X., Yang, J., Hong, Y., 2022. Research progress on cosmetic microneedle systems: Preparation, property and application. Eur. Polym. J. 163, 110942. https://doi.org/10.1016/J.EURPOLYMJ.2021.110942

Ibad, A., Khalid, R., Thompson, P.D., 2016. Chelation therapy in the treatment of cardiovascular diseases. J. Clin. Lipidol. 10, 58–62. https://doi.org/10.1016/j.jacl.2015.09.005

Im, S.H., Jung, Y., Kim, S.H., 2017. Current status and future direction of biodegradable metallic and polymeric vascular scaffolds for next-generation stents. Acta Biomater. 60, 3–22. https://doi.org/10.1016/j.actbio.2017.07.019

Indermun, S., Luttge, R., Choonara, Y.E., Kumar, P., Du Toit, L.C., Modi, G., Pillay, V., 2014. Current advances in the fabrication of microneedles for transdermal delivery. J. Control. Release 185, 130–138. https://doi.org/10.1016/j.jconrel.2014.04.052

Jaiswal, A.N., Vagga, A., 2022. Cryopreservation: A Review Article. Cureus 14, 1–6. https://doi.org/10.7759/cureus.31564

Jang, T.S., Cheon, K.H., Ahn, J.H., Song, E.H., Kim, H.E., Jung, H. Do, 2019. In-vitro blood and vascular compatibility of sirolimus-eluting organic/inorganic hybrid stent coatings. Colloids Surfaces B Biointerfaces 179, 405–413. https://doi.org/10.1016/j.colsurfb.2019.04.018

Johnson, A.R., Caudill, C.L., Tumbleston, J.R., Bloomquist, C.J., Moga, K.A., Ermoshkin, A., Shirvanyants, D., Mecham, S.J., Luft, J.C., De Simone, J.M., 2016. Single-step fabrication of computationally designed microneedles by continuous liquid interface production. PLoS One 11, 1–17. https://doi.org/10.1371/journal.pone.0162518

Karamched, S.R., Nosoudi, N., Moreland, H.E., Chowdhury, A., Vyavahare, N.R., 2019. Site-specific chelation therapy with EDTA-loaded albumin nanoparticles reverses arterial calcification in a rat model of chronic kidney disease. Sci. Rep. 9, 1–11. https://doi.org/10.1038/s41598-019-39639-8

Kaushik, S., Hord, A.H., Denson, D.D., McAllister, D. V., Smitra, S., Allen, M.G., Prausnitz, M.R., 2001. Lack of pain associated with microfabricated microneedles. Anesth. Analg. 92, 502–504. https://doi.org/10.1213/00000539-200102000-00041

Keane, K.N., Calton, E.K., Cruzat, V.F., Soares, M.J., Newsholme, P., 2015. The impact of cryopreservation on human peripheral blood leucocyte bioenergetics. Clin. Sci. 128, 723–733. https://doi.org/10.1042/CS20140725

Kim, D.-H., Hwa Jang, E., Ju Lee, K., Yong Lee, J., Hyun Park, S., Ho Seo, I., Woog Lee, K., Hyun Lee, S., Ryu, W., Youn, Y.-N., 2017. A biodegradable microneedle cuff for comparison of drug effects through perivascular delivery to balloon-injured arteries. https://doi.org/10.3390/polym9020056

Krieger, K.J., Bertollo, N., Dangol, M., Sheridan, J.T., Lowery, M.M., O'Cearbhaill, E.D., 2019. Simple and customizable method for fabrication of high-aspect ratio microneedle molds using low-cost 3D printing. Microsystems Nanoeng. 5. https://doi.org/10.1038/s41378-

019-0088-8

Kundu, A., Gabriela Nogueira Campos, M., Santra, S., Rajaraman, S., 2019. Precision vascular delivery of agrochemicals with micromilled microneedles (μMMNs). https://doi.org/10.1038/s41598-019-50386-8

Lanigan, K.C., Pidsosny, K., 2007. Reflectance FTIR spectroscopic analysis of metal complexation to EDTA and EDDS. Vib. Spectrosc. 45, 2–9. https://doi.org/10.1016/j.vibspec.2007.03.003

Lee, J.W., Prausnitz, M.R., 2018. Drug delivery using microneedle patches: not just for skin. Expert Opin. Drug Deliv. ISSN. https://doi.org/10.1080/17425247.2018.1471059

Lee, J.Y., Jang, E.H., Kim, Jae Ho, Park, S.H., Kang, Y., Park, S., Lee, K.J., Kim, Jung Hwan, Youn, Y.N., Ryu, W.H., 2021. Highly flexible and porous silk fibroin microneedle wraps for perivascular drug delivery. J. Control. Release 340, 125–135. https://doi.org/10.1016/J.JCONREL.2021.10.024

Lee, J.Y., Kim, D.H., Lee, K.J., Seo, I.H., Park, S.H., Jang, E.H., Park, Y., Youn, Y.N., Ryu, W.H., 2017. Transfer-molded wrappable microneedle meshes for perivascular drug delivery. J. Control. Release 268, 237–246. https://doi.org/10.1016/J.JCONREL.2017.10.007

Lee, K., Lee, H.C., Lee, D., Jung, H., 2010. Drawing lithography: three-dimensional fabrication of an ultrahigh-aspect-ratio microneedle 483–486. https://doi.org/10.1002/adma.200902418

Lee, K., Park, H., Lee, J., Ryu, S., Joo, C., Ryu, W., 2019. Three-step thermal drawing for rapid prototyping of highly customizable microneedles for vascular tissue insertion. MDPI. https://doi.org/10.3390/pharmaceutics11030100

Lee, K.J., Goudie, M.J., Tebon, P., Sun, W., Luo, Z., Lee, J., Zhang, S., Fetah, K., Kim, H.J., Xue, Y., Darabi, M.A., Ahadian, S., Sarikhani, E., Ryu, W.H., Gu, Z., Weiss, P.S., Dokmeci, M.R., Ashammakhi, N., Khademhosseini, A., 2020a. Non-transdermal microneedles for advanced drug delivery. Adv. Drug Deliv. Rev. 165–166, 41–59. https://doi.org/10.1016/J.ADDR.2019.11.010

Lee, K.J., Goudie, M.J., Tebon, P., Sun, W., Luo, Z., Lee, J., Zhang, S., Fetah, K., Kim, H.J., Xue, Y., Darabi, M.A., Ahadian, S., Sarikhani, E., Ryu, W.H., Gu, Z., Weiss, P.S., Dokmeci, M.R., Ashammakhi, N., Khademhosseini, A., 2020b. Non-transdermal microneedles for advanced drug delivery. Adv. Drug Deliv. Rev. 165–166, 41–59. https://doi.org/10.1016/J.ADDR.2019.11.010

Lee, K.J., Lee, J.Y., Lee, S.G., Park, S.H., Yang, D.S., Lee, J.J., Khademhosseini, A., Kim, J.S., Ryu, W.H., 2020c. Microneedle drug eluting balloon for enhanced drug delivery to vascular tissue. J. Control. Release 321, 174–183. https://doi.org/10.1016/j.jconrel.2020.02.012

Lee, K.J., Lee, J.Y., Lee, S.G., Park, S.H., Yang, D.S., Lee, J.J., Khademhosseini, A., Kim, J.S., Ryu, W.H., 2020d. Microneedle drug eluting balloon for enhanced drug delivery to vascular tissue. J. Control. Release 321, 174–183. https://doi.org/10.1016/J.JCONREL.2020.02.012

Lee, K.J., Park, S.H., Lee, J.Y., Joo, H.C., Jang, E.H., Youn, Y.N., Ryu, W., 2014a. Perivascular biodegradable microneedle cuff for reduction of neointima formation after vascular injury. J. Control. Release 192, 174–181. https://doi.org/10.1016/J.JCONREL.2014.07.007

Lee, K.J., Park, S.H., Lee, J.Y., Joo, H.C., Jang, E.H., Youn, Y.N., Ryu, W., 2014b. Perivascular biodegradable microneedle cuff for reduction of neointima formation after vascular injury. J. Control. Release 192, 174–181. https://doi.org/10.1016/j.jconrel.2014.07.007

Lei, Y., Grover, A., Sinha, A., Vyavahare, N., 2013. Efficacy of reversal of aortic calcification by chelating agents. Calcif. Tissue Int. 93, 426–435. https://doi.org/10.1007/s00223-013-9780-0

Lei, Y., Nosoudi, N., Vyavahare, N., 2014a. Targeted chelation therapy with EDTA-loaded albumin nanoparticles regresses arterial calcification without causing systemic side effects. J. Control. Release. https://doi.org/10.1016/j.jconrel.2014.09.029

Lei, Y., Nosoudi, N., Vyavahare, N., 2014b. Targeted chelation therapy with EDTA-loaded albumin nanoparticles regresses arterial calcification without causing systemic side effects. J. Control. Release 196, 79–86. https://doi.org/10.1016/j.jconrel.2014.09.029

Li, J., Wu, Y., He, J., Huang, Y., 2016. A new insight to the effect of calcium concentration on gelation process and physical properties of alginate films. J. Mater. Sci. 51, 5791–5801. https://doi.org/10.1007/s10853-016-9880-0

Li, Q.Y., Zhang, J.N., Chen, B.Z., Wang, Q.L., Guo, X.D., 2017. A solid polymer microneedle patch pretreatment enhances the permeation of drug molecules into the skin. RSC Adv. 7, 15408–15415. https://doi.org/10.1039/c6ra26759a

Li, S., Li, W., Prausnitz, M., 2018. Individually coated microneedles for co-delivery of multiple compounds with different properties. Drug Deliv. Transl. Res. 8, 1043–1052.

https://doi.org/10.1007/s13346-018-0549-x

Liu, Y., Long, L., Zhang, F., Hu, X., Zhang, J., Hu, C., Wang, Y., Xu, J., 2021. Microneedle-mediated vascular endothelial growth factor delivery promotes angiogenesis and functional recovery after stroke. J. Control. Release 338, 610–622. https://doi.org/10.1016/J.JCONREL.2021.08.057

Luzuriaga, M.A., Berry, D.R., Reagan, J.C., Smaldone, R.A., Gassensmith, J.J., 2018. Biodegradable 3D printed polymer microneedles for transdermal drug delivery. Lab Chip 18, 1223–1230. https://doi.org/10.1039/c8lc00098k

Mansur, H.S., Sadahira, C.M., Souza, A.N., Mansur, A.A.P., 2008. FTIR spectroscopy characterization of poly (vinyl alcohol) hydrogel with different hydrolysis degree and chemically crosslinked with glutaraldehyde. Mater. Sci. Eng. C 28, 539–548. https://doi.org/10.1016/j.msec.2007.10.088

Martanto, W., Davis, S.P., Holiday, N.R., Wang, J., Gill, H.S., Prausnitz, M.R., 2004. Transdermal delivery of insulin using microneedle rollers in vivo. Int. J. Pharm. 392, 127–133. https://doi.org/10.1016/j.ijpharm.2010.03.041

Nagarkar, R., Patel, J., 2019. Polyvinyl alcohol: a comprehensive study. Acta Sci. Pharm. Sci. (ISSN 2581-5423) 3, 34–44.

Najjar, D.M., Cohen, E.J., Rapuano, C.J., Laibson, P.R., 2004. EDTA chelation for calcific band keratopathy: Results and long-term follow-up. Am. J. Ophthalmol. 137, 1056–1064. https://doi.org/10.1016/j.ajo.2004.01.036

Nejad, H.R., Sadeqi, A., Kiaee, G., Sonkusale, S., 2018. Low-cost and cleanroom-free fabrication of microneedles. Microsystems Nanoeng. 4, 1–7. https://doi.org/10.1038/MICRONANO.2017.73

Nkuna, R., Ijoma, G.N., Matambo, T.S., 2022. Applying EDTA in chelating excess metal ions to improve downstream DNA recovery from mine tailings for long-read amplicon sequencing of acidophilic fungi communities. J. Fungi 8. https://doi.org/10.3390/jof8050419

Panda, A., Matadh, · V Anusha, Suresh, S., Shivakumar, · H N, Narasimha Murthy, · S, 2021. Non-dermal applications of microneedle drug delivery systems 1, 3. https://doi.org/10.1007/s13346-021-00922-9

Pérennès, F., Marmiroli, B., Matteucci, M., Tormen, M., Vaccari, L., Di Fabrizio, E., 2006. Sharp beveled tip hollow microneedle arrays fabricated by LIGA and 3D soft lithography

with polyvinyl alcohol. J. Micromechanics Microengineering 16, 473–479. https://doi.org/10.1088/0960-1317/16/3/001

Pradeep Narayanan, S., Raghavan, S., 2019. Fabrication and characterization of gold-coated solid silicon microneedles with improved biocompatibility. Int. J. Adv. Manuf. Technol. 104, 3327–3333. https://doi.org/10.1007/s00170-018-2596-3

Pradeep Narayanan, S., Raghavan, S., 2017. Solid silicon microneedles for drug delivery applications. Int. J. Adv. Manuf. Technol. 93, 407–422. https://doi.org/10.1007/s00170-016-9698-6

Queiroz, M.F., Melo, K.R.T., Sabry, D.A., Sassaki, G.L., Rocha, H.A.O., 2015. Does the use of chitosan contribute to oxalate kidney stone formation? Mar. Drugs 13, 141–158. https://doi.org/10.3390/md13010141

Rad, Z.F., Prewett, P.D., Davies, G.J., 2021. An overview of microneedle applications, materials, and fabrication methods. Beilstein J. Nanotechnol. 12, 1034–1046. https://doi.org/10.3762/BJNANO.12.77

Rafiei, P., Haddadi, A., 2019. A robust systematic design: Optimization and preparation of polymeric nanoparticles of PLGA for docetaxel intravenous delivery. Mater. Sci. Eng. C 104, 1–11. https://doi.org/10.1016/j.msec.2019.109950

Raghib, M.F., Mutzenbach, J.S., Rösler, C., Otto, F., Coy, M.M., Müller-Thies-Broussalis, E., Pikija, S., 2018. Acute treatment of stroke due to spontaneous calcified cerebral emboli causing large vessel occlusion. J. Clin. Neurosci. 47, 56–61. https://doi.org/10.1016/j.jocn.2017.10.042

Rajamannan, N.M., Evans, F.J., Aikawa, E., Grande-Allen, K.J., Demer, L.L., Heistad, D.D., Simmons, C.A., Masters, K.S., Mathieu, P., O'Brien, K.D., Schoen, F.J., Towler, D.A., Yoganathan, A.P., Otto, C.M., 2011. Calcific aortic valve disease: Not simply a degenerative process: A review and agenda for research from the national heart and lung and blood institute aortic stenosis working group. Circulation 124, 1783–1791. https://doi.org/10.1161/CIRCULATIONAHA.110.006767

Rambhia, K.J., Ma, P.X., 2015. Controlled Drug Release for Tissue Engineering Graphical Abstract HHS Public Access. J Control Release 219, 119–128. https://doi.org/10.1016/j.jconrel.2015.08.049

Russo, R., Malinconico, M., Santagata, G., 2007. Effect of cross-linking with calcium ions on the physical properties of alginate films. Biomacromolecules 8, 3193–3197. https://doi.org/10.1021/bm700565h

Sadeghi, A.M.M., Dorkoosh, F.A., Avadi, M.R., Weinhold, M., Bayat, A., Delie, F., Gurny, R., Larijani, B., Rafiee-Tehrani, M., Junginger, H.E., 2008. Permeation enhancer effect of chitosan and chitosan derivatives: Comparison of formulations as soluble polymers and nanoparticulate systems on insulin absorption in Caco-2 cells. Eur. J. Pharm. Biopharm. 70, 270–278. https://doi.org/10.1016/j.ejpb.2008.03.004

Schantl, A.E., Ivarsson, M.E., Leroux, J.-C., 2019. Investigational pharmacological treatments for vascular calcification. Adv. Ther. 2, 1800094. https://doi.org/10.1002/adtp.201800094

Schweighofer, N., Aigelsreiter, A., Trummer, O., Graf-Rechberger, M., Hacker, N., Kniepeiss, D., Wagner, D., Stiegler, P., Trummer, C., Pieber, T., Obermayer-Pietsch, B., Müller, H., 2016. Direct comparison of regulators of calcification between bone and vessels in humans. Bone 88, 31–38. https://doi.org/10.1016/j.bone.2016.04.016

Shakya, A.K., Ingrole, R.S.J., Joshi, G., Uddin, J., Anvari, S., Davis, C.M., Gill, H.S., 2019. Microneedles coated with peanut allergen enable desensitization of peanut sensitized mice. J Control Release. 176, 139–148. https://doi.org/10.1016/j.jconrel.2019.09.022.Microneedles

Shioi, A., Morioka, T., Shoji, T., Emoto, M., 2020. The inhibitory roles of vitamin K in progression of vascular calcification. MDPI. https://doi.org/10.3390/nu12020583

Siepmann, J., Peppas, N.A., 2012. Modeling of drug release from delivery systems based on hydroxypropyl methylcellulose (HPMC). Adv. Drug Deliv. Rev. 64, 163–174. https://doi.org/10.1016/j.addr.2012.09.028

Singh, K., Suri, R., Tiwary, A.K., Rana, V., 2012. Chitosan films: Crosslinking with EDTA modifies physicochemical and mechanical properties. J. Mater. Sci. Mater. Med. 23, 687–695. https://doi.org/10.1007/s10856-012-4554-1

Stoeber, B., Liepmann, D., 2000. Fluid injection through out-of-plane microneedles. https://doi.org/10.1109/MMB.2000.893777

Su, Y., Andrabi, S.M., Shahriar, S.M.S., Wong, S.L., Wang, G., Xie, J., 2023. Triggered release of antimicrobial peptide from microneedle patches for treatment of wound biofilms. J. Control. Release 356, 131–141. https://doi.org/10.1016/J.JCONREL.2023.02.030

Tang, J., Wang, J., Huang, K., Ye, Y., Su, T., Qiao, L., Hensley, M.T., Caranasos, T.G., Zhang, J., Gu, Z., Cheng, K., 2018. Cardiac cell–integrated microneedle patch for treating myocardial infarction. Sci. Adv. 4, 1–13. https://doi.org/10.1126/sciadv.aat9365

Tiraton, T., Suwantong, O., Chuysinuan, P., Ekabutr, P., Niamlang, P., Khampieng, T., Supaphol, P., 2022. Biodegradable microneedle fabricated from sodium alginate-gelatin for transdermal delivery of clindamycin. Mater. Today Commun. 32, 104158. https://doi.org/10.1016/j.mtcomm.2022.104158

Topuz, F., Henke, A., Richtering, W., Groll, J., 2012. Magnesium ions and alginate do form hydrogels: A rheological study. Soft Matter 8, 4877–4881. https://doi.org/10.1039/C2SM07465F

Waghule, T., Singhvi, G., Dubey, S.K., Pandey, M.M., Gupta, G., Singh, M., Dua, K., 2019. Microneedles: A smart approach and increasing potential for transdermal drug delivery system. Biomed. Pharmacother. 109, 1249–1258. https://doi.org/10.1016/J.BIOPHA.2018.10.078

Wei, H., Liu, S., Tong, Z., Chen, T., Yang, M., Guo, Y., Sun, H., Wu, Y., Chu, Y., Fan, L., 2022. Hydrogel-based microneedles of chitosan derivatives for drug delivery. React. Funct. Polym. 172, 105200. https://doi.org/10.1016/j.reactfunctpolym.2022.105200

Wilke, N., Mulcahy, A., Ye, S.R., Morrissey, A., 2005. Process optimization and characterization of silicon microneedles fabricated by wet etch technology. Microelectronics J. 36, 650–656. https://doi.org/10.1016/j.mejo.2005.04.044

Witeska, M., Wargocka, W., 2011. Disodium EDTA used as anticoagulant causes hemolysis in common carp blood. Turkish J. Vet. Anim. Sci. 35, 99–104. https://doi.org/10.3906/vet-0908-51

Wu, C.H., Sun, M.K., Kung, Y., Wang, Y.C., Chen, S.L., Shen, H.H., Chen, W.S., Young, T.H., 2020. One injection for one-week controlled release: In vitro and in vivo assessment of ultrasound-triggered drug release from injectable thermoresponsive biocompatible hydrogels. Ultrason. Sonochem. 62, 104875. https://doi.org/10.1016/j.ultsonch.2019.104875

Wu, M., Rementer, C., Giachelli, C.M., 2013. Vascular calcification: an update on mechanisms and challenges in treatment. Calcif. Tissue Int 93, 365–373. https://doi.org/10.1007/s00223-013-9712-z.Vascular

Wu, Q.X., Lin, D.Q., Yao, S.J., 2014. Design of chitosan and its water soluble derivatives-based drug carriers with polyelectrolyte complexes. Mar. Drugs 12, 6236–6253. https://doi.org/10.3390/md12126236

Wu, T., You, X., Chen, Z., 2022. Hollow microneedles on a paper fabricated by standard photolithography for the screening test of prediabetes. Sensors 22.

https://doi.org/10.3390/s22114253

Yang, M., Zahn, J.D., 2004. Microneedle insertion force reduction using vibratory actuation. Biomed. Microdevices 6, 177–182.

Yang, Q., Zhong, W., Xu, L., Li, H., Yan, Q., She, Y., Yang, G., 2021. Recent progress of 3D-printed microneedles for transdermal drug delivery. Int. J. Pharm. 593, 120106. https://doi.org/10.1016/J.IJPHARM.2020.120106

Yao, W., Li, D., Zhao, Y., Zhan, Z., Jin, G., Liang, H., Yang, R., 2020. 3D printed multi-functional hydrogel microneedles based on high-precision digital light processing. 3. IF2.9 Micromachines 11. https://doi.org/doi:10.3390/mi11010017

Yu, W., Jiang, G., Zhang, Y., Liu, D., Xu, B., Zhou, J., 2017. Polymer microneedles fabricated from alginate and hyaluronate for transdermal delivery of insulin. Mater. Sci. Eng. C 80, 187–196. https://doi.org/10.1016/j.msec.2017.05.143

Zhang, Y., Jiang, G., Yu, W., Liu, D., Xu, B., 2018a. Microneedles fabricated from alginate and maltose for transdermal delivery of insulin on diabetic rats. Mater. Sci. Eng. C 85, 18–26. https://doi.org/10.1016/J.MSEC.2017.12.006

Zhang, Y., Jiang, G., Yu, W., Liu, D., Xu, B., 2018b. Microneedles fabricated from alginate and maltose for transdermal delivery of insulin on diabetic rats. Mater. Sci. Eng. C 85, 18–26. https://doi.org/10.1016/j.msec.2017.12.006

Zhou, R., Yu, J., Gu, Z., Zhang, Y., 2022. Microneedle-mediated therapy for cardiovascular diseases. Drug Deliv. Transl. Res. 12, 472–483. https://doi.org/10.1007/S13346-021-01073-7

Zhou, R., Yu, J., Gu, Z., Zhang, Y., 2021. Microneedle-mediated therapy for cardiovascular diseases. Drug Deliv. Transl. Res. https://doi.org/10.1007/s13346-021-01073-7

Zhou, Z., Xing, M., Zhang, S., Yang, G., Gao, Y., 2022. Process optimization of Ca2+ cross-linked alginate-based swellable microneedles for enhanced transdermal permeability: More applicable to acidic drugs. Int. J. Pharm. 618, 121669. https://doi.org/10.1016/J.IJPHARM.2022.121669

Zhu, D.D., Wang, Q.L., Liu, X.B., Guo, X.D., 2016. Rapidly separating microneedles for transdermal drug delivery. Acta Biomater. 41, 312–319. https://doi.org/10.1016/j.actbio.2016.06.005

Appendix 1 - Ethical Certificates

UNIVERSITY OF THE WITWATERSRAND JOHANNESBURG

R49 Professor YE Choonara

HUMAN RESEARCH ETHICS COMMITTEE (MEDICAL)
CLEARANCE CERTIFICATE NO. M180978

NAME: (Principal Investigator)	Professor YE Choonara
DEPARTMENT:	School of Therapeutic Sciences Department of Pharmacy and Pharmacology Medical School University
PROJECT TITLE:	*Development of a biohybrid, platelet-based drug-delivery vehicle for the potential treatment of ischaemic stroke*
DATE CONSIDERED:	28/09/2018
DECISION:	Approved unconditionally
CONDITIONS:	Change of Principal Investigator noted on 02/09/2021
NOTE:	If contact information regarding student study participants is required, please contact the Registrar's office - <Nicoleen.Potgieter@wits.ac.za>
SUPERVISOR:	Not applicable
APPROVED BY:	CB Penny Dr CB Penny, Chairperson, HREC (Medical)
DATE OF APPROVAL:	16/11/2018

This Clearance Certificate is valid for 5 years from the date of approval. An extension may be applied for.

DECLARATION OF INVESTIGATORS

To be completed in duplicate and **ONE COPY** returned to the Research Office secretariat on the 3rd floor, Phillip Tobias Building, Parktown, University of the Witwatersrand, Johannesburg.

I/we fully understand the conditions under which I am/we are authorized to carry out the above-mentioned research and I/we undertake to ensure compliance with these conditions. Should any departure be contemplated from the research protocol as approved, I/we undertake to submit details to the Committee. **I agree to submit a yearly progress report**. When a funder requires annual re-certification, the application date will be one year after the date when the study was initially reviewed. In this case, the study was initially reviewed in **«Missing mail merge field»** and therefore reports and re-certification will be due in the month of **«Missing mail merge field»** each year. Unreported changes to the study may invalidate the clearance given by the HREC (Medical).

Signature of Principal Investigator _____ Date _____

ANIMAL RESEARCH ETHICS COMMITTEE
Registration number: AREC-101210-002

Date: 19/05/2022

Certificate reference: Waiver 19-05-2022-O
Category: O
Applicant: Yahya Choonara
Department: Department of Pharmacy and Pharmacology (WITS)
Tel: 011 717 2552; **Email**: Yahya.Choonara@wits.ac.za

Re: Waiver from the Animal Ethics Research Committee of the University of the Witwatersrand

This letter is to confirm that Professor Yahya Choonara (Department of Pharmacy and Pharmacology), does not require full Animal Ethics Research Committee clearance for the use of porcine tissues obtained commercially or from the Wits Animal Research Facility (WRAF).

Reason for waiver
The project is using already available tissue collected from
1) pigs euthanized for other purposes (such as animals terminated after experimental procedures and old stock animals being terminated) at WRAF,
2) commercially available animals from local accredited and registered abattoirs in the Gauteng area. (McKenzie Piggery & Abattoir (Pty) Ltd, Tarlton)

Details of the study
The applicant will perform *in vitro* drug diffusion studies on various tissue from Sus scrofa domesticus (domestic pig). Permeability experiments will be performed on 7 tissue replicates for each tissue sample and 6 diffusion experiments will be performed for each drug tested. Equilibration of 10 minutes was allowed in the donor as well the acceptor compartments of the diffusion cells. Thereafter the PBS solution of the donor cell will be removed and replaced with the specific drug in PBS solution. PBS at 20°C will be pumped through the acceptor chambers at a rate of 1.5 ml/h and collected, by means of a fraction collector, at 2-h intervals for 24 hours. The study will be performed under sink conditions (i.e. the concentration in the acceptor cell never reached 10% of the donor cell concentration). Drug concentrations will be analyzed by means of RP C18-HPLC .

The individuals covered by the waiver is Prof Yahya Choonara (Department of Pharmacy and Pharmacology, WITS).

Condition:
An annual report stating the number of animals used, the title of the different projects that made use of the porcine tissue and the students and coworkers involved in each project will be sent by the end of January to Dept-Secretary-AREC@wits.ac.za

Please contact me should you require further information.

Yours sincerely



Prof Frederic Michel
Chair: Animal Research Ethics Committee
University of the Witwatersrand

Appendix 2 - Research Presentations

Design and Characterization of EDTA loaded: Polymer Microneedles Fabricated from Chitosan or Alginate

K. Moodley[1], T. Marimuthu[1] , P. Kumar[1] and Y.E. Choonara[1]

Wits Advanced Drug Delivery Platform, Department of Pharmacy and Pharmacology, School of Therapeutic Sciences, Faculty of Health Sciences, University of the Witwatersrand, Johannesburg, 7 York Road, Parktown, 2193, South Africa

Aim: This study aims to design and compare EDTA-loaded chitosan and alginate microneedle patches for the treatment of calcified blood tissue.

Methods: Alginate and chitosan solutions were made and mold-based approach was used for the synthesis of the microneedle arrays of both polymers mixtures. Physicomechanical and physicochemical characteristics of the arrays have been analysed using SEM, FTIR, DSC, XRD and texture analysis.

Results: FTIR analysis of the chitosan array showed an intensity of the peak at 1578.26 cm^{-1} whereas the alginate array showed the presence of a new peak at 3377.15 cm^{-1} indicative of successful combination of bioactive and the polymer. Texture analyzer results showed that although the chitosan array exhibited a greater compression strength than the alginate array, both polymer arrays display the mechanical strengths withstanding a force of 30N adequate for the insertion and penetration into the vasculature. Designed microneedles possess a square based pyramidal shape with a base of 100 µm and a needle height of 300 µm.

Conclusions/Impact: The developed microneedles possess the physical attributes required for their potential use as a vascular drug delivery system.

Future work: the penetrating ability of the arrays is currently being tested using a PVA phantom model of both healthy and calcified vascular tissue. The hemocompatibility of the arrays will be evaluated by assessing hemolysis.

Design and Characterisation of EDTA Loaded Polymer Microneedles: Fabricated from Chitosan and Alginate

K. Moodley[1], T. Marimuthu[1], P. Kumar[1], A. Van Eyk[2], Y.E. Choonara[1]

[1]Wits Advanced Drug Delivery Platform, Department of Pharmacy and Pharmacology, School of Therapeutic Sciences, Faculty of Health Sciences, University of the Witwatersrand, Johannesburg, 7 York Road, Parktown, 2193, South Africa

[2]Department of Pharmacy and Pharmacology, School of Therapeutic Sciences, Faculty of Health Sciences, University of the Witwatersrand, Johannesburg, 7 York Road, Parktown, 2193, South Africa

Introduction:

Vascular calcification occurs when calcium and phosphate minerals are deposited within the walls of the vasculature[1]. Vascular calcification results in stiffening of vessels and obstruction to regular blood flow leading to acute coronary syndromes, decreased organ perfusion and increased blood pressure[2,3]. Current treatment options for calcification of blood vessels mainly include physical mechanisms such as surgical procedures and while many pharmaceutics have been evaluated as potential treatments, no therapeutic currently exists[3,4]. This study addresses the need for a suitable therapy to treat calcification of vascular tissue by providing a polymeric microneedle array loaded with EDTA, a novel therapeutic for the sustained, local delivery of EDTA for calcium removal by chelation.

Methods and Materials:

- Materials: Chitosan, Sodium Alginate, Polyvinyl Alcohol (PVA), Hydroxypropyl methylcellulose (HPMC), Disodium ethylenediaminetetraacetic acid (EDTA)
- Microneedle Formulation:

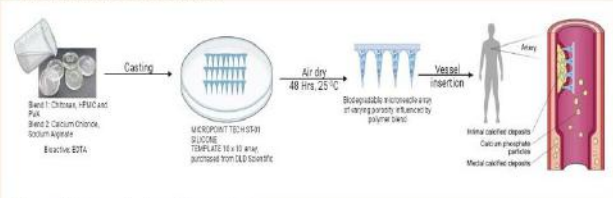


Figure 1 Microneedle formulation method

- Methods:

Table 1 characterisation parameters and methods

Parameter	Array aspects affected by parameter	Methods and Instrument
Array composition	Drug loading, mechanical strength and drug release	Fourier Transform Infrared Spectroscopy (FTIR) using a PerkinElmer Spectrum 2000 ATR-FTIR
Array dimensions and needle shape	Drug loading, drug delivery site, depth of penetration, mechanical strength and drug release	Scanning Electron Microscopy (SEM) using a Zeiss Sigma 03-39 Field Emission Scanning Electron Microscope
Array mechanical strength	Drug delivery site, depth of penetration and drug release	Texture Analysis (Compression testing) using a TA.XT.plus Texture Analyser, Stable Microsystems®
Crystallinity	Drug loading, mechanical strength and drug release	X-Ray Diffraction (XRD) using a Rigaku MiniFlex 600 X-ray diffractometer

Conclusion

The developed microneedles successfully incorporate EDTA as a therapeutic agent, possess the necessary adhesion properties, mechanical strength and dimensions required for their potential use as a much needed vascular drug delivery system.

Future work: The drug release profile and haemocompatibility of the arrays will be evaluated by tissue permeation studies and assessing hemolysis of whole blood respectively.

Acknowledgements

WADDP Wits Advanced Drug Delivery Platform

NRF National Research Foundation

Results and Discussion:

- Assessment of microneedle array composition using FTIR analysis:

Analysis confirms the successful incorporation of bioactive (EDTA) into the optimised blended polymer mixtures

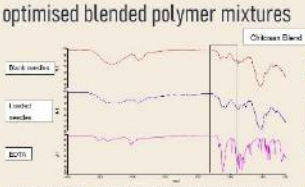


Figure 2 FTIR spectra of EDTA disodium, blank chitosan microneedles and EDTA loaded chitosan microneedles.

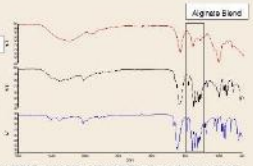


Figure 3 FTIR spectra of EDTA disodium, blank alginate microneedles and EDTA loaded alginate microneedles

- Assessment of microneedle array mechanical strength using texture analysis:

Both needle arrays withstand a 30N compressive force, above the required mechanical strength adequate for the insertion of the array into calcified tissue without breakage.

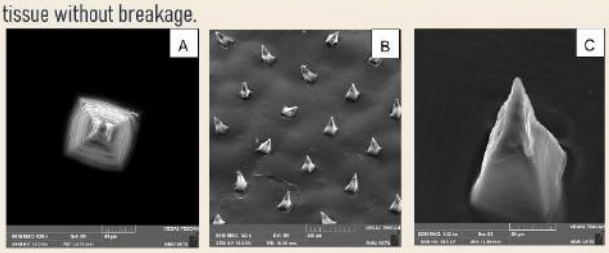


Figure 4 SEM images of deformation of needles after a 30N force application at magnification (A) 926X, (B) 143X and (C) 1320X.

- Assessment of microneedle array dimensions and needle shape using SEM:

The designed microneedles possess a square based pyramidal shape with a base of 100 µm and a needle height of 300 µm allowing for optimized insertion and a size small enough to prevent vascular occlusion.

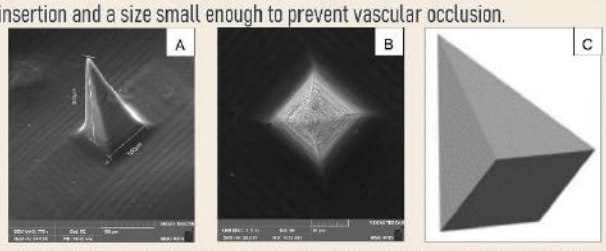


Figure 5 SEM images of individual needle tips with a square pyramidal base within the fabricated array at magnification (A) 779X and (B) 1110X. (C) 3D representation of ideal microneedle shape.

- Assessment of microneedle array crystallinity using XRD

XRD results indicate that both formulations are amorphous in nature.

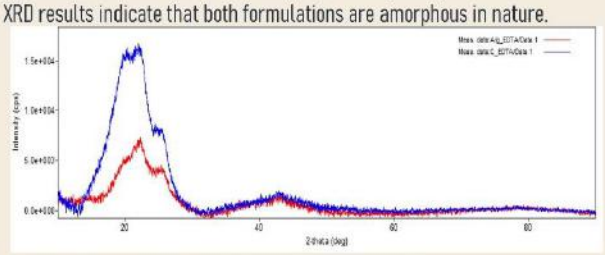


Figure 6 XRD graph of EDTA loaded alginate and chitosan microneedles

References:

1. Schwaighofer A, et al. Direct comparison of drug-eluting and bare metal stents in human coronary vessels in vivo. Nat Rev Drug Discov. 2016;15(12):824-33.
2. Tabrizi AR, et al. Investigation of Pharmacological Treatments for Vascular Calcification. Adv Pharm Bull. 2017;7(3):333-341.
4. Bell S, et al. Drug delivery to the coronary vasculature: challenges and opportunities. Int J Cardiol. 2016;203:1-11.